PH.D. THESIS

Control of Smart Actuators

by Xiaobo Tan
Advisor: John S. Baras and P. S. Krishnaprasad

CDCSS PhD 2002-1
(ISR PhD 2002-8)

The Center for Dynamics and Control of Smart Structures (CDCSS) is a joint Harvard University, Boston University, University of Maryland center, supported by the Army Research Office under the ODDR&E MURI97 Program Grant No. DAAG55-97-1-0114 (through Harvard University). This document is a technical report in the CDCSS series originating at the University of Maryland.

Web site http://www.isr.umd.edu/CDCSS/cdcss.html

ABSTRACT

Title of Dissertation: Control of Smart Actuators

Xiaobo Tan, Doctor of Philosophy, 2002

Dissertation directed by: Professor John S. Baras
Professor P. S. Krishnaprasad
Department of Electrical and Computer Engineering

Hysteresis in smart materials hinders wider applicability of such materials in actuators and sensors. In this dissertation we study modeling, identification and control of hysteresis in smart actuators. While the approaches are applicable to control of a wide class of smart actuators, we illustrate the ideas through the example of controlling a magnetostrictive actuator.

Hysteresis exhibited by magnetostrictive actuators is rate-independent when the input frequency is low and we can model it by a Preisach operator. It becomes rate-dependent when the input frequency gets high due to the eddy current effect and the magnetoelastic dynamics. In this case, we propose a new dynamic hysteresis model, consisting of a Preisach operator coupled to an ordinary differential equation in an unusual way. We establish its well-posedness and study its various system-theoretic properties. Existence of periodic solutions under periodic forcing

is proved. Algorithms for simulation of the model are also studied. Parameter identification methods for both the Preisach operator and the dynamic model are investigated.

We pursue the problem of hysteresis control along three different but connected paths: inverse control, robust control and optimal control.

The idea of inverse control is to construct an inverse operator to cancel out the hysteretic nonlinearity. Efficient inversion schemes are proposed for both the Preisach model and the dynamic hysteresis model. We also formulate and study a novel inversion problem, called the value inversion problem, and apply it to micro-positioning control.

Inverse compensation is open-loop in nature and therefore susceptible to model uncertainties and to errors introduced in the inverse schemes. We propose a robust control framework for smart actuators by combining inverse compensation with robust control techniques. We present systematic controller design methods which guarantee robust stability and robust trajectory tracking while taking actuator saturation into account.

Finally we study optimal control of hysteresis in smart actuators based on a low dimensional hysteresis model. We characterize the value function as the (unique) viscosity solution to a Hamilton-Jacobi-Bellman equation of a hybrid form, and provide a numerical scheme to approximate the solution.

Control of Smart Actuators

by

Xiaobo Tan

Dissertation submitted to the Faculty of the Graduate School of the
University of Maryland, College Park in partial fulfillment
of the requirements for the degree of
Doctor of Philosophy
2002

Advisory Committee:

Professor John S. Baras, Chairman / Advisor
Professor P. S. Krishnaprasad, Coadvisor
Professor Reza Ghodssi
Professor Isaak Mayergoyz
Professor Stuart Antman

DEDICATION

To Mom and Dad, and my wife Youyu

ACKNOWLEDGEMENTS

It has been my privilege to have both Professor John S. Baras and Professor P. S. Krishnaprasad as my advisors. I am grateful to them for their thoughtful guidance and enthusiastic encouragement. They inspired me with their vision and expertise during the course of my PhD study. Apart from providing technical directions, they have also offered me with invaluable advices on how to improve myself as a researcher.

I would like to thank Professor Ramakrishnan Venkataraman, who led me into the area of hysteresis modeling and control. Venkat also helped me a lot in my modeling effort through numerous discussions.

I thank Professor Reza Ghodssi, Professor Isaak Mayergoyz and Professor Stuart Antman for kindly joining the advisory committee and providing many insightful suggestions and comments. I also thank Professor Ghodssi for his advice on my job search.

I would like to thank Professor Andre Tits for taking time to review my work and offering me useful comments. I also benefited a lot from his robust control course, which enabled me to successfully accomplish the work in Chapter 4.

I gratefully acknowledge the inspiring discussions with Professor Martin Brokate on the well-posedness of the dynamic hysteresis model during the Hysteresis and Micromagnetics Modeling Symposium (HMM'01) at the George Washington University.

I am grateful to my colleagues and friends at Maryland who have offered help in various ways: Sean Andersson, Fumin Zhang, Dr. George Kantor, Dr. Andrew Newman, Dr. Amir Handzel, Dr. Eric Justh, Dr. Sameer Joshi, Jia-Shiang Jou, Chang Zhang, Sudhir Varma, Maben Rabi, Huigang Chen, Zhu Han, Dr. Hongjun Li, Shah-An Yang, Vijay Bharadwaj and many others. Special thanks are due to Andrew for creating the thesis template, which makes thesis writing much easier and more pleasant.

I also want to thank the computing and administrative staff of ISR for their assistance during my study and life here. Special thanks are due to Althia Kirlew, Pamela White, Jean Lafonta, Trevor Vaughan and Margaret Jayant.

I am grateful for the financial support of my studies and research by the Army Research Office under the ODDR&E MURI97 Program Grant No. DAAG55-97-1-0114 to the Center for Dynamics and Control of Smart Structures (through Harvard University), and from the Lockheed Martin Chair endowment funds.

Last, but certainly not the least, I am deeply indebted to my wife, Youyu Feng, for her constant love, support and encouragement.

TABLE OF CONTENTS

LIST OF FIGURES

Chapter 1

Introduction

Smart materials, such as magnetostrictives, piezoelectrics, electroactive polymers (EAPs), shape memory alloys (SMAs), electrorheological (ER) fluids and magnetorheological (MR) fluids, all display certain coupling phenomena between applied electromagnetic/thermal fields and their mechanical/rheological properties. Actuators and sensors made of these materials can be built into structures, often called *smart structures*, with the ability to sense and respond to environmental changes to achieve desired goals. Smart materials and smart structures have been receiving tremendous interest in the past decade, due to their broad applications in areas of aerospace, manufacturing, defense, and civil infrastructure systems, to name a few. Hysteresis widely existing in smart materials, however, makes the effective use of smart actuators and sensors quite challenging.

A fundamental idea in coping with hysteresis is to formulate the mathematical model of hysteresis and use inverse compensation to cancel out the hysteretic effect. This idea can be found in [45, 80, 71, 35, 79, 62]. There have been a few monographs devoted to modeling of hysteresis and study of dynamical systems with hysteresis [55, 58, 86, 20, 81].

Hysteresis models can be roughly classified into physics-based models and phenomenological models. An example of a physics-based model is the Jiles-Atherton model of ferromagnetic hysteresis [51], where hysteresis is considered to arise from pinning of domain walls on defect sites. The most popular phenomenological hysteresis model used in control of smart actuators has been the Preisach model [1, 45, 46, 36, 38, 79, 62]. A similar type of operator, called Krasnosel'skii-Pokrovskii (KP) operator has also been used [7, 35]. Although in general the Preisach model does not provide physical insight into the problem, it provides a means of developing phenomenological models that are capable of producing behaviors similar to those of physical systems (see Mayergoyz [58] for an excellent exposition).

In this dissertation we study control methodologies for smart actuators exhibiting hysteresis. We illustrate the ideas through the example of controlling a commercially available magnetostrictive actuator. Magnetostriction is the phenomenon of strong coupling between magnetic properties and mechanical properties of some ferromagnetic materials (e.g., Terfenol-D): strains are generated in response to an applied magnetic field, while conversely, mechanical stresses in the materials produce measurable changes in magnetization. This phenomenon can be used for actuation and sensing. Magnetostrictive actuators have applications to micro-positioning, robotics, ultrasonics, vibration control, etc. Figure 1.1 shows a sectional view of a Terfenol-D actuator manufactured by Etrema Products, Inc. By varying the current in the coil, we vary the magnetic field in the Terfenol-D rod and thus control the motion of the rod head. Figure 1.2 displays the hysteresis observed in the magnetostrictive actuator.

We study the problem of control of hysteresis from two perspectives. The first

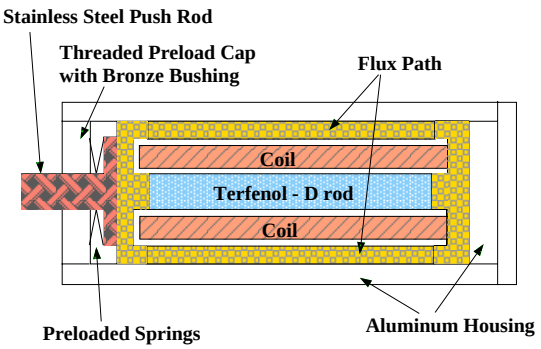

Figure 1.1: Sectional view of a Terfenol-D actuator [82](Original source: Etrema Products, Inc.).

one is based on the Preisach model and the theme is to develop accurate and fast inverse control algorithms. The second perspective is optimal control based on the low dimensional bulk ferromagnetic hysteresis model [82, 84], a modification of the Jiles-Atherton model. We now outline the contributions of this dissertation.

1.1 Contributions of the Dissertation

We note that although the dissertation is based on controlling a magnetostrictive actuator, our work is applicable to control of a wide class of smart actuators for two reasons: 1) the Preisach operator is able to model hysteresis in various smart actuators; 2) a low dimensional ferroelectric hysteresis model has been proposed [72] and therefore the viscosity solutions approach in Chapter 5 applies well to optimal control of actuators made of ferroelectric materials, e.g., piezoelectrics and electrostrictives.

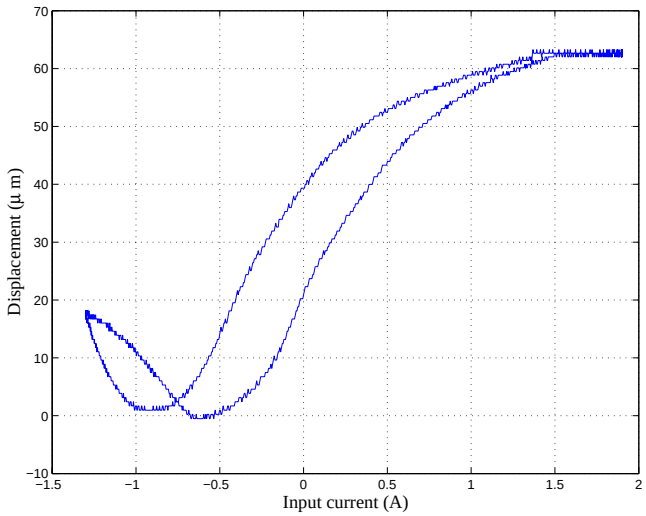

Figure 1.2: Hysteresis in the magnetostrictive actuator.

1.1.1 Modeling and control of hysteresis based on the Preisach operator

When the input frequency is very low (typically below 5 Hz), the magnetostrictive hysteresis is rate-independent and can be modeled by a Preisach operator alone. We propose a constrained least squares algorithm to obtain a discrete approximation to the Preisach measure, and present several algorithms to invert the Preisach operator efficiently.

By inverse compensation, one usually refers to the *trajectory* inversion. In many applications, such as micro-positioning, we are more interested in the following problem: given a desired output *value*, find an input trajectory such that the final value of the output matches the desired value. To distinguish this problem from the trajectory inversion problem, we call it the *value inversion* problem. The discretized Preisach operator is a finite state machine (FSM). We formulate the value inversion problem as a state reachability problem for the FSM. We show

that the FSM is reachable and propose a state space reduction scheme, which significantly saves storage space and computation time.

When the input frequency gets high, the magnetostrictive hysteresis is rate-dependent due to the eddy current effect and the magnetoelastic dynamics of the actuator rod. We propose a novel dynamic hysteresis model, consisting of a Preisach operator coupled to an ordinary differential equation (ODE) in an unusual way. We establish the well-posedness of the model and study its various system-theoretic properties. Existence of periodic solutions under periodic forcing is proved. Algorithms for simulation of the model are also studied. Methods for parameter identification and inverse compensation for this dynamic model are proposed.

Inverse compensation is open-loop in nature and therefore susceptible to model uncertainties and to errors introduced in the inverse schemes. We propose a robust control framework for smart actuators by combining inverse compensation with robust control techniques. We present systematic controller design methods which guarantee robust stability and robust trajectory tracking while taking actuator saturation into account.

Ideas and theories are backed by extensive simulation and experimental results.

1.1.2 Optimal control of hysteresis based on the low dimensional model

Optimal control of the magnetostrictive actuator is investigated based on the low dimensional ferromagnetic hysteresis model proposed by Venkataraman and Krishnaprasad [84, 82]. We study an infinte time horizon optimal control problem in details. The value function is characterized as the (unique) viscosity solution to

a Hamilton-Jacobi-Bellman equation (HJB) of a hybrid form. We also provide a numerical scheme to approximate the solution.

The viscosity solutions approach is also extended to other control problems of practical interest, e.g., the finite time horizon problem, the time-optimal control problem, the exit problem, and the nonlinear $\mathcal{H}_\infty$ control problem.

1.2 Organization of the Dissertation

In Chapter 2 we provide an introduction to the Preisach operator, and present identification and inversion schemes for the Preisach operator. The dynamic hysteresis model is proposed and studied in Chapter 3. In Chapter 4 we discuss the robust control framework for smart actuators. In Chapter 5, we present the viscosity solutions approach for optimal control of hysteresis based on the low dimensional model. Conclusions and future work are provided in Chapter 6.

Chapter 2

Identification and Approximate Inversion of the Preisach Operator

When the input frequency is low (typically below 5 Hz), the magnetostrictive hysteresis is rate-independent and can be modeled by a Preisach operator alone. In this chapter we first give an introduction to the Preisach operator. Then we discuss how to identify the Preisach measure. Finally we study two types of inversion problems for the Preisach operator: the trajectory inversion problem and the value inversion problem.

2.1 Introduction to the Preisach Operator

In this section we introduce the Preisach operator and some of its properties.

2.1.1 The Preisach operator in (β, α) coordinates

For a pair of thresholds (β, α) with $\beta \leq \alpha$, consider a simple hysteretic element $\widehat{\gamma}_{\beta,\alpha}[\cdot, \cdot]$, as illustrated in Figure 2.1. For $u \in C([0, T])$ and an initial configuration $\zeta \in \{-1, 1\}$, the function

$$v = \widehat{\gamma}_{\beta,\alpha}[u, \zeta] : [0, T] \to \{-1, 1\}$$

is defined as follows [86]:

$$v(0) \stackrel{\triangle}{=} \begin{cases} -1 & \text{if } u(0) \leq \beta \\ \zeta & \text{if } \beta < u(0) < \alpha \\ 1 & \text{if } u(0) \geq \alpha \end{cases},$$

and for $t \in (0, T]$, setting $X_t \stackrel{\triangle}{=} \{\tau \in (0, t] : u(\tau) = \beta \text{ or } \alpha\}$,

$$v(t) \stackrel{\triangle}{=} \begin{cases} v(0) & \text{if } X_t = \emptyset \\ -1 & \text{if } X_t \neq \emptyset \text{ and } u(\max X_t) = \beta \\ 1 & \text{if } X_t \neq \emptyset \text{ and } u(\max X_t) = \alpha \end{cases}.$$

This operator is sometimes referred to as an *elementary Preisach hysteron* (we will call it a *hysteron* in this dissertation), since it is a building block for the Preisach operator.

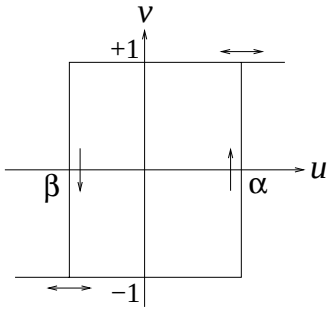

Figure 2.1: The elementary Preisach hysteron.

The Preisach operator is a weighted superposition of all possible hysterons. Define $P_0 \triangleq \{(\beta, \alpha) \in \mathbb{R}^2 : \beta \leq \alpha\}$. P_0 is called the *Preisach plane*, and each $(\beta, \alpha) \in P_0$ is identified with the hysteron $\widehat{\gamma}_{\beta,\alpha}$. For $u \in C([0, T])$ and a Borel measurable initial configuration ζ_0 of all hysterons:

$$\zeta_0 : P_0 \to \{-1, 1\}.$$

the output of the Preisach operator Γ is defined as [86]:

$$y(t) = \Gamma[u, \zeta_0](t) = \int_{P_0} \widehat{\gamma}_{\beta,\alpha}[u, \zeta_0(\beta, \alpha)](t) d\nu(\beta, \alpha), \tag{2.1}$$

where ν is a finite, signed Borel measure on P_0, called the *Preisach measure*. Appendix B provides an introduction to the measure theory.

In this dissertation, we call the Preisach measure ν *nonsingular* if $|\nu|$ is absolutely continuous with respect to the two-dimensional Lebesgue measure, and *singular* otherwise. By the Radon-Nikodym theorem, if ν is nonsingular, there exists a Borel measurable function μ, such that

$$\Gamma[u, \zeta_0](t) = \int\int_{P_0} \mu(\beta, \alpha) \widehat{\gamma}_{\beta,\alpha}[u, \zeta_0(\beta, \alpha)](t) d\beta d\alpha. \tag{2.2}$$

The weighting function μ is often referred to as the *Preisach function* [58] or the *density function* [20].

To simplify the discussion, throughout the dissertation we assume that μ has a compact support, i.e., $\mu(\beta, \alpha) = 0$ if $\beta < \beta_0$ or $\alpha > \alpha_0$ for some β_0, α_0. In this case it suffices to consider the finite triangular area

$$P \triangleq \{(\beta, \alpha) \in \mathbb{R}^2 | \alpha \geq \beta, \beta \geq \beta_0, \alpha \leq \alpha_0\}, \tag{2.3}$$

as shown in Figure 2.2(a). Without loss of generality, we further assume that $\alpha_0 = -\beta_0 =: r_0 > 0$.

The memory effect of the Preisach operator can be captured by curves in P. At each time instant t, define

$$\begin{aligned} P_-(t) &\triangleq \{(\beta,\alpha)\in P| \quad \text{output of } \widehat{\gamma}_{\beta,\alpha} \text{ at } t \text{ is} -1\}, \\ P_+(t) &\triangleq \{(\beta,\alpha)\in P| \quad \text{output of } \widehat{\gamma}_{\beta,\alpha} \text{ at } t \text{ is} +1\}, \end{aligned}$$

so that $P = P_-(t)\cup P_+(t)$, $\forall\, t$. Eq. (2.2) can be rewritten as:

$$y(t) = \int\int_{P_+(t)} \mu(\beta,\alpha)d\beta d\alpha - \int\int_{P_-(t)} \mu(\beta,\alpha)d\beta d\alpha. \tag{2.4}$$

Now assume that at some initial time t_0, the input $u(t_0) = u_0 < \beta_0$. Then the output of every hysteron is -1. Therefore $P_-(t_0) = P$, $P_+(t_0) = \emptyset$ and it corresponds to the "negative saturation" (Figure 2.2(b)). Next we assume that the input is monotonically increased to some maximum value at t_1 with $u(t_1) = u_1$. The output of $\widehat{\gamma}_{\beta,\alpha}$ is switched to $+1$ as the input $u(t)$ increases past α. Thus at time t_1, the boundary between $P_-(t_1)$ and $P_+(t_1)$ is the horizontal line $\alpha = u_1$ (Figure 2.2(c)). Next we assume that the input starts to decrease monotonically until it stops at t_2 with $u(t_2) = u_2$. It's easy to see that the output of $\widehat{\gamma}_{\beta,\alpha}$ becomes -1 as $u(t)$ sweeps past β, and correspondingly, a vertical line segment $\beta = u_2$ is generated as part of the boundary (Figure 2.2(d)). Further input reversals generate additional horizontal or vertical boundary segments.

From the above illustration, we can see that each of P_- and P_+ is a connected set, and the output of the Preisach operator is determined by the boundary between P_- and P_+. The boundary is called the *memory curve*. The memory curve has a staircase structure and its intersection with the line $\alpha = \beta$ gives the current input value. The memory curve ψ_0 at $t = 0$ is called the *initial memory curve* and it represents the initial condition of the Preisach operator.

If the Preisach measure is nonsingular, we can identify a configuration of hys-

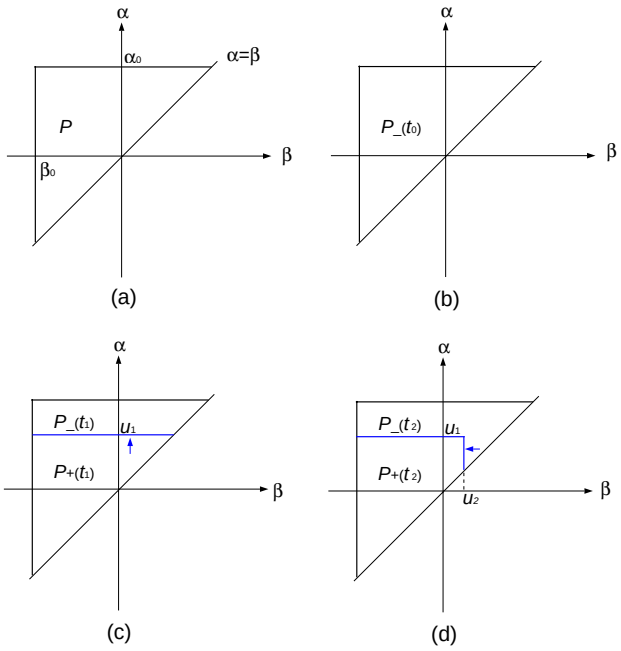

Figure 2.2: Memory curves in the Preisach plane.

terons ζ_ψ with a memory curve ψ in the following way: $\zeta_\psi(\beta, \alpha) = 1\,(-1, \text{resp.})$ if (β, α) is below (above, resp.) the graph of ψ. Note that it does not matter whether ζ_ψ takes 1 or -1 on the graph of ψ.

In the sequel we will put the initial memory curve ψ_0 as the second argument of Γ, where

$$\Gamma[\cdot, \psi_0] \stackrel{\triangle}{=} \Gamma[\cdot, \zeta_{\psi_0}].$$

2.1.2 The Preisach operator in (r, s) coordinates

Sometimes it is more convenient to describe the Preisach operator using the (r, s) coordinates with $r = \frac{\alpha-\beta}{2}$ and $s = \frac{\alpha+\beta}{2}$. If the Preisach measure is nonsingular, the output of the Preisach operator can be expressed in terms of (r, s) as:

$$y(t) = \Gamma[u, \psi_0](t) = \int_0^\infty \int_{-\infty}^\infty \omega(r, s)\widehat{\gamma}_{s-r,s+r}[u, \zeta_{\psi_0}(s - r, s + r)](t)dsdr, \qquad (2.5)$$

where $\omega(\cdot,\cdot)$ is the density function expressed in the (r,s) coordinates. In the new coordinates, a memory curve $\psi[t]$ at time t is the graph of a function of r, and $\psi[t](0)$ gives the current input value $u(t)$ (Figure 2.3). Eq. (2.5) can be rewritten as:

$$y(t) = \Gamma[u,\psi_0](t) = \nu_0 - 2\int_0^\infty \int_{\psi[t](r)}^\infty \omega(r,s)dsdr, \tag{2.6}$$

where ν_0 is the output corresponding to the positive saturation.

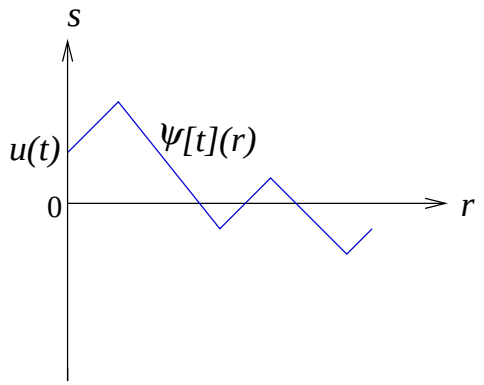

Figure 2.3: The Preisach plane in (r,s) coordinates.

Although practically a memory curve is only composed of segments of slope ± 1 in (r,s) coordinates, we make the following definition:

Definition 2.1.1 *[20, 37] The set of memory curves Ψ is defined to be the set of continuous functions $\psi : [0, r_0] \to \mathbb{R}$ such that*

1. $|\psi(r_1) - \psi(r_2)| \leq |r_1 - r_2|$, $\forall r_1, r_2 \in [0, r_0]$,

2. $\psi(r_0) = 0$,

where r_0 is the constant defined in Subsection 2.1.1.

The graph of any $\psi \in \Psi$ is confined in the triangular region P_r, as shown in Figure 2.4.

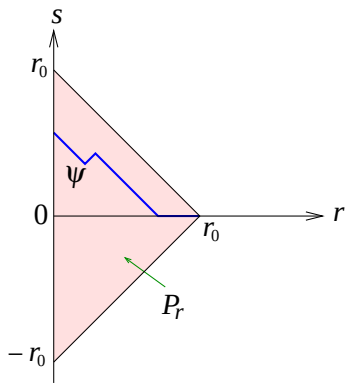

Figure 2.4: The set Ψ of memory curves.

Remark 2.1.2 *Including in Ψ all functions with Lipschitz constant 1 leads to a complete metric space [37], which will facilitate analysis in the sequel. In addition this will allow one to include certain initial hysteron configurations carrying physical interpretations, e.g., $\psi(r) = 0, \forall r \in [0, r_0]$, can represent the demagnetized virgin state in ferromagnetics [58, 86].*

We will switch between the (β, α) coordinates and the (r, s) coordinates in this dissertation.

2.1.3 Properties of the Preisach operator

The Preisach operator has a number of important properties [58, 86, 20]. The following theorems summarize some properties which will be useful for development of results in this dissertation.

Theorem 2.1.3 *[86] Let ν be a Preisach measure. Let $u, u_1, u_2 \in C([0, T])$ and $\psi_0 \in \Psi$. Then the following hold:*

1. **(Rate-independence)** *If $\phi : [0, T] \to [0, T]$ is an increasing continuous*

function satisfying $\phi(0) = 0$ *and* $\phi(T) = T$*, then*

$$\Gamma[u \circ \phi, \psi_0](t) = \Gamma[u, \psi_0](\phi(t)),\ \forall t \in [0, T],$$

where "$\circ$*" denotes composition of functions.*

2. **(Strong continuity)** *If* ν *is nonsingular, then* $\Gamma[\cdot, \psi_0] : C([0,T]) \to C([0,T])$ *is strongly continuous (in the* sup *norm).*

3. **(Piecewise monotonicity)** *Assume* $\nu \geq 0$*. If* u *is either nondecreasing or nonincreasing on some interval in* $[0, T]$*, then so is* $\Gamma[u, \psi_0]$*.*

4. **(Order preservation)** *Assume* $\nu \geq 0$*. If* $u_1 \leq u_2$ *on* $[0, T]$*, then*

$$\Gamma[u_1, \psi_0] \leq \Gamma[u_2, \psi_0]$$

on $[0, T]$*.*

Theorem 2.1.4 (Lipschitz continuity) *[20]* [1] *Assume that the Preisach measure* ν *is nonsingular. Let* ω *be the Preisach density function in* (r, s) *coordinates. Then for any* $\psi_0 \in \Psi$*,* $\Gamma[\cdot, \psi_0]$ *is Lipschitz continuous on* $C([0,T])$ *with Lipschitz constant* $2C_1$ *if*

$$C_1 \stackrel{\triangle}{=} \int_0^\infty \sup_{s \in \mathbb{R}} |\omega(r, s)| dr < \infty. \tag{2.7}$$

2.2 Identification of the Preisach Measure

2.2.1 Review of measure identification methods

For the Preisach operator, the only parameter is the Preisach measure. A classical method for identifying the Preisach density function is using the so called *first*

[1] See also [86] for a slightly different version.

order reversal curves, detailed in Mayergoyz [58]. A first order reversal curve can be generated by first bringing the input to β_0, followed by a monotonic increase to α, then a monotonic decrease to β. The term "first order reversal" comes from that each of these curves is formed after the first reversal of the input. Denote the output value as $f(\beta, \alpha)$ when the input reaches β. Then the density $\mu(\beta, \alpha)$ can be obtained as

$$\mu(\beta, \alpha) = \frac{1}{2} \frac{\partial^2 f(\beta, \alpha)}{\partial \beta \partial \alpha}. \tag{2.8}$$

Since it involves twice differentiation, a smooth approximating surface is fit to the data points in practice [45, 46, 38]. Hughes and Wen [45, 46] approximated the surface by polynomials using a least squares method. Gorbet, Wang and Morris employed functions with specific forms, and the parameters were obtained via a weighted least squares algorithm [38]. A fuzzy approximator was adopted to approximate the surface in [62]. As pointed out in [38], deriving the density by differentiating a fitted surface is inherently imprecise, since different types of approximating functions lead to quite different density distributions.

Hoffmann and Sprekels [53] proposed a scheme to identify the Preisach measure directly. By devising the input sequence carefully, they set up independent blocks of linear equations involving the output measurements and the weighting masses in the discretized Preisach plane, with the number of measurements equal to that of unknowns. Each block of equations can be solved successively to obtain the weighting masses. This scheme is very sensitive to experimental errors as one can easily see. Using the identified weighting masses [53], Hoffman and Meyer [52] approximated the density function in terms of a set of basis functions. A least squares method was applied to compute the coefficients.

Another method for measure identification is driving the system with a "rea-

sonably" rich input signal, measuring the output and then estimating the density by a least squares method. This idea appeared in the work of Banks and his colleagues [7, 8], where they investigated the identification problem of the KP operator. Galinaitis and Rogers [35] used the same idea to identify the weights for a discretized KP operator. We also adopt the least squares method for identification of the Preisach measure [79].

2.2.2 An identification scheme

Smart actuators, due to the capacity of the windings or other practical reasons, have to be operated with their inputs within specific ranges. As a consequence, we will not be able to visit the whole Preisach plane and identify the density function everywhere during the identification process. We assume that the input range is $[u_{min}, u_{max}]$. In Figure 2.5, the bigger triangle represents the set P (recall the definition (2.3)), while the smaller triangle is the region Ω_1 that we can visit. The region outside Ω_1 but inside the set P is denoted by Ω_0. Since the input $u(t)$ never goes beyond the limits, the states of the hysterons in Ω_0 remain unchanged. Thus the bulk contribution to the output from Ω_0 is a constant and we denote it by ν_0.

The input is discretized into $L+1$ levels uniformly (we will call this *discretization of level L*) and we label the cells in the grid as illustrated in Figure 2.5 for $L = 9$. The Preisach measure within each cell is assumed to concentrate as a discrete mass at the cell center. The quantities we want to identify include weighting masses $\nu_{ij}, i = 1, \cdots, L, j = 1, \cdots, i$ and ν_0. To simplify the discussion, with a slight abuse of notation, we write $\{\nu_{ij}\}$ as a column vector $\{\nu_k\}_{k=1}^{K}$, where $K = \frac{L(L+1)}{2}$. We note that discretization of the Preisach plane leads to a discretized Preisach operator, which is a weighted sum of K hysterons (see Figure 2.6).

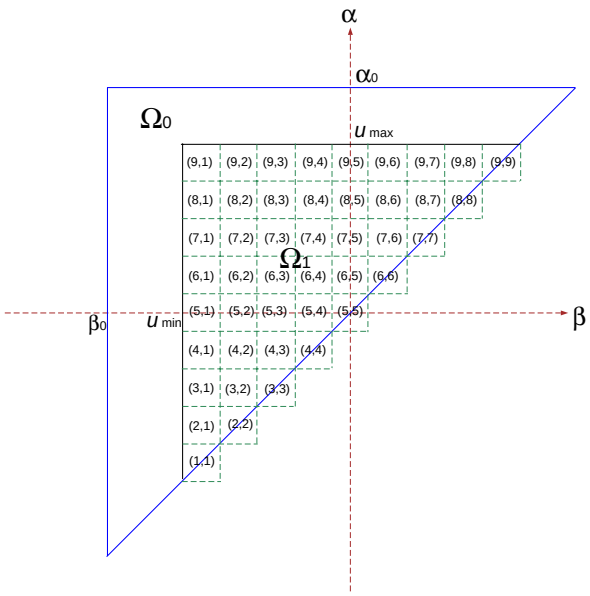

Figure 2.5: Discretization of the Preisach plane ($L = 9$) [79].

To initialize the states of hysterons, we decrease the input to u_{min}. This sets the state of each hysteron in Ω_1 to -1. We then apply some piecewise monotone, continuous input $u(t)$, and measure the output $y(t)$. The input $u(t)$ should be chosen in such a way that the contribution of each weighting mass can be singled out, and one candidate for such $u(t)$ is the concatenation of the first order reversal inputs. Signals $u(t), y(t)$ are then sampled into sequences $\{u[n]\}_{n=1}^{N}$, $\{y[n]\}_{n=1}^{N}$. The input sequence $\{u[n]\}$ (after discretization) is fed into the discretized Preisach operator and the state of each hysteron, $\{\widehat{\gamma}_k[n]\}$, $k = 1, \cdots, K$, is computed. The output of the Preisach model at time instant n can be expressed as:

$$\widetilde{y}[n] = \nu_0 + \sum_{k=1}^{K} \nu_k \widehat{\gamma}_k[n], \tag{2.9}$$

where $\{\nu_k\}_{k=0}^{K}$ is yet to be found.

We use the least squares method to estimate the parameters, i.e., the parame-

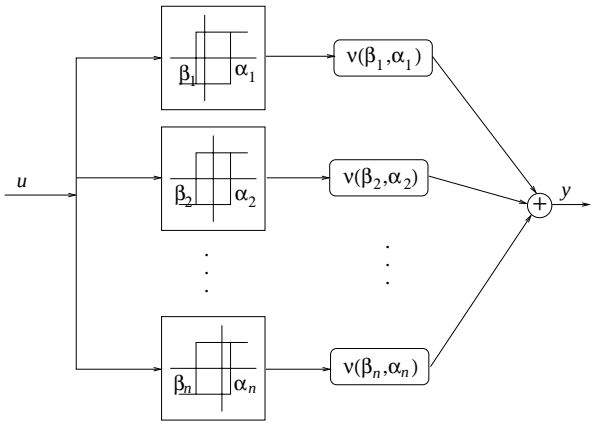

Figure 2.6: The discretized Preisach operator.

ters are determined in such a way that

$$\sum_{n=1}^{N} |y[n] - \widetilde{y}[n]|^2 \tag{2.10}$$

is minimized. Since we require $\nu_k \geq 0, k = 1, \cdots, K$, it is a constrained least squares problem.

Remark 2.2.1 *Theoretically the weighting masses can be computed directly from the first order reversal curves. This works if the signals are noise-free, which is usually not the case. Therefore we use the least squares method.*

2.2.3 Experimental results

In general the magnetostriction depends on both the mechanical pre-stress σ and the magnetic field H [30]. Pre-stress is applied to the magnetostrictive actuator through preloaded springs (see Figure 1.1) and that improves magnetostriction. The pre-stress is not adjustable once the actuator is manufactured, and it does not change much during operation considering the magnitude of magnetostriction (less than 1500 parts per million for Terfenol-D). Therefore we assume that the magnetostriction is only dependent on the magnetic field H.

For the purpose of control, we define the magnetostriction λ to be

$$\lambda = \frac{\Delta l}{l_{rod}}, \tag{2.11}$$

where l_{rod} is the length of the magnetostrictive rod in the demagnetized state, and Δl is the change of the rod length from l_{rod}. The saturation magnetostriction λ_s is defined in an obvious way. Note our definition of λ_s is slightly different from that in [23].

When the input frequency is low, the magnetostrictive hysteresis is rate independent: roughly speaking, the shape of the hysteresis loop does not depend on the input frequency. In this case, we can relate λ to the bulk magnetization M along the rod direction by a square law [82]

$$\lambda = a_1 M^2, \tag{2.12}$$

and relate the input current I to the magnetic field H (assumed uniform) along the rod direction by

$$H = c_0 I + H_{bias}, \tag{2.13}$$

where c_0 is the so called *coil factor*, and H_{bias} is the bias field produced by permanent magnets or a dc current. H_{bias} is necessary for generating bidirectional strains. Hence we can capture the hysteretic relationship between λ and I by the ferromagnetic $M - H$ hysteresis. Venkataraman employed a low dimensional ferromagnetic hysteresis model in [82]. We will use a Preisach operator to model $M - H$ hysteresis.

Remark 2.2.2 *Due to the thin rod geometry, we approximate the continuum magnetization in the magnetostrictive rod by the bulk magnetization. The square law*

(2.12) follows from the continuum theory of micromagnetics, where the magnetoelastic energy is of the form linear in the strain and quadratic in the direction cosines of the magnetization vector [22].

Remark 2.2.3 *Mayergoyz has shown that, the necessary and sufficient conditions for a hysteretic nonlinearity to be represented by the Preisach model are the wiping-out property and the congruency property [58]. While the wiping-out property for the ferromagnetic hysteresis can be directly verified, we will indirectly verify the congruency property by a trajectory tracking experiment based on inversion of the Preisach operator.*

The following parameters are available from the manufacturer: the saturation magnetization $M_s = 7.87 \times 10^5$A/m, $l_{rod} = 5.13 \times 10^{-2}$m, $c_0 = 1.54 \times 10^4$/m. We can easily identify $\lambda_s = 1.313 \times 10^{-3}$ by applying an input of relatively large magnitude, and then get the coefficient $a_1 = \frac{\lambda_s}{M_s^2}$. The bias field H_{bias} is identified to be 1.23×10^4A/m.

Given a measurement of λ, we compute $M = \pm\sqrt{\frac{\lambda}{a_1}}$ and the sign of M is determined with further information on the input. The Preisach weighting masses can be identified with the constrained least squares algorithm as described in the previous subsection.

Our experimental setup is as shown in Figure 2.7 . DSpace ControlDesk is a tool for real-time simulation and control. The displacement of the actuator is measured with a LVDT sensor, which has a precision of about 1 μm.

The magnetic field input H is limited to $[1.57\times10^3\text{A/m}, 3.25\times10^4\text{A/m}]$ and we discretize the Preisach plane into 25 levels. Figure 2.8 shows the distribution of the identified weighting masses. The constant contribution ν_0 from Ω_0 (see Figure 2.5) is estimated to be 4.99×10^5A/m.

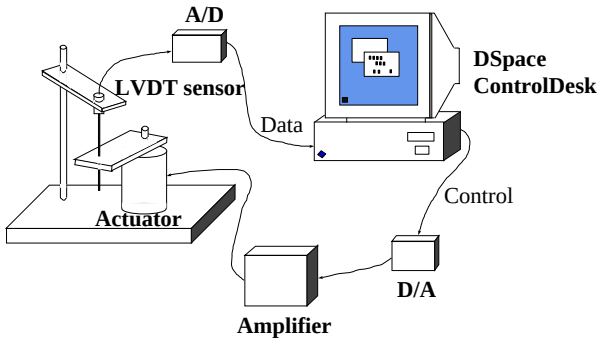

Figure 2.7: Experimental setup.

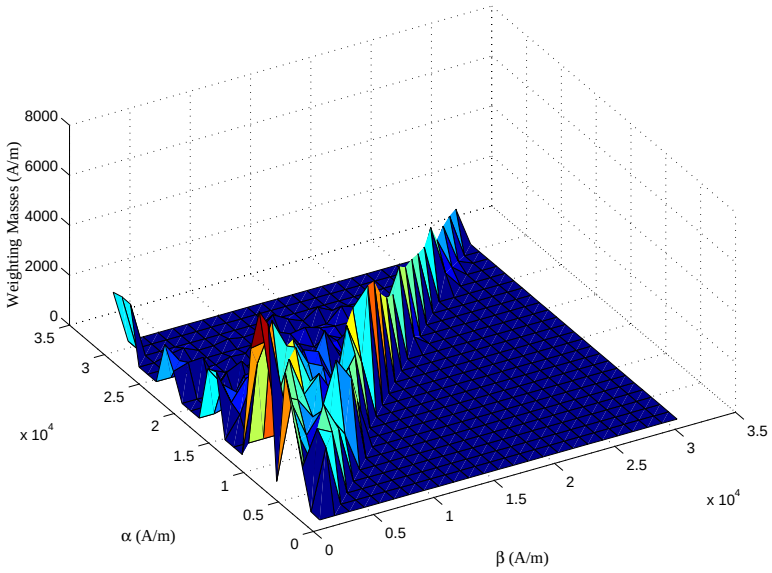

Figure 2.8: Distribution of the Preisach weighting masses.

Remark 2.2.4 *Due to the bias field H_{bias} and the constraint on the input current, we can not trace the major loop of the M - H hysteresis; instead we can only visit a certain region inside the major loop. As a result, the magnetostrictive hysteresis loop (the butterfly curve) is asymmetric (Figure 1.2).*

2.3 Inversion of the Preisach Operator

The general structure of models for smart actuators that capture both hysteresis and dynamic behaviour is shown in Figure 2.9 [85] . In the figure, $G(s)$ represents the transfer function of the linear part in the actuator, while W denotes a rate-independent hysteretic nonlinearity. Venkataraman [82] has shown that a key component of a low dimensional model for magnetostriction in Terfenol-D has a structure resembling Figure 2.9 .

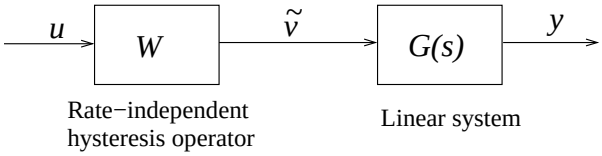

Figure 2.9: Structure of models for smart actuators [85].

A basic idea for controller synthesis for such systems is to design a right inverse operator W^{-1} for W as shown in Figure 2.10. Then $\widetilde{v}(\cdot) = v(\cdot)$ and the controller design problem is reduced to designing a linear controller $K(s)$ for the linear system $G(s)$.

In the context of this dissertation, we consider W to be a Preisach operator. The Preisach operator is highly nonlinear, and in general, we cannot find a closed-form formula for the inverse operator, unless the density function is of some special form, as in the work of Galinaitis and Rogers [34]. Hughes and Wen

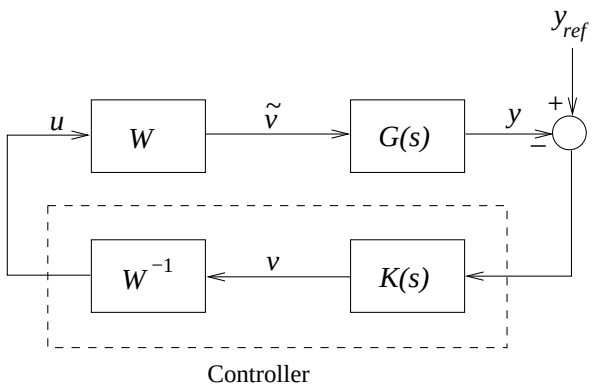

Figure 2.10: Controller design schematic [85].

[45, 46] utilized the first order reversal curves in computing the numerical inverse of the Preisach operator. This method relies on measurement of all first order reversal curves and involves solving nonlinear equations. Natale and his colleagues proposed using another Preisach operator as a "pseudo-compensator" to approximate the inverse of a Preisach operator [62], where the Preisach density of the compensator is identified with the same set of experimental data used in identification of the original Preisach operator, but with the roles of input and output swapped. The compensator is "pseudo" because it is well known that in general, the inverse of a Preisach operator is not a Preisach operator. Venkataraman and Krishnaprasad [85] utilized piecewise monotonicity and Lipschitz continuity of the Preisach operator, and proposed an inversion algorithm based on the contraction mapping principle.

The Preisach operator is rate-independent, and at any time t, the memory curve (and thus the output) depends only on the dominant maximum and minimum values in the past input. Therefore we are mainly interested in the inversion problem in the discrete-time setting.

2.3.1 Inversion of the discretized Preisach operator

First we study inversion of a discretized Preisach operator obtained as a result of input discretization.

Let U be the discrete control set, i.e., $U \stackrel{\triangle}{=} \{u_l, 1 \leq l \leq L+1\}$ with

$$u_l = u_{min} + (l-1)\delta_u, \text{ where } \delta_u = \frac{u_{max} - u_{min}}{L}.$$

Let S^n be the set of input strings of length n taking values in U, i.e., if $s \in S^n$, then $s[i] \in U$, $1 \leq i \leq n$. Let Ψ_d be the set of memory curves for the discretized Preisach operator.

Trajectory Inversion Problem of Length N: *Given an initial memory curve $\psi_0 \in \Psi_d$ and a desired output sequence $\bar{y}$ of length N, find $s^* \in S^N$, such that*

$$\max_{1 \leq i \leq N} |\Gamma[s^*, \psi_0][i] - \bar{y}[i]| = \min_{s \in S^N} \max_{1 \leq i \leq N} |\Gamma[s, \psi_0][i] - \bar{y}[i]|. \tag{2.14}$$

We call this the *trajectory inversion* problem, to distinguish it from the *value inversion* problem we will discuss in the next section.

Remark 2.3.1 *We put a sequence instead of a continuous time function as the first argument of Γ in (2.14). To avoid ambiguity, it is tacitly understood that the input is changed monotonically from $s[i]$ to $s[i+1]$. Throughout the dissertation we may use a sequence or a continuous time function as the first argument of Γ depending on the context.*

Remark 2.3.2 *A discretized Preisach operator is not "onto" since its output takes values in a finite set. Therefore we don't seek an exact inverse in the problem formulation.*

Before we present the solution to the problem above, we first look at the case when $N = 1$:

Trajectory Inversion Problem of Length 1: *Given an initial memory curve $\psi_0 \in \Psi_d$ and a desired output $\bar{y}_0$, find $u^* \in U$, such that*

$$|\Gamma[u^*, \psi_0] - \bar{y}_0| = \min_{u \in U} |\Gamma[u, \psi_0] - \bar{y}_0|. \tag{2.15}$$

There is a simple algorithm for solving the problem of length 1, which is based on the piecewise monotonicity of the Preisach operator [79]. We name it the *closest match algorithm* because it always generates an input whose output matches the desired output most closely among all possible inputs.

The idea of the closest match algorithm is as follows. One can obtain the initial input $u^{(0)}$ and output $y^{(0)}$ from the initial memory curve ψ_0. Consider the case $y^{(0)} < \bar{y}_0$ (the case $y^{(0)} > \bar{y}_0$ is treated in exactly the same way with some obvious modification). We keep increasing the input by one level in each iteration until, say at iteration n, the input $u^{(n)}$ reaches u_{max}, or the output $y^{(n)}$ corresponding to $u^{(n)}$ exceeds $\bar{y}_0$. For the first case, the optimal input is clearly u_{max}; for the second case, two candidates for the optimal input u^* are $u^{(n-1)}$ and $u^{(n)}$. We then take u^* to be the one with the smaller output error. Note that we need back up the memory curve whenever we increase the input, so that we can always retrieve the consistent memory curve with u^*.

The above algorithm yields the optimal input u^* in at most L iterations. And in each iteration, the evaluation of $y^{(n)}$ is very fast since the input has changed by one level and thus we need only update states of hysterons corresponding to that level. These factors combine to make this algorithm simple and efficient.

The trajectory inversion problem of length N is solved by combining the closest match algorithm and the dynamic programming principle [13].

Let $\Xi_d : \Psi_d \times U \to \Psi_d$ be the evolution map for the memory curve, i.e., if $\psi \in \Psi_d$ is the initial memory curve, then $\Xi_d(u, \psi)$ is the new memory curve when the input $u \in U$ is applied.

Given N and the sequence $\bar{y}$, for $1 \leq k \leq N$, we define

$$J_k(\psi, s) = \max_{k \leq i \leq N} |\Gamma[s, \psi][i] - \bar{y}[i]|, \; s \in S^{N-k+1}, \tag{2.16}$$

$$V_k(\psi) = \min_{s \in S^{N-k+1}} J_k(\psi, s), \tag{2.17}$$

where we call J_k the cost function and V_k the value function.

Proposition 2.3.3 *The value functions V_k, $1 \leq k \leq N$, can be solved successively via:*

$$V_N(\psi) = \min_{u \in U} |\Gamma[u, \psi] - \bar{y}[N]|, \tag{2.18}$$

$$V_k(\psi) = \min_{u \in U} \max\{|\Gamma[u, \psi] - \bar{y}[k]|, V_{k+1}(\Xi_d(u, \psi))\}. \tag{2.19}$$

Define maps $\pi_k^* : \Psi_d \to U$, $1 \leq k \leq N$, so that $\pi_k^*(\psi)$ is the $\arg\min$ *in (2.18) and (2.19). Then for the trajectory inversion problem of length N, π_k^*, $1 \leq k \leq N$, gives the optimal control policy at time k.*

Proof Straightforward from Bellman's optimality principle. ∎

The closest match algorithm can be used in solving (2.18) and (2.19). Proposition 2.3.3 entails pre-computing and storage of the optimal maps, which is undesirable when N or the cardinality of Ψ_d is large. A sub-optimal approach is to decompose the inversion problem of length N into N successive inversion problems of length 1 and solve them using the closest match algorithm. The experimental result of trajectory tracking based on this approach can be found in [79].

2.3.2 Inversion of the Preisach operator with nonsingular measure

We now discuss the inversion problem for a Preisach operator with nonsingular Preisach measure. In this case, the Preisach operator can be inverted with arbitrary accuracy, and it suffices to study an inversion problem of length 1: given $\psi_0 \in \Psi$ and $\bar{M} \in [M_{min}, M_{max}]$, find $\bar{H} \in [H_{min}, H_{max}]$, such that

$$\bar{M} = \Gamma[\bar{H}, \psi_0],$$

where $[H_{min}, H_{max}]$ and $[M_{min}, M_{max}]$ are the ranges of the input and the output of the Preisach operator, respectively. The notation used in this subsection is slightly different from that in Subsection 2.3.1, but it will be consistent with the notation in Chapter 3.

Proposition 2.3.4 *Let the Preisach measure be nonnegative and nonsingular with a density function μ. Let*

$$\bar{\nu} \stackrel{\triangle}{=} \max\{\sup_{\alpha} \int_{\beta_0}^{\alpha} \mu(\beta, \alpha) d\beta, \sup_{\beta} \int_{\beta}^{\alpha_0} \mu(\beta, \alpha) d\alpha\} < \infty. \tag{2.20}$$

Let the current memory curve be ψ_0, and let the input and the output of the Preisach operator corresponding to ψ_0 be H_0 and M_0, respectively. Given $\bar{M} \in [M_{min}, M_{max}]$, consider the following algorithm:

$$\begin{cases} H^{(n+1)} = H^{(n)} + \frac{\bar{M} - M^{(n)}}{\bar{\nu}} \\ M^{(n+1)} = \Gamma[H^{(n+1)}, \psi^{(n)}] \end{cases}, \tag{2.21}$$

where $\psi^{(0)} = \psi_0$, $H^{(0)} = H_0$, $M^{(0)} = M_0$, and $\psi^{(n)}$ is the memory curve after $\{H^{(k)}\}_{k=1}^{n}$ is applied. Then $M^{(n)} \to \bar{M}$ as $n \to \infty$.

Proof The proposition follows directly from the piecewise monotonicity property and the continuity property of the Preisach operator. ■

Remark 2.3.5 *The algorithm (2.21) also appeared in [85], where approximate inversion of the Preisach operator was studied for the class of continuous, piecewise monotone functions.*

What we have identified in Subsection 2.2.2 is a set of Preisach weighting masses, which forms a singular Preisach measure. We can obtain a nonsingular Preisach measure ν_p by assuming that each identified mass is distributed uniformly over the corresponding cell in the discretization grid. Note that the diagonal cells are triangular, while other cells are square (refer to Figure 2.13(a)). The density function μ_p corresponding to ν_p is piecewise uniform, which enables us to solve the inversion problem exactly, as described next.

We consider the case $\bar{M} > M_0$ and the other case can be treated analogously. It's obvious that $\bar{H} > H_0$ and we will increase the input in every iteration. At iteration n, let $d_1^{(n)} > 0$ be such that $H^{(n)} + d_1^{(n)}$ equals the next input level, and let $d_2^{(n)} > 0$ be the minimum amount such that applying $H^{(n)} + d_2^{(n)}$ will eliminate the next corner of the memory curve (see Figure 2.11 for illustration). Since μ_p is piecewise constant, for $d < \min\{d_1^{(n)}, d_2^{(n)}\}$, we have

$$\Gamma[H^{(n)} + d, \psi^{(n)}] - \Gamma[H^{(n)}, \psi^{(n)}] = a_2^{(n)} d^2 + a_1^{(n)} d,$$

where $a_1^{(n)}, a_2^{(n)} > 0$ can be computed from μ_p, and the square term is due to the contribution from the triangular region inside the diagonal cell. Let $d_0^{(n)}$ be such that

$$\bar{M} - \Gamma[H^{(n)}, \psi^{(n)}] = a_2^{(n)} (d_0^{(n)})^2 + a_1^{(n)} d_0^{(n)}.$$

The inversion algorithm now works as follows:

$$\begin{cases} d^{(n)} = \min\{d_0^{(n)},\, d_1^{(n)},\, d_2^{(n)}\} \\ H^{(n+1)} = H^{(n)} + d^{(n)} \\ M^{(n+1)} = \Gamma[H^{(n+1)}, \psi^{(n)}] \end{cases} . \tag{2.22}$$

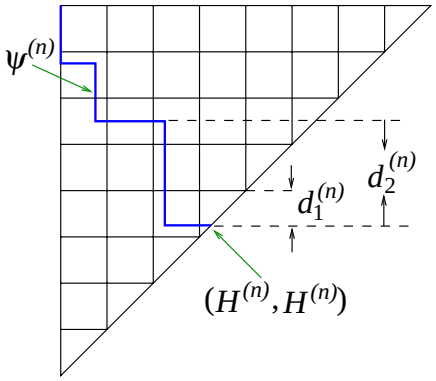

Figure 2.11: Illustration of $d_1^{(n)}$ and $d_2^{(n)}$.

If at iteration n^*, $d^{(n^*)} = d_0^{(n^*)}$, then the iteration stops and $\bar{H} = H^{(n^*+1)}$. Let $n_c(\psi_0)$ be the number of corners of ψ_0, and L the discretization level of the Preisach plane. It's easy to see the algorithm (2.22) yields the (exact) solution in no more than $\bar{n} = n_c(\psi_0) + L$ iterations.

Figure 2.12 shows the result of an open-loop tracking experiment using the algorithm (2.22). The desired trajectory was obtained from the output of a Van der Pol oscillator to make the tracking task more challenging. In Figure 2.12, the displacement trajectories (both the desired and the measured), the tracking error and the input current are displayed. The overall performance is satisfactory since the error magnitude is less than 4 μm most of the time with a tracking range of 60 μm. We can see that the tracking error slightly exceeds 4 μm when the desired output (and thus the input) undergoes abrupt changes, in which case the rate-independence assumption no longer holds.

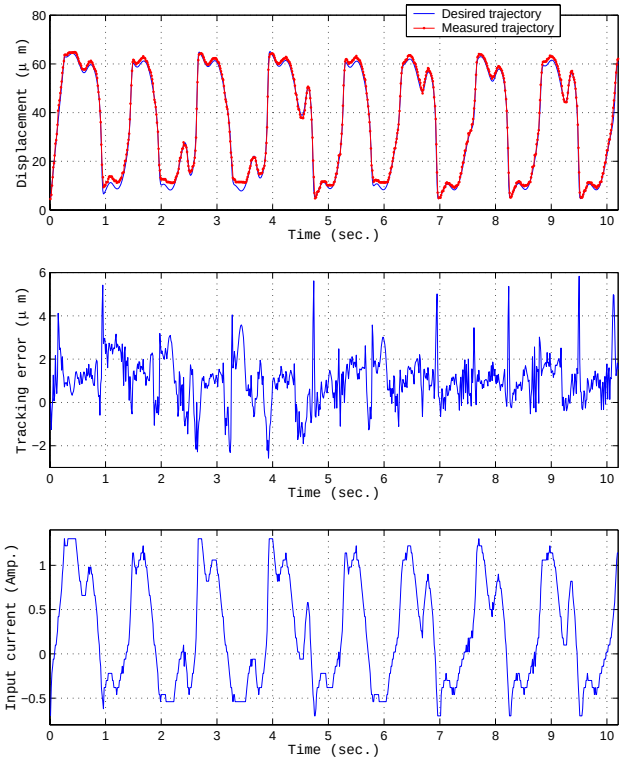

Figure 2.12: Trajectory tracking based on inversion of the Preisach operator.

2.4 The Value Inversion Problem and Its Application to Micro-Positioning Control

By inverse compensation, one usually refers to the trajectory inversion problem: given a desired output trajectory, compute an input trajectory whose corresponding output trajectory matches the desired one. In many applications, such as micro-positioning, we are more interested in the following problem: given a desired output *value*, find an input trajectory such that the final value of the output matches the desired value. To distinguish this problem from the trajectory inversion problem, we call it the *value inversion* problem. This problem has been well studied for linear systems, but to our best knowledge, very little has been done in the context of hysteretic systems.

The Preisach operator becomes a finite state machine (FSM) after discretization, and the value inversion problem can be transformed into a state reachability problem for the FSM. We show that the FSM is reachable and indicate how to construct the input sequence for the state transition. After observing that, for practical reasons, there may exist a large number of equivalent states in the FSM, we propose a state space reduction scheme, which can significantly save storage space and computation time. An algorithm for generating the optimal (the sense of "optimality" will be clear) representative state in each equivalent class is presented.

2.4.1 The value inversion problem

In any practical identification scheme for the Preisach measure, a discretization step is involved in one form or another. Figure 2.13(a) shows our discretization scheme used earlier in measure identification, where the Preisach measure inside

each cell is assumed to concentrate at the cell center (represented by dark dots in Figure 2.13(a)). As noted in Subsection 2.2.2, this results in a discretized Preisach operator. We note that although uniform discretization is considered here, the results of this section apply directly to the case of non-uniform discretization.

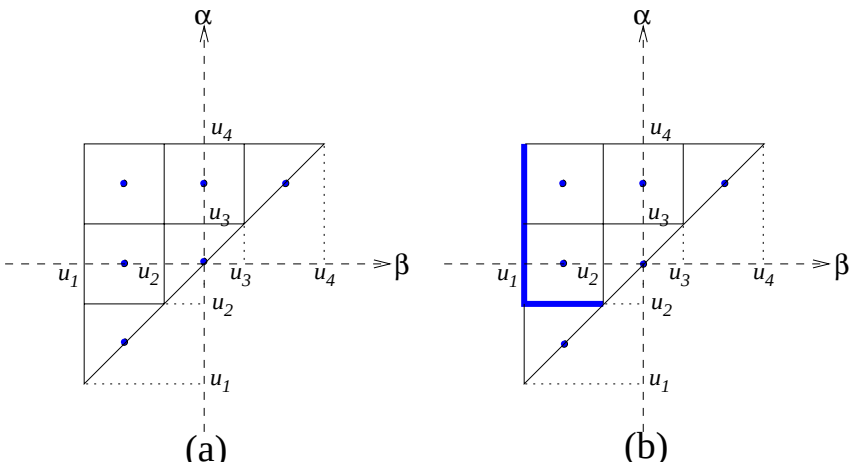

Figure 2.13: (a) Discretization of the Preisach plane ($L = 3$); (b) Memory cuve "001" (bolded lines).

Let S be the set of input strings taking values in U, where U is as defined in Subsection 2.3.1. Let S_A be the set of alternating input strings [20] in U, in the sense that, if $s_a \in S_A$, then $(s_a[i+2] - s_a[i+1])(s_a[i+1] - s_a[i]) < 0,\ \forall i > 0$. The value inversion problem is formulated as:

Value Inversion Problem: *Given a desired output value $\bar{y}_0$ and an initial memory curve $\psi_0 \in \Psi_d$, find $s_a^* \in S_A$, such that*

$$|\Gamma_f[s_a^*, \psi_0] - \bar{y}_0| = \min_{s_a \in S_A} |\Gamma_f[s_a, \psi_0] - \bar{y}_0|, \tag{2.23}$$

where $\Gamma_f[s, \psi_0]$ denotes the final value of the output of the Preisach operator under input sequence s. If there is more than one such string achieving (2.23), find the one with the minimum length.

Remark 2.4.1 *Any $s \in S$ can be reduced to some $s_a \in S_A$ using the following rules, starting from $i = 1$: if $(s[i+1] - s[i])(s[i+2] - s[i+1]) \geq 0$, delete $s[i+1]$ and re-index. For example, $s = (u_1, u_3, u_3, u_5, u_4, u_2) \in S$ can be reduced to $s_a = (u_1, u_5, u_2) \in S_A$. The final values of the output under s and s_a are identical (easy to verify), hence we only need search the optimal input sequence in S_A.*

Remark 2.4.2 *The length of an alternating input string is directly linked to the number of input reversals and thus the complexity of implementing that input. Therefore we seek s_a^* with the minimum length.*

The discretized Preisach operator can be treated as a finite state machine (FSM). Since there are $\frac{L(L+1)}{2}$ hysterons for a discretized Preisach model with discretization level L and the output of each hysteron takes values in $\{-1, 1\}$, the number of states appears to be $2^{L(L+1)/2}$. This is not the case in general, recalling that the true state is the memory curve.

Proposition 2.4.3 *For a discretized Preisach operator with discretization level L, the number of states is 2^L.*

Proof In the (β, α) coordinates, each memory curve consists of L horizontal or vertical segments of length δ_u, so the total number of memory curves is 2^L. ■

The proof motivates an indexing scheme for the memory curve. Starting from the upper left corner, we number each memory curve with L bits corresponding to the L segments: 0 represents vertical, and 1 represents horizontal. For instance, the memory curve represented by the bolded lines in Figure 2.13(b) reads "001".

We can now give a complete description for the FSM. It has state space

$$\Psi_d = \{\psi : \psi = (\alpha^L, \alpha^{L-1}, \cdots, \alpha^1),\ \alpha^j \in \{0, 1\},\ j = 1, \cdots, L\}$$

and input space U. It is a *state output* automaton [15] since the output y of the Preisach operator depends only on the memory curve ψ. Therefore *the value inversion problem is solved if any state of the FSM is reachable*, because then all we have to do is to find the state whose corresponding output is closest to the desired $\bar{y}_0$.

The state transition function $\Xi_d : \Psi_d \times U \to \Psi_d$ can be best described in terms of two state operations, INC: $\Psi_d \to \Psi_d$ and DEC: $\Psi_d \to \Psi_d$. For any state $\psi \in \Psi_d$, we can immediately determine the current input $\widetilde{u}(\psi)$: $\widetilde{u}(\psi) = u_{n+1}$ if ψ contains n "1"s. For $\psi \in \Psi_d$, we define

$$INC(\psi) \triangleq \begin{cases} \psi \text{ if } \widetilde{u}(\psi) = u_{L+1} \\ \text{the state after the input is increased by one level if } \widetilde{u}(\psi) \neq u_{L+1} \end{cases},$$

and

$$DEC(\psi) \triangleq \begin{cases} \psi \text{ if } \widetilde{u}(\psi) = u_1 \\ \text{the state after the input is decreased by one level if } \widetilde{u}(\psi) \neq u_1 \end{cases}.$$

As one can easily verify, INC changes the first "0" bit counting from the right to "1" and leave other bits untouched. A symmetric remark applies to the operation DEC. Therefore bit L (bit 1, resp.) is the most (least, resp.) important bit, in the sense that, if you want to switch bit j from 0 (1, resp.) to 1 (0, resp.), you must first switch all the lower bits to 1 (0, resp.). Figure 2.14 illustrates the INC and DEC operations for the case of $L = 3$.

Now given $u \in U$, the state transition function is expressed as:

$$\Xi_d(\psi, u) = \begin{cases} \psi, \text{ if } u - \widetilde{u}(\psi) = 0 \\ \underbrace{INC \circ \cdots INC}_{n \; INCs}(\psi), \text{ if } u - \widetilde{u}(\psi) = n\delta_u \\ \underbrace{DEC \circ \cdots DEC}_{n \; DECs}(\psi), \text{ if } u - \widetilde{u}(\psi) = -n\delta_u \end{cases},$$

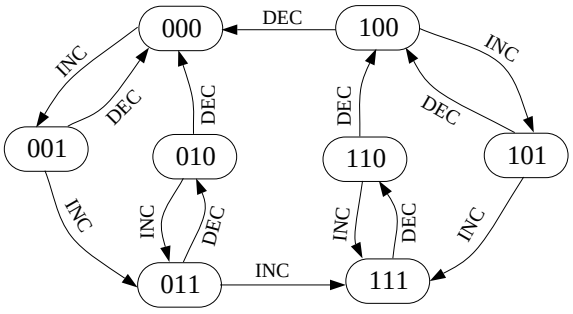

Figure 2.14: Operations INC and DEC for $L = 3$.

where "$\circ$" denotes composition of functions.

Proposition 2.4.4 *Any state is reachable. Let ψ_i, $i = 1, 2$, be two states. Let bit n_0 be the leftmost bit at which ψ_1 and ψ_2 differ, and let n_a be the number of alternating bit pairs in ψ_2 from bit n_0 through bit 1. Then ψ_2 is reachable from ψ_1 by applying an input string $s_a^* \in S_A$ of length $n_a + 1$, and the length of any other $s_a \in S_A$ achieving the state transition from ψ_1 to ψ_2 is no less than $n_a + 1$.*

The proposition is a straightforward consequence of the state transition map Ξ_d. The following example illustrates the proposition as well as how to actually construct the input string.

Example 2.4.5 Assume $L = 5$, $\psi_1 = 00100$, $\psi_2 = 01011$. Then $n_0 = 4$, $n_a = 2$, and the alternating input string s_a^* for achieving the state transition has length 3. Now let's detail the procedure of state transition:

- **Step 0.** ψ_1 contains one "1", so the current input value is u_2;
- **Step 1.** Apply u_5 (3 consecutive INCs) to make bit 4 "1" and the state becomes 01111;
- **Step 2.** Apply u_2 (3 consecutive DECs) to make bit 3 "0" and the state becomes 01000;

- **Step 3.** Apply u_4 (2 consecutive INCs) to get ψ_2.

Remark 2.4.6 *A state-space representation of a general Preisach operator can be found in [37] and it is shown there that the state space is approximately reachable*, see Proposition 3.4.10. This "approximate reachability" result was also stated in [58, 86] (in a more casual way).

Corollary 2.4.7 *Any state is reachable from any other state with some $s_a^* \in S_A$ of length no more than L.*

2.4.2 A state space reduction scheme

Reduction of the state space

In general we need store output values of 2^L states for the value inversion problem. For a reasonable discretization level L, this may take lots of memory. In addition, computation cost for sorting and searching these states will be very high. Therefore reducing the number of states without compromising control accuracy is of practical interest.

Two states $\psi_1, \psi_2 \in \Psi_d$ are *equivalent*, denoted as $\psi_1 \equiv \psi_2$, if

$$\Gamma[s, \psi_1] = \Gamma[s, \psi_2], \ \forall s \in S.$$

We say a hysteron in the discretized Preisach operator is *non-trivial* if its associated weight is not zero, and is *trivial* otherwise. Existence of trivial hysterons leads to equivalent states. Let's look at an example. In Figure 2.15(a), the hysterons marked with "•"(and labeled by $\gamma_1, \cdots, \gamma_5$) are assumed to be non-trivial and those marked with "○" are assumed to be trivial. It's easy to verify that the following states in Figure 2.15(a) are equivalent: 0101, 0110, 1001 and 1010.

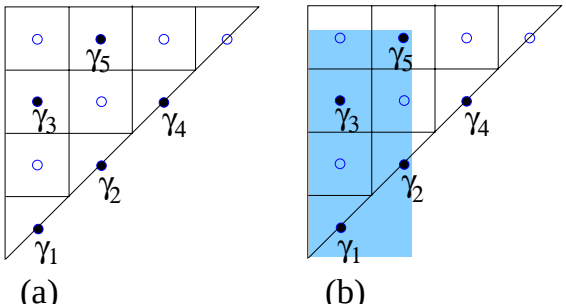

Figure 2.15: (a) Existence of equivalent states ($L = 4$); (b) Illustration of the shaded set.

For $\psi \in \Psi_d$, define $\mathcal{S}(\psi)$ to be the set of non-trivial hysterons underneath the memory curve corresponding to ψ. From the example above, we can see that $\psi_1 \equiv \psi_2$ if and only if $\mathcal{S}(\psi_1) = \mathcal{S}(\psi_2)$. From the experimental result of measure identification (see Figure 2.8), we see that indeed many hysterons carry weights of zero or close to zero, and this provides room for the state space reduction.

The original state space Ψ_d is thus a disjoint union of equivalent classes of states. A reduced state space $\widetilde{\Psi}$ is obtained such that each element in $\widetilde{\Psi}$ is an equivalent class in Ψ_d, i.e., $\widetilde{\Psi} = \Psi_d/\equiv$. Denote the set of non-trivial hysterons as $\mathcal{N}$, i.e., $\mathcal{N} \stackrel{\triangle}{=} \{\widehat{\gamma}_{\beta,\alpha} : \nu_{\beta,\alpha} > 0\}$, where $\nu_{\beta,\alpha}$ is the weight of $\widehat{\gamma}_{\beta,\alpha}$. Then a subset $\widetilde{\psi}$ of $\mathcal{N}$ can be identified with a member of $\widetilde{\Psi}$ if and only if $\exists\, \psi \in \Psi_d$, such that $\widetilde{\psi} = \mathcal{S}(\psi)$. To better capture the latter property, we introduce the notion of a *Lower-Left-Shaded Set* . The Lower-Left-Shaded Set (abbreviated as the shaded set hereafter) $\mathcal{A}(\widehat{\gamma}_{\beta,\alpha})$ of a hysteron $\widehat{\gamma}_{\beta,\alpha} \in \mathcal{N}$ is defined to be

$$\mathcal{A}(\widehat{\gamma}_{\beta,\alpha}) = \{\widehat{\gamma}_{\beta',\alpha'} \in \mathcal{N} :\ \widehat{\gamma}_{\beta',\alpha'} \neq \widehat{\gamma}_{\beta,\alpha}, \beta' \leq \beta, \alpha' \leq \alpha\}.$$

The geometric interpretation of the shaded set of $\widehat{\gamma}_{\beta,\alpha}$ is clear: imagining two rays from $\widehat{\gamma}_{\beta,\alpha}$ in the Preisach plane, one pointing downwards and the other to the left, the shaded set consists of non-trivial hysterons lying between the two rays.

For example, in Figure 2.15(b), $\mathcal{A}(\gamma_5) = \{\gamma_1, \gamma_2, \gamma_3\}$. If $\widehat{\gamma}_{\beta,\alpha}$ lies underneath some memory curve ψ', all elements of $\mathcal{A}(\widehat{\gamma}_{\beta,\alpha})$ must do so too. Therefore we conclude that $\widetilde{\psi} \subset \mathcal{N}$ is identified with a member of $\widetilde{\Psi}$ if and only if the following holds:

$$\mathcal{A}(\widehat{\gamma}_{\beta,\alpha}) \subset \widetilde{\psi}\ , \forall\, \widehat{\gamma}_{\beta,\alpha} \in\ \widetilde{\psi}. \tag{2.24}$$

To ease presentation, from now on we will simply write $\widetilde{\psi} \in \widetilde{\Psi}$ if (2.24) is satisfied. Now we can list all members in $\widetilde{\Psi}$ using a tree-structured algorithm:

- **Step 1.** List the equivalent class having no non-trivial hysterons (negative saturation);
- **Step 2.** List equivalent classes with one constituent non-trivial hysteron, i.e., the shaded set of every such hysteron is empty;
- **Step 3.** Starting from each equivalent class (*parent class*) $\widetilde{\psi}$ with n non-trivial hysterons, we list equivalent classes (*children classes*) with $n+1$ non-trivial hysterons by finding another hysteron $\widehat{\gamma} \in \mathcal{N}$ such that:
  - $\widehat{\gamma}$ is not included in $\widetilde{\psi}$,
  - $\mathcal{A}(\widehat{\gamma}) \subset \widetilde{\psi}$, i.e., $\widetilde{\psi} \cup \widehat{\gamma}$ is an eligible member of $\widetilde{\Psi}$, and
  - $\widetilde{\psi} \cup \widehat{\gamma}$ does not coincide with any other equivalent class $\widetilde{\psi}'$ with $n+1$ constituent hysterons that has been listed so far;
- **Step 4.** Continue Step 3 until $\widetilde{\psi} = \mathcal{N}$ (positive saturation) is listed.

The equivalent classes are sorted according to their output values during the above enumeration process, and we save computation time by using the fact that the output of a child class is always greater than that of its parent.

Generating best representative states

For the purpose of realizing state transition, we need find a representative state $\psi \in \Psi_d$ for every $\widetilde{\psi} \in \widetilde{\Psi}$. From Proposition 2.4.4, the number of alternating bit pairs of a state ψ is closely related to the number of input reversals required for the state transition. Therefore the best representative state $\psi^* \in \Psi_d$ for $\widetilde{\psi} \in \widetilde{\Psi}$ should have the least number of alternating bit pairs among all states in the equivalent class $\widetilde{\psi}$.

We generate a representative ψ^* for $\widetilde{\psi} \in \widetilde{\Psi}$ by first drawing two memory curves $\psi^*_{\downarrow}$ and $\psi^*_{\rightarrow}$ and then picking ψ^* to be the one whose number of alternating bit pairs is less. When we draw a memory curve, at most two directions are possible for each segment: going downwards (denoted by "$\downarrow$") or going to the right (denoted by "$\rightarrow$"). $\psi^*_{\downarrow}$ is obtained as follows: start from the left upper corner with "$\downarrow$" and continue that direction as long as it is feasible to do so (i.e., no constituent hysteron of $\widetilde{\psi}$ is left out); when it is infeasible to continue "$\downarrow$", we switch to "$\rightarrow$" and keep going with that direction until it is infeasible for $\widetilde{\psi}$ (i.e., non-constituent hysterons will be included). We continue until all L segments are drawn. Similarly we obtain $\psi^*_{\rightarrow}$ by starting with "$\rightarrow$". Note it's easy to see that "$\rightarrow$" is feasible whenever "$\downarrow$" is not, and vice versa.

Proposition 2.4.8 *The representative ψ^* obtained in the above scheme has the least number of alternating bit pairs among all states in the equivalent class $\widetilde{\psi}$.*

Proof For any state ψ starting with "$\downarrow$", we can show its number of alternating bit pairs is no less than that of $\psi^*_{\downarrow}$ by exploiting the strategy in generating $\psi^*_{\downarrow}$.

Instead of giving a general proof, we will illustrate the essential idea by looking at a concrete example with discretization level $L = 8$ (Figure 2.16). In the figure,

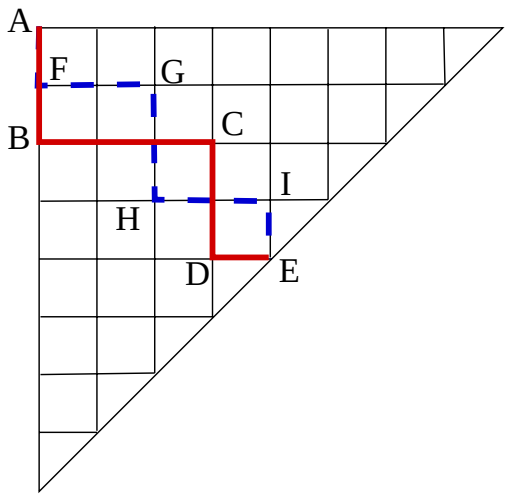

Figure 2.16: Illustration of the proof of Proposition 2.4.8.

we assume that the memory curve represented by the bolded lines A-B-C-D-E ("00111001") is $\psi^*_{\downarrow}$. Let ψ be any other state in the same equivalent class $\widetilde{\psi}$ starting with "$\downarrow$". Now imagine we are growing the two curves $\psi^*_{\downarrow}$ and ψ segment by segment, starting from the left upper corner. The curve ψ has to switch to "$\rightarrow$" no later than it reaches the point B (since otherwise it will be infeasible). This implies that when we encounter the first alternating bit pair in $\psi^*_{\rightarrow}$, we must have encountered at least one alternating bit pair in ψ. For the same reason, ψ has to switch to "$\downarrow$" before $\psi^*_{\downarrow}$ does so at point C. This argument goes on until we hit the line $\alpha = \beta$ and stop. Therefore whenever one alternating bit pair occurs in $\psi^*_{\downarrow}$, at least one alternating pair occurs in ψ. Hence the number of alternating bit pairs in ψ is no less than that in $\psi^*_{\downarrow}$. The curve represented by the dashed lines A-F-G-H-I-E in Figure 2.16 gives an example of such ψ.

Analogously for any state ψ starting with "$\rightarrow$", we can show its number of alternating bit pairs is no less than that of $\psi^*_{\rightarrow}$. The proof is now complete. ■

Example 2.4.9 For the equivalent class $\{\gamma_1, \gamma_2, \gamma_3\}$ in Figure 2.15(a), $\psi^*_{\downarrow} = 0110$

with 2 alternating bit pairs and $\psi^*_{\rightarrow} = 1001$ with the same number of alternating bit pairs. So $\psi^* = \psi^*_{\downarrow}$ (or $\psi^*_{\rightarrow}$).

2.4.3 Experimental results

We now apply the value inversion scheme and the state space reduction scheme to micro-positioning control of a magnetostrictive actuator. The Preisach plane is discretized with $L = 25$, which results in 300 hysterons. By treating 201 hysterons whose weights are zero or very small as trivial, we are left with 99 non-trivial hysterons. The final number of states in the reduced state space is 99,217, compared with 33,554,432, the number of states in the original state space.

Given a sequence of 8 desired displacement values (10 μm, 30 μm, 15 μm, 40 μm, 20 μm, 40 μm, 60 μm and 50 μm), we want to drive the actuator head to these positions consecutively. Three control schemes are implemented to achieve the positioning goals. The first one is based on the value inversion scheme, the second one is based on the closest match algorithm, and the third scheme is based on a non-hysteretic model where the input-output relationship is approximated by a single-valued function $y = -7.44I^3 - 2.63I^2 + 40.81I + 30.34$. The current input and the measured displacement are shown in Figure 2.17 through Figure 2.19. We intentionally hold the input current constant for about 1 second after each positioning is completed. Figure 2.20 compares the errors of the three schemes for the eight positioning tasks. We see that Scheme 1 yields the minimum positioning error. As a trajectory inversion algorithm, Scheme 2 does not allow input reversals for each desired output value and thus has less control freedom than Scheme 1 does. This can explain why scheme 1 is better than scheme 2. Scheme 3 delivers the worst performance because hysteresis is not taken into account.

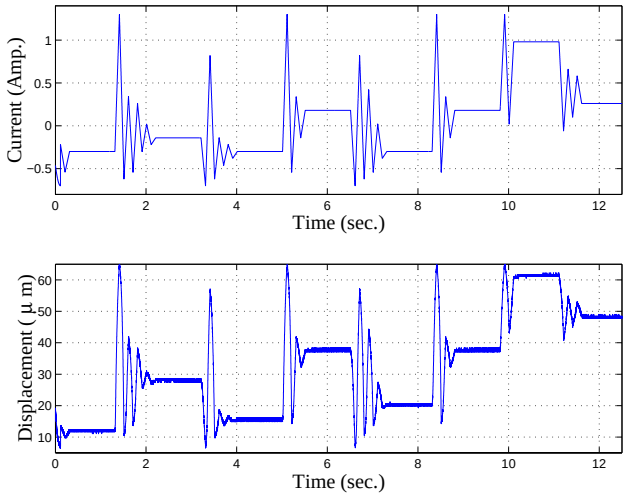

Figure 2.17: Micro-positioning control based on the value inversion scheme.

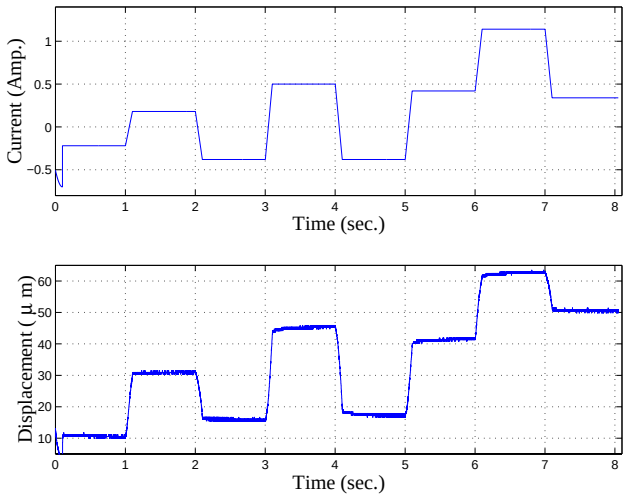

Figure 2.18: Micro-positioning control based on the closest match algorithm.

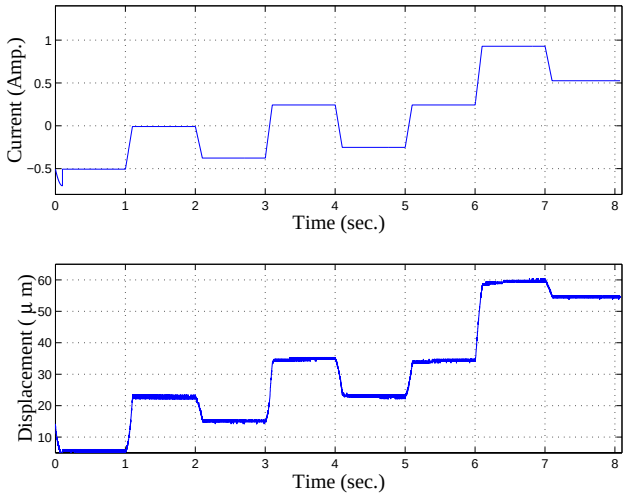

Figure 2.19: Micro-positioning control based on a non-hysteretic model.

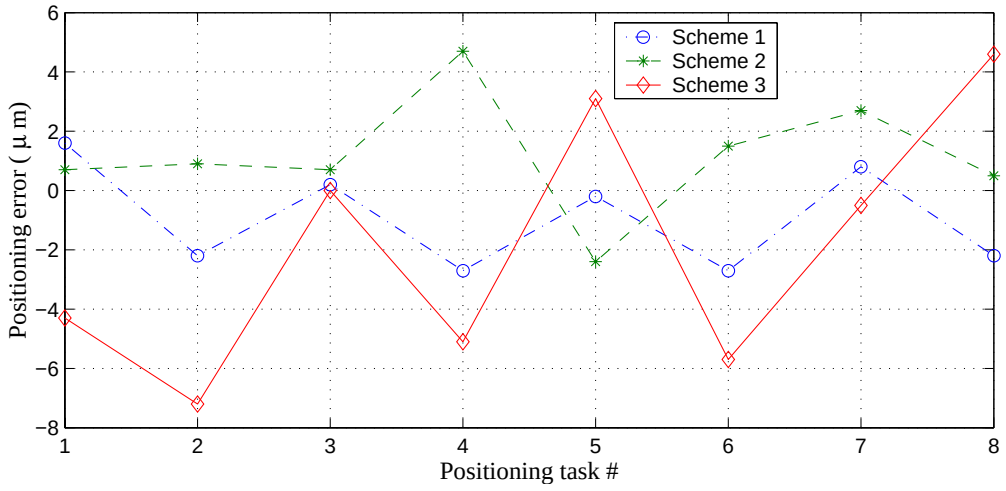

Figure 2.20: Comparison of three schemes. Scheme 1: the value inversion algorithm; Scheme 2: the closest match algorithm; Scheme 3: the inversion algorithm based on a non-hysteretic model.

Chapter 3

A Dynamic Model for Magnetostrictive Hysteresis

When the input frequency gets high, the magnetostrictive hysteresis is rate dependent[1] (Figure 3.1) due to the eddy current effect and the magnetoelastic dynamics of the actuator rod [82, 83]. The rate-dependent hysteresis can no longer be modeled by a Preisach operator alone. In this chapter, we propose a novel dynamic model for the magnetostrictive hysteresis, consisting of a Preisach operator coupled to an ordinary differential equation (ODE) in an unusual way. Due to its special structure, the model presents interesting problems in analysis and computation. We establish the well-posedness of the model and study its various system-theoretic properties. Existence of periodic solutions is proved. Numerical integration schemes, parameter identification methods and an inverse control scheme are presented.

[1] In some literature, e.g., [86, 20], the word *hysteresis* is referred to rate-independent memory effects only. We use "hysteresis" in the more general sense in this dissertation.

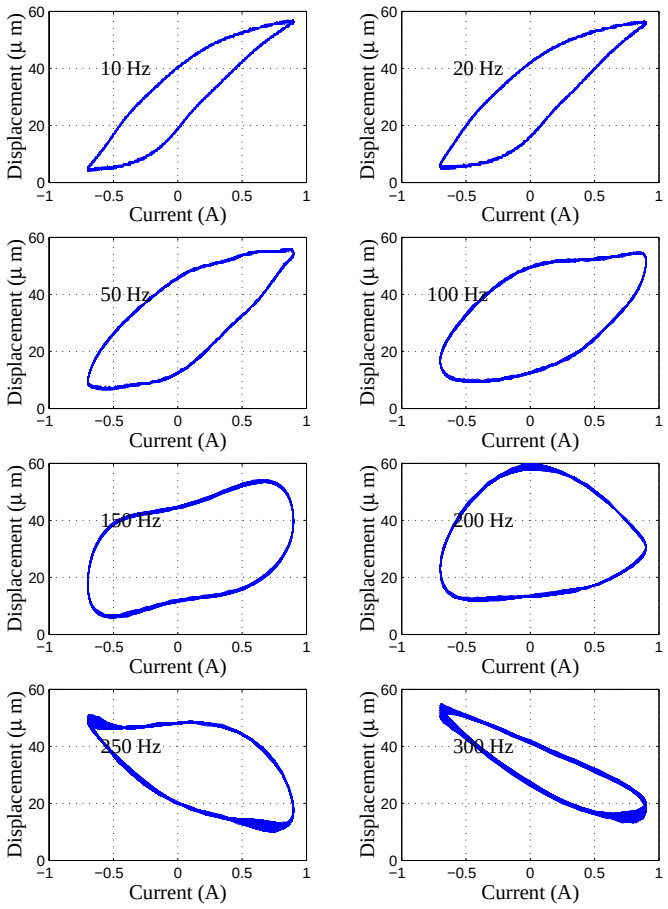

Figure 3.1: The rate-dependent magnetostrictive hysteresis.

3.1 A Dynamic Hysteresis Model

Venkataraman and Krishnaprasad proposed a bulk magnetostrictive hysteresis model based on energy balancing principles [82, 83]. The model has a cascaded structure as shown in Figure 3.2. The block W takes care of the $M - H$ hysteresis and the eddy current losses. $G(s)$ is a lumped second order linear system modeling the magnetoelastic dynamics of the rod.

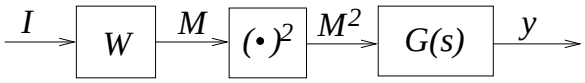

Figure 3.2: Model structure of a magnetostrictive actuator.

We now have a closer look at the block W. Due to the finite resistivity of the magnetostrictive material, there are eddy currents circulating inside the rod. One way to represent the eddy current losses is to place a resistor R_{eddy} in parallel with a hysteretic inductor [23, 82], as shown in Figure 3.3. We note that this is a phenomenological approach and the underlying details of the eddy current dynamics are ignored here. Considering the thin structure of the rod, we assume that the magnetic flux density B is uniform over the cross section of the magnetostrictive rod. Then the voltage V across the nonlinear inductor is $N_m A_m \frac{dB}{dt}$, where N_m is the number of turns of the coil, and A_m is the cross sectional area. Let I be the input current applied, and I_1 be the current flowing in the inductor branch. Since $V = (I - I_1)R_{eddy}$, we have

$$\frac{dB}{dt} = \frac{R_{eddy}}{N_m A_m}(I - I_1). \tag{3.1}$$

In SI units, $B = \mu_0(H + M)$, where $\mu_0 = 4\pi \times 10^{-7}$Henry/m is the permeability of vacuum. H is related to I_1 via $H = c_0 I_1$, where c_0 is the coil factor. The

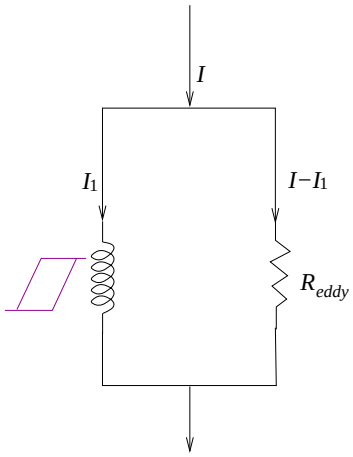

Figure 3.3: Representation of eddy current losses in a magnetostrictive actuator [82].

constitutive relationship between M and H was modeled by a low dimensional bulk ferromagnetic hysteresis model in [82] and that led to an overall model described by switching ordinary differential equations. We use a Preisach operator Γ to model $M - H$ hysteresis and obtain the following new model for the block W:

$$\begin{cases} \dot{H} + \dot{M} = c_1(I - \frac{H}{c_0}) \\ M = \Gamma[H, \psi_0] \end{cases}, \tag{3.2}$$

where ψ_0 represents the initial memory curve and

$$c_1 \triangleq \frac{R_{eddy}}{\mu_0 N_m A_m}.$$

$G(s)$ has a state space representation [82, 83] (after some manipulations):

$$\ddot{y}(t) + 2\xi\omega_0\dot{y}(t) + \omega_0^2 y(t) = \frac{\omega_0^2 l_{rod}\lambda_s}{M_s^2} M^2(t), \tag{3.3}$$

where y is the displacement, $\omega_0 = 2\pi f_0$, f_0 is the first resonant frequency of the actuator, ξ is the damping coefficient, l_{rod} is the length of the rod, λ_s is the saturation magnetostriction and M_s is the saturation magnetization.

Note if we set derivatives in (3.2) and (3.3) to zero, the dynamic model degenerates to the static hysteresis model we have discussed in Chapter 2:

$$\begin{cases} H(t) = c_0 I(t) \\ M(t) = \Gamma[H(\cdot), \psi_0](t) \\ y(t) = \frac{l_{rod}\lambda_s}{M_s^2} M^2(t) \end{cases} . \tag{3.4}$$

3.2 Well-posedness of the Model

Eq. (3.3) is just an ODE, therefore we will focus on the well-posedness of (3.2).

3.2.1 Existence and uniqueness

Eq. (3.2) involves time derivatives of both H and M. It is well known that, in general, a Preisach operator does not map C^1 into C^1. Indeed, when corners in the memory curve are eliminated, discontinuities occur in the output derivative if the Preisach measure does not vanish in a neighbourhood of the corner [86]. Hence we will interpret (3.2) in the sense of Carathéodory [87]. Some partial differential equations with hysteretic operators appearing in the principal parts have been studied, see [86, 20] and references therein. Existence and uniqueness proof of solutions to equations of the form

$$\dot{y} = f(t, y, \Gamma(y)), \tag{3.5}$$

where Γ is some hysteresis operator, can be found in [20]. To our best knowledge, no such result has been published for equations like (3.2).

The following lemma will be used in the proof of uniqueness of the solution to (3.2).

Lemma 3.2.1 (The Gronwall inequality) *[24] Let $\lambda(t)$ be a real continuous function and $\nu(t)$ a nonnegative continuous function on the interval $[a, b]$. If a continuous function $y(t)$ has the property that*

$$y(t) \leq \lambda(t) + \int_a^t \nu(s)y(s)ds$$

for $a \leq t \leq b$, then on the same interval

$$y(t) \leq \lambda(t) + \int_a^t \lambda(s)\nu(s)e^{\int_s^t \nu(\tau)d\tau}ds.$$

In particular, if $\lambda(t) \equiv \lambda_0$, where λ_0 is a constant, then

$$y(t) \leq \lambda_0 e^{\int_a^t \nu(s)ds}.$$

Theorem 3.2.2 *If the Preisach measure ν is nonnegative and nonsingular, and $I(\cdot)$ is piecewise continuous, then for any $\psi_0 \in \Psi$, for any $T > 0$, there exists a unique pair $\{H(\cdot), M(\cdot)\} \in C([0,T]) \times C([0,T])$ satisfying (3.2) almost everywhere.*

Proof 1. We first show the existence. From ψ_0, one can evaluate initial values $H(0)$ and $M(0)$. Eq. (3.2) is equivalent to the following: $\forall t \in [0,T]$,

$$\begin{cases} H(t) + M(t) = H(0) + M(0) + \int_0^t c_1(I(s) - \frac{H(s)}{c_0})ds \\ M(t) = \Gamma[H(\cdot), \psi_0](t) \end{cases} . \tag{3.6}$$

As in the proof of the existence of solutions to the heat equation with hysteresis in [20], we use an Euler polygon method to approximate (3.2): for $N > 0$ and $h_N = \frac{T}{N}$, solve consecutively

$$\begin{cases} \frac{H_N^{(m+1)} - H_N^{(m)}}{h_N} + \frac{M_N^{(m+1)} - M_N^{(m)}}{h_N} = c_1(I_N^{(m)} - \frac{H_N^{(m)}}{c_0}) \\ M_N^{(m+1)} = \Gamma[H_N^{(m+1)}, \psi_m] \end{cases} , \tag{3.7}$$

for $0 \le m \le N-1$, with $H_N^{(0)} = H(0)$, $M_N^{(0)} = M(0)$, $I_N^{(m)} = \frac{1}{h_N}\int_{mh_N}^{(m+1)h_N} I(s)ds$, and ψ_m the memory curve resulting from application of the sequence $\{H_N^{(i)}\}_{i=1}^m$. As discussed in Chapter 2, we tacitly understand that the input of Γ is changed monotonically from $H_N^{(m)}$ to $H_N^{(m+1)}$. From the continuity and the piecewise monotonicity properties of $\Gamma[\cdot, \psi_m]$ (Theorem 2.1.3), (3.7) admits a unique solution for $H_N^{(m+1)}$ and thus for $M_N^{(m+1)}$. Furthermore, by the piecewise monotonicity, $H_N^{(m+1)} - H_N^{(m)}$ and $M_N^{(m+1)} - M_N^{(m)}$ have the same sign, from which we have

$$\begin{aligned} |\frac{H_N^{(m+1)} - H_N^{(m)}}{h_N}| &\le c_1 |I_N^{(m)} - \frac{H_N^{(m)}}{c_0}| \\ &\le c_1(|I_N^{(m)}| + \frac{|H_N^{(m)}|}{c_0}). \end{aligned} \tag{3.8}$$

Since $I(\cdot)$ is piecewise continuous, we have $\forall m$, $I_N^{(m)} \le C_I$, with $C_I > 0$ independent of N. From (3.8), we can get

$$\begin{aligned} |H_N^{(m)}| &\le (1 + \frac{c_1 T}{c_0 N})^N (|H(0)| + c_0 C_I) - c_0 C_I \\ &< e^{\frac{c_1 T}{c_0}} (|H(0)| + c_0 C_I) - c_0 C_I =: C, \end{aligned} \tag{3.9}$$

for all m, and C is independent of N. Boundedness of $M_N^{(m)}$ is a natural consequence of (3.9).

We obtain $H_N(\cdot), M_N(\cdot) \in C([0,T])$ by linearly interpolating $\{H_N^{(m)}\}$ and $\{M_N^{(m)}\}$, i.e., $H_N(t) = \tau H_N^{(m)} + (1-\tau) H_N^{(m+1)}$, for $t = (m+\tau)h_N$, $0 \le \tau \le 1$, and analogously for $M_N(\cdot)$. Combining (3.8) and (3.9) we see that $H_N(\cdot)$ is Lipschitz continuous with Lipschitz constant $L = c_1(C_I + \frac{C}{c_0})$ and the same is true for $M_N(\cdot)$. Therefore $\{H_N(\cdot)\}_{N \ge 1}$ is an equicontinuous and equibounded family of functions, and by Ascoli-Arzelá Theorem, by extracting a subsequence if necessary, $H_N(\cdot) \to \widetilde{H}(\cdot) \in C([0,T])$ uniformly as $N \to \infty$. It's easy to see that $\widetilde{H}(\cdot)$ is also Lipschitz continuous and thus differentiable almost everywhere. Similarly $M_N(\cdot) \to \widetilde{M}(\cdot) \in C([0,T])$ uniformly.

Now define $e_N(t) = \dot{H}_N(t)+\dot{M}_N(t)-c_1(I(t)-\frac{H_N(t)}{c_0})$ at t where $\dot{H}_N(t)$ and $\dot{M}_N(t)$ exist. By the definitions of $H_N(\cdot)$ and $M_N(\cdot)$, we know $e_N(t)$ is well defined a.e. and $e_N(t) = c_1(I_N^{(m)} - I(t)) - \frac{c_1(H_N^{(m)}-H_N(t))}{c_0}$, for $t \in (mh_N, (m+1)h_N)$. Integrating

$$\dot{H}_N(t) + \dot{M}_N(t) = c_1(I(t) - \frac{H_N(t)}{c_0}) + e_N(t)$$

from 0 to t, and letting $N \to \infty$, one can show $\widetilde{H}(\cdot)$ and $\widetilde{M}(\cdot)$ satisfy the first part of (3.6) and we are left to show $\widetilde{M}(t) = \Gamma[\widetilde{H}(\cdot), \psi_0](t)$, $\forall t \in [0, T]$.

Let $\bar{M}_N = \Gamma[H_N(\cdot), \psi_0]$. By the strong continuity of Γ, $\bar{M}_N \to \Gamma[\widetilde{H}(\cdot), \psi_0]$ since $H_N(\cdot) \to \widetilde{H}(\cdot)$. Furthermore we have $\bar{M}_N(mh_N) = M_N(mh_N)$, $0 \le m \le N$. This together with the piecewise monotonicity of Γ enables us to conclude

$$\sup_{t\in[0,T]} |M_N(t) - \bar{M}_N(t)| \le Lh_N.$$

Therefore as $N \to \infty$, $\{M_N\}$ and $\{\bar{M}_N\}$ have the same limit, i.e.,

$$\widetilde{M}(t) = \Gamma[\widetilde{H}(\cdot), \psi_0](t), \ \forall t \in [0, T].$$

2. We now prove the uniqueness. By contradiction we assume that there exist two solutions $\{H_1(\cdot), M_1(\cdot)\}$ and $\{H_2(\cdot), M_2(\cdot)\}$ and $H_1(t') \neq H_2(t')$ for some $t' > 0$ (we know $H_1(0) = H_2(0)$). Define $e_H = H_2 - H_1$ and $e_M = M_2 - M_1$. Using (3.2), we get

$$e_H(t) + e_M(t) = -\frac{c_1}{c_0} \int_0^t e_H(s)ds. \tag{3.10}$$

Define $\bar{t}$ to be

$$\bar{t} = \sup_{t\le t'}\{t : \ e_H(\tau) \equiv 0, \forall \tau \in [0, t]\}.$$

By the continuity of e_H, there exists $\delta > 0$ such that $e_H(t)$ has a constant sign, say, > 0 (without loss of generality), on $(\bar{t}, \bar{t} + \delta]$. Using the order preservation property of Γ (Theorem 2.1.3), $e_M(t) \ge 0$, $\forall t \in [\bar{t}, \bar{t}+\delta]$. This together with (3.10)

leads to

$$|e_H(t)| \leq \frac{c_1}{c_0} \int_0^t |e_H(s)| ds, \forall t \in [0, \bar{t} + \delta], \tag{3.11}$$

which implies $|e_H(t)| \leq 0$ by the Gronwall inequality, $\forall t \in [0, \bar{t} + \delta]$, and this contradicts $|e_H(t)| > 0$, $\forall t \in (\bar{t}, \bar{t} + \delta]$. ■

Remark 3.2.3 *With minor modification, the above proof can be used to show existence and uniqueness of solutions to more general systems where the right hand side of the first equation in (3.2) is replaced by some function $f(H, I)$ continuous in I and Lipschitz continuous in H.*

3.2.2 Continuous dependence on parameters

Continuous dependence of the solution to (3.2) on the parameters and the initial condition can be proved using the properties of the Preisach operator and analysis techniques for ODEs [24].

Before we go to the main result of this subsection, we first look at some lemmas about the Preisach operator. In this subsection we deal with nonsingular Preisach measures exclusively. Since we will discuss a sequence of Preisach operators, a Preisach operator with a density function μ will be denoted as Γ_μ.

Lemma 3.2.4 *If $\{\mu_n\}$ and μ satisfy*

$$\int \int_P |\mu_n(\beta, \alpha) - \mu(\beta, \alpha)| d\beta d\alpha \to 0,$$

then $\forall \psi_0 \in \Psi$, $\forall u \in C([0, T])$, $\Gamma_{\mu_n}[u, \psi_0] \to \Gamma_\mu[u, \psi_0]$ uniformly on $[0, T]$.

Proof For any $t \in [0, T]$, for any n, Γ_{μ_n} and Γ_μ have the same memory curve. Therefore

$$|\Gamma_{\mu_n}[u, \psi_0](t) - \Gamma_\mu[u, \psi_0](t)| \leq \int \int_P |\mu_n(\beta, \alpha) - \mu(\beta, \alpha)| d\beta d\alpha,$$

and the conclusion follows. ∎

Recall the definition of ζ_ψ (Subsection 2.1.1).

Lemma 3.2.5 *Let μ be a density function. Let $\{\psi_{n0} \in \Psi\}$ be a sequence of memory curves such that $\int\int_P \mu(\beta,\alpha)|\zeta_{\psi_{n0}}(\beta,\alpha) - \zeta_{\psi_0}(\beta,\alpha)|d\beta d\alpha \to 0$ for some $\psi_0 \in \Psi$. Let the sequence $u_n \in C([0,T]) \to u \in C([0,T])$ uniformly. Then*

$$\Gamma_\mu[u_n, \psi_{n0}] \to \Gamma_\mu[u, \psi_0] \text{ uniformly on } [0,T].$$

Proof This follows from Theorem IV.3.4 in [86], page 114. ∎

Lemma 3.2.6 *Let $\{\mu_n\}$ be a sequence of density functions such that $\int\int_P |\mu_n(\beta,\alpha) - \mu(\beta,\alpha)|d\beta d\alpha \to 0$ for some Borel measurable function μ. Let $\{\psi_{n0} \in \Psi\}$ be a sequence of memory curves such that*

$$\int\int_P \mu(\beta,\alpha)|\zeta_{\psi_{n0}}(\beta,\alpha) - \zeta_{\psi_0}(\beta,\alpha)|d\beta d\alpha \to 0,$$

for some $\psi_0 \in \Psi$. Let the sequence $u_n \in C([0,T]) \to u \in C([0,T])$ uniformly. Then $\Gamma_{\mu_n}[u_n, \psi_{n0}] \to \Gamma_\mu[u, \psi_0]$ uniformly on $[0,T]$.

Proof We get this by combining Lemma 3.2.4 and Lemma 3.2.5. ∎

Remark 3.2.7 *Theorem IV.2.5 in [86] shows continuous dependence of $\Gamma_\mu[u, \psi_0]$ on μ, u, ψ_0, and there convergence of the Preisach measure in the weak* sense is assumed which enables one to conclude only pointwise convergence for the output. We use a stronger assumption $\mu_n \to \mu$ in the L_1 norm in Lemma 3.2.6 and the payoff is that we get the uniform convergence for the output.*

Theorem 3.2.8 *Let $\{H(\cdot), M(\cdot)\}$ be the solution to (3.2) with the initial condition $\psi_0 \in \Psi$. Assume that the Preisach measure ν for Γ in (3.2) is nonnegative and nonsingular, and let μ be the corresponding density function. Consider a sequence of equations:*

$$\begin{cases} \dot{H}_n + \dot{M}_n = c_{n1}(I_n - \frac{H_n}{c_{n0}}) \\ M_n = \Gamma_{\mu_n}[H_n, \psi_{n0}] \end{cases}, \tag{3.12}$$

where $\{\mu_n\}$ is a sequence of nonnegative density functions, $\{I_n \in PC([0,T])\}$ is a sequence of piecewise continuous functions. From ψ_0 and ψ_{n0}, we get $H(0)$ and $H_n(0)$, respectively. If the following assumptions are satisfied:

$$c_{ni} \to c_i,\ i = 0, 1, \tag{3.13}$$

$$I_n \to I \text{ uniformly on } [0,T], \tag{3.14}$$

$$H_n(0) \to H(0), \tag{3.15}$$

$$\int\int_P |\mu_n(\beta,\alpha) - \mu(\beta,\alpha)| d\beta d\alpha \to 0, \tag{3.16}$$

$$\int\int_P \mu(\beta,\alpha)|\zeta_{\psi_{n0}}(\beta,\alpha) - \zeta_{\psi_0}(\beta,\alpha)| d\beta d\alpha \to 0, \tag{3.17}$$

then $\{H_n(\cdot), M_n(\cdot)\} \to \{H(\cdot), M(\cdot)\}$ uniformly on $[0,T]$.

Proof From Theorem 3.2.2, (3.12) has a unique solution

$$\{H_n(\cdot), M_n(\cdot)\} \in C([0,T]) \times C([0,T]).$$

Let $E \subset \mathbb{R}^2$ be a compact set containing in its interior the graph of $H = H(t)$ for $0 \le t \le T$. Let $Q > 0$ be such that

$$|c_1(I(s) - \frac{\widehat{H}}{c_0})| \le Q,\ \forall (s, \widehat{H}) \in E.$$

From (3.13) and (3.14), there exists $\bar{n}_1$, such that when $n > \bar{n}_1$ (by increasing Q if necessary)

$$|c_{n1}(I_n(s) - \frac{\widehat{H}}{c_{n0}})| \le Q,\ \forall (s, \widehat{H}) \in E.$$

Choose $\delta > 0$ such that the rectangle

$$R = \{(s, \widehat{H}) : \ 0 \le s \le \delta, \, |\widehat{H} - H(0)| \le 2Q\delta\} \subset E.$$

By (3.15), there exists $\bar{n}_2$, such that when $n > \bar{n}_2$, $|H_n(0) - H(0)| \le Q\delta$ and hence $(0, H_n(0)) \in R$. Now from the piecewise monotonicity of Γ_{μ_n}, $\dot{H}_n \dot{M}_n \ge 0$, which implies $|\dot{H}_n| \le Q$. Therefore $(t, H_n(t)) \in R$ for $0 \le t \le \delta$.

$\{H_n(\cdot)\}$ is a sequence of equicontinuous (with same Lipschitz constant Q) and equibounded functions on $[0, \delta]$. From the Ascoli-Arzelá Theorem, by extracting a subsequence if necessary, $H_n \to \bar{H} \in C([0, \delta])$ uniformly. Using Lemma 3.2.6,

$$M_n \to \bar{M} \stackrel{\triangle}{=} \Gamma_\mu[\bar{H}, \psi_0] \text{ uniformly on } [0, \delta].$$

It's easy to show that $\{\bar{H}(\cdot), \bar{M}(\cdot)\}$ solves (3.2) on $[0, \delta]$. By the uniqueness of the solution to (3.2), we have $\{\bar{H}(\cdot), \bar{M}(\cdot)\} = \{H(\cdot), M(\cdot)\}$ on $[0, \delta]$. Hence we have shown any subsequence of (and thus the whole sequence) $\{H_n(\cdot), M_n(\cdot)\}$ converges to $\{H(\cdot), M(\cdot)\}$ uniformly on $[0, \delta]$. Following a standard argument for ODEs (see, e.g., [24]), the region of uniform convergence can be extended to $[0, T]$. ■

3.3 A New Perspective to Study the Model

In this section, we look at (3.2) from a different perspective. This will lead to an alternative proof for the well-posedness as well as provide insight into understanding of various properties of the model.

We define an operator $\mathcal{B} : C([0, T]) \times \Psi \to C([0, T])$, such that

$$\mathcal{B}[H, \psi_0](t) = H(t) + \Gamma[H, \psi_0](t), \, \forall H \in C([0, T]), \, \forall \psi_0 \in \Psi, \tag{3.18}$$

where Γ is the Preisach operator. Let $\widetilde{B} = \mathcal{B}[H, \psi_0]$. Recall $B = \mu_0(H + M)$

(Section 3.1), hence the physical interpretation of $\widetilde{B}$ is the scaled magnetic flux density.

If for any $\widetilde{B} \in C([0,T])$ and any $\psi_0 \in \Psi$, there exists a unique $H \in C([0,T])$, satisfying $\widetilde{B} = \mathcal{B}[H, \psi_0]$, then in terms of $\widetilde{B}$, (3.2) can be written as:

$$\dot{\widetilde{B}} = c_1(I - \frac{\mathcal{B}^{-1}[\widetilde{B}, \psi_0]}{c_0}), \tag{3.19}$$

where $\mathcal{B}^{-1}$ denotes the inverse operator of $\mathcal{B}$. Eq. (3.19) is of a more amenable form and people have studied such systems, see [20] and the references therein.

For an interval J, we define

$$C_J([0,T]) \triangleq \{u \in C([0,T]) : u(t) \in J, \forall t \in [0,T]\}.$$

Let $J_H = [H_{min}, H_{max}] \subset \mathbb{R}$ be the range of H. Then the Preisach operator $\Gamma : C_{J_H}([0,T]) \times \Psi \to C_{J_M}([0,T])$, where $J_M = [M_{min}, M_{max}]$ and M_{min} (M_{max}, resp.) is the negative (positive, resp.) saturation corresponding to H_{min} (H_{max}, resp.)

Proposition 3.3.1 *Let the Preisach measure of* Γ *be nonsingular and nonnegative. Then for any* $\psi_0 \in \Psi$*, the mapping*

$$\mathcal{B}[\cdot, \psi_0] : C_{J_H}([0,T]) \to C_{J_B}([0,T])$$

is piecewise monotone, continuous and injective, where

$$J_B = [H_{min} + M_{min}, H_{max} + M_{max}].$$

Proof It's obvious that the range of $\mathcal{B} \subset C_{J_B}([0,T])$ and $\mathcal{B}$ is piecewise monotone. Continuity of $\mathcal{B}[\cdot, \psi_0]$ follows from that of $\Gamma[\cdot, \psi_0]$. To show $\mathcal{B}[\cdot, \psi_0]$ is injective,

consider H_1, $H_2 \in C_{J_H}([0,T])$ and $H_1(\widetilde{t}) \neq H_2(\widetilde{t})$ for some $\widetilde{t} \in (0,T)$. We can find t', $0 \leq t' < \widetilde{t}$, and $\delta > 0$, such that $H_1(t) = H_2(t)$, $\forall\, t \in [0,t']$ and (without loss of generality) $H_1(t) - H_2(t) > 0$, $\forall\, t \in (t', t'+\delta]$. From the order preservation property of Γ, we have $\mathcal{B}[H_1,\psi_0](t) > \mathcal{B}[H_2,\psi_0](t)$, $\forall t \in (t', t'+\delta]$, which proves the claim. ■

We can also show $\mathcal{B}$ is surjective. We first present a lemma which will be used in the sequel.

Lemma 3.3.2 *[86] Let X, Y be metric spaces, $f : X \to Y$ be continuous and $\widetilde{Y} \subset f(X)$ be dense in Y. Also assume that for any relatively compact set $K \subset \widetilde{Y}$, the set $f^{-1}(K) \stackrel{\triangle}{=} \{x \in X : f(x) \in K\}$ is relatively compact. Then $f(X) = Y$. If moreover f is injective, then $f^{-1} : Y \to X$ is continuous.*

Proof For any $y \in Y$, we can find a sequence $\{y_n \in \widetilde{Y}\}$ convergent to y. Then for any choice of $x_n \in f^{-1}(y_n)$, the sequence $\{x_n\}$ is relatively compact, hence $x_{n'} \to x$ for some subsequence $\{x_{n'}\}$ and some $x \in X$. Since f is continuous, we have $f(x) = y$ and therefore f is surjective.

Let now f be injective. By the same argument as above, if $y_n \to y \in Y$, we get $f^{-1}(y_n) \to x = f^{-1}(y)$ since x is unique and independent of the choice of the subsequence. ■

For $u \in C([0,T])$, we define

$$\underset{[t_1,t_2]}{osc}\, u \stackrel{\triangle}{=} \max_{[t_1,t_2]} u - \min_{[t_1,t_2]} u,\ \forall\, [t_1,t_2] \subset [0,T].$$

Lemma 3.3.3 *Let the assumption in Proposition 3.3.1 hold. Then $\forall \psi_0 \in \Psi$,*

$$\underset{[t_1,t_2]}{osc}\, H \leq \underset{[t_1,t_2]}{osc}\, \mathcal{B}[H,\psi_0],\ \forall\, H \in C([0,T]),\ \forall\, [t_1,t_2] \subset [0,T]. \tag{3.20}$$

Proof Let

$$t^* = \arg\max_{[t_1,t_2]} H,\ t_* = \arg\min_{[t_1,t_2]} H.$$

It's easy to verify that $\Gamma[H,\psi_0](t^*) \geq \Gamma[H,\psi_0](t_*)$. Hence

$$\operatorname*{osc}_{[t_1,t_2]} \mathcal{B}[H,\psi_0] \geq \mathcal{B}[H,\psi_0](t^*) - \mathcal{B}[H,\psi_0](t_*) \geq \operatorname*{osc}_{[t_1,t_2]} H.$$

■

Proposition 3.3.4 *Let the assumption in Proposition 3.3.1 hold. Then for any* $\psi_0 \in \Psi$, $\mathcal{B}[\cdot,\psi_0] : C_{J_H}([0,T]) \to C_{J_B}([0,T])$ *is surjective, and its inverse*

$$\mathcal{B}^{-1}[\cdot,\psi_0] : C_{J_B}([0,T]) \to C_{J_H}([0,T])$$

is continuous.

Proof The results will follow from Lemma 3.3.2, by letting $X = C_{J_H}([0,T])$, $Y = C_{J_B}([0,T])$, $f = \mathcal{B}[\cdot,\psi_0]$, and

$$\widetilde{Y} = C_{pm,J_B}([0,T]) \stackrel{\triangle}{=} \{u \in C_{J_B}([0,T]) : u \text{ is piecewise monotone}\}.$$

We now verify that the assumptions in Lemma 3.3.2 are satisfied.

From Proposition 3.3.1, f is continuous and injective. $\widetilde{Y}$ is obviously dense in Y. To show $\widetilde{Y} \subset f(X)$, we adopt a technique used in [85]. Given $\psi_0 \in \Psi$, we evaluate $H(0)$ and $M(0)$. Without loss of generality, we assume $\widetilde{B} \in C_{pm,J_B}([0,T])$ has only one monotonicity partition with $\widetilde{B}(0) < \widetilde{B}(T)$ (The argument extends to the case of multiple partition regions easily). We assume the compatibility condition is satisfied[2], i.e., $\widetilde{B}(0) = H(0) + M(0)$. We want to find $H \in C_{pm,J_H}([0,T])$, such

[2]If this condition fails, we will have to "blow up" the point of input discontinuity into an interval with nonzero length and make the input continuous by linear interpolation, see [55], page 55, or [20], page 51.

that $\mathcal{B}[H,\psi_0]=\widetilde{B}$. Let $\bar{H}(t)=H(0)+t$. By the (strict) piecewise monotonicity of $\mathcal{B}$, there exists $\bar{T}$, such that $\mathcal{B}[\bar{H},\psi_0](\bar{T})=\widetilde{B}(T)$. Let $H_1(t)=H(0)+\frac{\bar{T}}{T}t$, and $\widetilde{B}_1=\mathcal{B}[H_1,\psi_0]$. Then $\widetilde{B}_1$ is strictly monotone increasing, $\widetilde{B}_1(0)=\widetilde{B}(0)$ and $\widetilde{B}_1(T)=\widetilde{B}(T)$. Now we introduce a time transformation $\phi:[0,T]\to[0,T]$ so that $\phi(t)=\widetilde{B}_1^{-1}\circ\widetilde{B}(t)$. It's easy to see $H=H_1\circ\phi$ will yield $\widetilde{B}$.

We are left to show $f^{-1}(K)$ is relatively compact for any relatively compact set $K\subset\widetilde{Y}$. Using Lemma 3.3.3, the set $\mathcal{B}^{-1}[K,\psi_0]$ is equicontinuous if $K\subset C_{pm,J_B}([0,T])$ is. Then we conclude with the Ascoli-Arzelá Theorem. ∎

Remark 3.3.5 *Properties of $\mathcal{B}$ and $\mathcal{B}^{-1}$ we have shown so far and the Lipschitz continuity of $\mathcal{B}^{-1}$ (to be shown next) parallel those of Γ and Γ^{-1} when the Preisach measure ν satisfies an extra assumption:*

$$\nu(\triangle(\lambda_1,\lambda_2))>0,\ \forall\,[\lambda_1,\lambda_2]\subset J_H,\lambda_1<\lambda_2, \tag{3.21}$$

where $\triangle(\lambda_1,\lambda_2)\stackrel{\triangle}{=}\{(\beta,\alpha)\in P:\lambda_1\le\beta\le\alpha\le\lambda_2\}$ [21, 86, 20]. This is not surprising since the operator $\mathcal{B}$ can be regarded as a Preisach operator Γ' with measure $\nu'=\nu+\nu_0$, where ν_0 is a strictly positive singular measure concentrated on the line $\alpha=\beta$.

Proposition 3.3.6 *Let the assumption in Proposition 3.3.1 hold. Then the operator $\mathcal{B}[\cdot,\cdot]$ is causal, rate-independent and order preserving.*

Proof Straightforward. ∎

Theorem 3.3.7 *Let the assumption in Proposition 3.3.1 hold. Then $\forall\,\psi_0\in\Psi$, $\mathcal{B}^{-1}[\cdot,\psi_0]$ is Lipschitz continuous with Lipschitz constant 2, i.e.,*

$$\sup_{t\in[0,T]}|H_1(t)-H_2(t)|\le 2\sup_{t\in[0,T]}|\mathcal{B}[H_1,\psi_0](t)-\mathcal{B}[H_2,\psi_0](t)|, \tag{3.22}$$

for H_1, $H_2\in C_{J_H}([0,T])$.

Proof Essential ideas of the proof are borrowed from [21], where the inverse of the Preisach operator Γ is shown to be Lipschitz continuous if (3.21) and the following condition are satisfied:

$$\chi(x) \geq Cx, \forall x > 0, \tag{3.23}$$

for some constant $C > 0$, where

$$\chi(x) \stackrel{\triangle}{=} \min\{\nu(\triangle(\lambda, \lambda + x)) : H_{min} \leq \lambda \leq H_{max} - x\}.$$

It suffices to show that, $\forall\, t \in [0, T]$,

$$|H_1(t) - H_2(t)| \leq 2 \sup_{\tau \in [0,t]} |\mathcal{B}[H_1, \psi_0](\tau) - \mathcal{B}[H_2, \psi_0](\tau)|. \tag{3.24}$$

If $H_1(t) = H_2(t)$, the claim is trivial. Assume $H_1(t) < H_2(t)$ (the case $H_1(t) > H_2(t)$ is similar). Let the corresponding memory curves at t be $\psi_1[t]$ and $\psi_2[t]$ in (r, s) coordinates. If $\psi_1[t](r) \leq \psi_2[t](r)$, $\forall r > 0$, (3.24) is obviously true. So we consider only the case that $\psi_1[t](r) > \psi_2[t](r)$, for some $r > 0$, as shown in Figure 3.4 (same as Figure 5.1 in [21] with different notation).

Define

$$r_* = \inf\{r \geq 0 : \psi_1[t](r) > \psi_2[t](r)\},$$
$$r^* = \inf\{r > r_* : \psi_1[t](r) = \psi_2[t](r)\}.$$

Since $\psi_1[t](0) < \psi_2[t](0)$ and we consider a compact support for the Preisach measure, $0 < r_* < r^* < \infty$. As illustrated in Figure 3.4, r_* indicates the first (counting from the left) bifurcation point of $\psi_1[t]$ and $\psi_2[t]$ after they first intersect, and r^* indicates the next intersection point of the two curves. Define regions:

$$D_1 = \{(r, s) : 0 \leq r \leq r_*,\, \psi_1[t](r) \leq s \leq \psi_2[t](r)\},$$
$$D_2 = \{(r, s) : r_* \leq r \leq r^*,\, \psi_2[t](r) \leq s \leq \psi_1[t](r)\}.$$

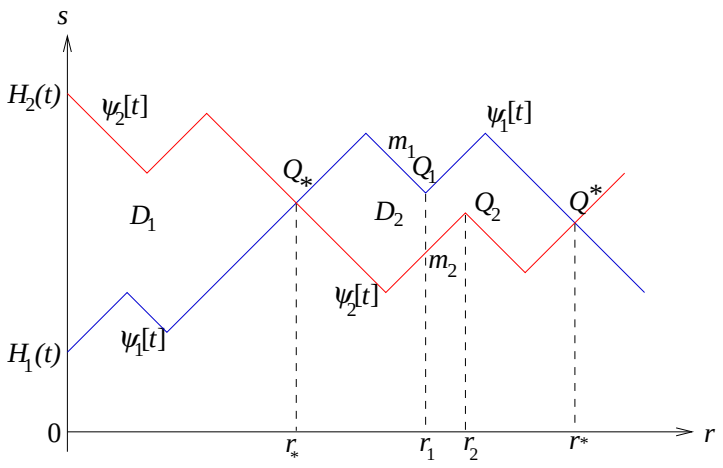

Figure 3.4: Illustration of the proof of Theorem 3.3.7.

Now

$$\Gamma[H_1,\psi_0](t)-\Gamma[H_2,\psi_0](t)=-2\int\int_{D_1}\omega(r,s)dsdr+2\int\int_{D_2}\omega(r,s)dsdr+\nu_\infty, \tag{3.25}$$

where ν_∞ represents the contribution from the region where $r>r^*$. Since $\omega\geq 0$, we get from (3.25)

$$H_2(t)-H_1(t)\leq \mathcal{B}[H_2,\psi_0](t)-\mathcal{B}[H_1,\psi_0](t)+2\int\int_{D_2}\omega(r,s)dsdr+\nu_\infty. \tag{3.26}$$

Our next goal is to show that we can find $\tau\in[0,t]$, such that

$$2\int\int_{D_2}\omega(r,s)dsdr+\nu_\infty\leq \mathcal{B}[H_1,\psi_0](\tau)-\mathcal{B}[H_2,\psi_0](\tau), \tag{3.27}$$

then (3.26) and (3.27) would imply (3.24).

We observe that both graphs of $\psi_1[t]$ and $\psi_2[t]$ when restricted to $[r_*,r^*]$, consist of at least two segments of different slopes and we let m_i be the second segment of $\psi_i[t]|[r_*,r^*]$ counting from the left, where "|" denotes restriction. Let t_i be the time when m_i is formed on $\psi_i[t]$. Let $\tau=\max\{t_1,t_2\}$. Clearly $\tau>0$. We claim τ

satisfies (3.27). To see this, let's assume, without loss of generality, $\tau = t_1$. Then

$$\begin{aligned}
\psi_1[\tau] &= \max\{\psi_1[t], \bar{\psi}_1\}, \\
\psi_2[\tau] &\leq \max\{\psi_2[t], \bar{\psi}_*\} \text{ in } [0, r_2], \\
\psi_2[\tau] &= \psi_2[t] \text{ in } [r_2, \infty],
\end{aligned}$$

where $\bar{\psi}_1$ and $\bar{\psi}_*$ are the straight lines with slope -1 through Q_1 and Q_*. Therefore $\Gamma[H_1, \psi_0](\tau) \geq \Gamma[H_2, \psi_0](\tau)$ and $H_1(\tau) > H_2(\tau)$, which implies (3.27). ■

Corollary 3.3.8 *Let the assumption in Proposition 3.3.1 hold. Then*

$$\mathcal{B}^{-1}[\cdot, \cdot] : C_{J_B}([0, T]) \times \Psi \to C_{J_H}([0, T])$$

is Lipschitz continuous: $\forall\, \psi_1, \psi_2 \in \Psi$, $\forall\, H_1, H_2 \in C_{J_H}([0, T])$,

$$\sup_{t\in[0,T]} |H_1(t) - H_2(t)| \leq 2 \sup_{t\in[0,T]} |\mathcal{B}[H_1, \psi_1](t) - \mathcal{B}[H_2, \psi_2](t)| + 2 \parallel \psi_1 - \psi_2 \parallel, \quad (3.28)$$

where

$$\parallel \psi_1 - \psi_2 \parallel \stackrel{\triangle}{=} \int\int_P |\zeta_{\psi_1}(\beta, \alpha) - \zeta_{\psi_2}(\beta, \alpha)| \mu(\beta, \alpha) d\beta d\alpha,$$

and ζ_ψ is as defined in Subsection 2.1.1.

Proof The proof is almost identical to that of Theorem 3.3.7, except that when $\psi_1 \neq \psi_2$, $\tau = \max\{t_1, t_2\}$ may be 0. But if that's the case, we immediately have

$$2 \int\int_{D_2} \omega(r, s) ds dr + \nu_\infty \leq 2 \parallel \psi_1 - \psi_2 \parallel, \quad (3.29)$$

which completes the proof. ■

Now we can provide another proof for Theorem 3.2.2 (see also Theorem 3.1.1 in [20], page 124):

Proof Define $\mathcal{B}$ as in (3.18) and rewrite (3.2) as (3.19). The latter is equivalent to

$$\widetilde{B}(t) = \widetilde{B}(0) + \int_0^t c_1 (I(s) - \frac{\mathcal{B}^{-1}[\widetilde{B}, \psi_0](s)}{c_0}) ds =: \mathcal{T}[\widetilde{B}](t), \quad (3.30)$$

where $\widetilde{B}(0) = H(0) + M(0)$. From Theorem 3.3.7, when τ is small enough, the operator $\mathcal{T}$ is a contraction mapping on a closed subset of $C([0,\tau])$. Therefore (3.30) has a unique solution $\widetilde{B}$ defined on $[0,\tau]$ by the contraction mapping theorem (Appendix A). Furthermore, the solution can be extended to the interval $[0,T]$. One can then obtain $H = \mathcal{B}^{-1}[\widetilde{B}, \psi_0]$ and $M = \Gamma[H, \psi_0]$. ∎

From Corollary 3.3.8, we can obtain an explicit formula for the continuous dependence of the solution to (3.2) on the initial condition:

Proposition 3.3.9 *Let the Preisach measure ν be nonsingular and nonnegative. Let ω_Γ be the modulus of continuity for Γ. For $i = 1, 2$, denote by $\{H_i(\cdot), M_i(\cdot)\}$ the solution to (3.2) corresponding to the initial memory curve $\psi_i \in \Psi$. Then for any $T > 0$, any $I(\cdot) \in PC([0,T])$, we have*

$$\| H_1 - H_2 \|_{C([0,T])} \leq 2(a_0 e^{\frac{2c_1 T}{c_0}} + \| \psi_1 - \psi_2 \|), \tag{3.31}$$

$$\| M_1 - M_2 \|_{C([0,T])} \leq \omega_\Gamma(\| H_1 - H_2 \|_{C([0,T])}), \tag{3.32}$$

where

$$a_0 \triangleq |H_1(0) + M_1(0) - H_2(0) - M_2(0)| + \frac{2c_1 T \| \psi_1 - \psi_2 \|}{c_0},$$

and $\| \cdot \|_{C([0,T])}$ denotes the sup *norm on $C([0,T])$.*

Proof Let $\widetilde{B}_i(t) = H_i(t) + M_i(t)$, $i = 1, 2$. Then for $i = 1, 2$,

$$\widetilde{B}_i(t) = \widetilde{B}_i(0) + \int_0^t c_1 (I(s) - \frac{\mathcal{B}^{-1}[\widetilde{B}_i, \psi_i](s)}{c_0}) ds,$$

which gives rise to

$$\widetilde{B}_1(t) - \widetilde{B}_2(t) = \widetilde{B}_1(0) - \widetilde{B}_2(0) - \frac{c_1}{c_0} \int_0^t (\mathcal{B}^{-1}[\widetilde{B}_1, \psi_1](s) - \mathcal{B}^{-1}[\widetilde{B}_2, \psi_2](s)) ds. \tag{3.33}$$

From Corollary 3.3.8 and the Gronwall inequality, we obtain

$$\| \widetilde{B}_1 - \widetilde{B}_2 \|_{C([0,T])} \leq a_0 e^{\frac{2c_1 T}{c_0}}. \tag{3.34}$$

Then (3.31) follows from Corollary 3.3.8 and (3.32) follows from the continuity of Γ. ■

3.4 System-Theoretic Properties of the Model

In this section we study system-theoretic properties associated with the model (3.2). In particular, we look at stability of equilibria, input-output stability, reachability and observability.

3.4.1 Stability of equilibria

The state for (3.2) is the (infinite-dimensional) memory curve $\psi \in \Psi$ since both H and M can be derived from ψ. We set the input $I \equiv 0$ in (3.2) and investigate stability of the equilibria of the following equation:

$$\begin{cases} \dot{H} + \dot{M} = -\frac{c_1}{c_0} H \\ M = \Gamma[H, \psi_0] \end{cases} . \tag{3.35}$$

To get the set of equilibria, we let $\dot{H} = \dot{M} = 0$ in (3.35) and obtain $H = 0$. Therefore the equilibria set

$$\Psi_0 = \{\psi \in \Psi : \text{ the graph of } \psi \text{ intersects the line } \alpha = \beta \text{ at } (0,0)\}.$$

In (r, s) coordinates, $\Psi_0 = \{\psi \in \Psi : \psi(0) = 0\}$. Note Ψ_0 forms a continuum and any $\psi \in \Psi$ whose graph is embraced by those of ψ_u and ψ_l in Figure 3.5(a) belongs to Ψ_0.

Stability of an equilibrium point is usually discussed in the sense of Lyapunov [54]. An equilibrium point is *stable* if all solutions starting at its nearby points stay nearby. It is *asymptotically stable* if it is stable and all solutions starting

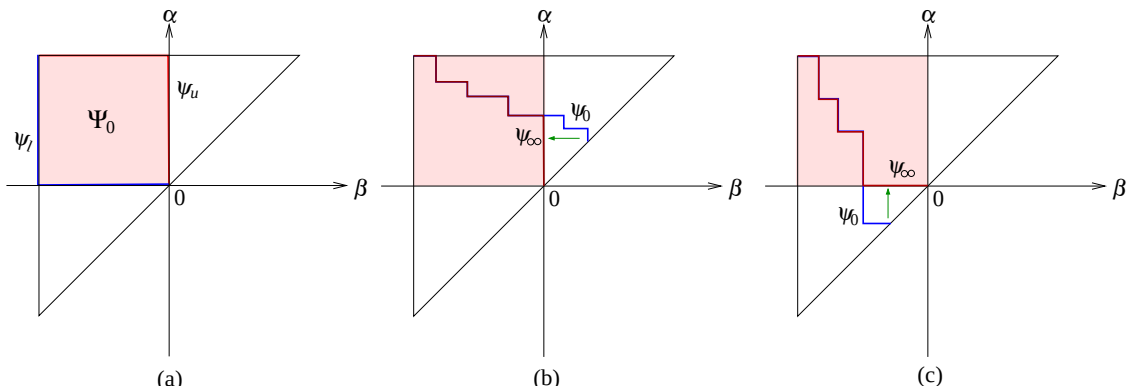

Figure 3.5: Stability of the equilibria: (a) the set Ψ_0; (b) evolution of ψ_t when $H(0) > 0$; (c) evolution of ψ_t when $H(0) < 0$.

at nearby points tend to it as time approaches infinity. Different metrics can be defined to measure the distance between two memory curves ψ_1, $\psi_2 \in \Psi$. Recall the definition for ζ_ψ (Subsection 2.1.1). We can define

$$\| \psi_1 - \psi_2 \|_{L_1} \stackrel{\triangle}{=} \int \int_P |\zeta_{\psi_1}(\beta, \alpha) - \zeta_{\psi_2}(\beta, \alpha)| d\beta d\alpha, \tag{3.36}$$

and

$$\| \psi_1 - \psi_2 \|_{L_{1,\mu}} \stackrel{\triangle}{=} \int \int_P |\zeta_{\psi_1}(\beta, \alpha) - \zeta_{\psi_2}(\beta, \alpha)| \mu(\beta, \alpha) d\beta d\alpha. \tag{3.37}$$

We use the notation $\| \cdot \|_{L_1}$ and $\| \cdot \|_{L_{1,\mu}}$ since the metrics (3.36) and (3.37) are defined in terms of the L_1 norm where the underlying measures are the Lebesgue measure in $\mathbb{R}^2$ and the Preisach measure with density μ, respectively.

A third metric uses the Hausdorff distance

$$\| \psi_1 - \psi_2 \|_H \stackrel{\triangle}{=} d_H(\text{graph of } \psi_1, \text{graph of } \psi_2), \tag{3.38}$$

and we recall for a metric space X with metric $d(\cdot, \cdot)$, the Hausdorff distance $d_H(S_1, S_2)$ between two sets S_1, $S_2 \subset X$ is defined

$$d_H(S_1, S_2) \stackrel{\triangle}{=} \max\{ \sup_{s_1 \in S_1} \inf_{s_2 \in S_2} d(s_1, s_2), \sup_{s_2 \in S_2} \inf_{s_1 \in S_1} d(s_1, s_2) \}.$$

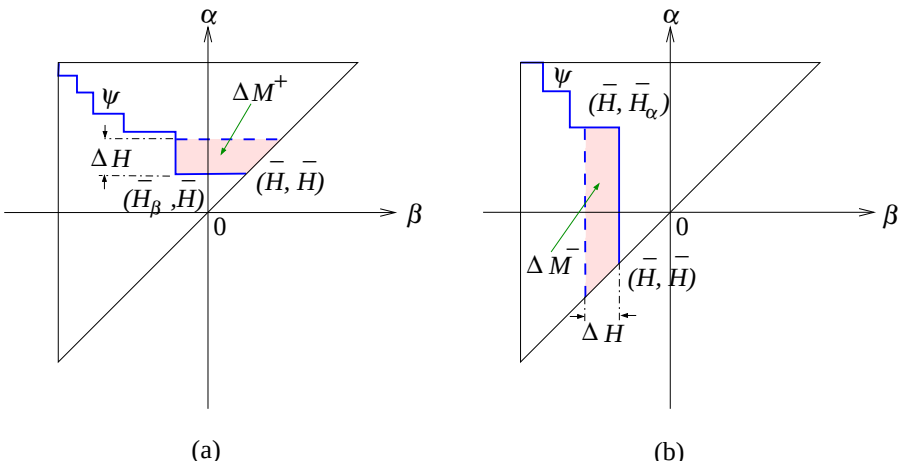

Figure 3.6: Illustration of the definition $\frac{dM}{dH}(\psi, \pm)$: (a) definition of $\frac{dM}{dH}(\psi, +)$; (b) definition of $\frac{dM}{dH}(\psi, -)$.

We now define two quantities, $\frac{dM}{dH}(\psi, +)$ and $\frac{dM}{dH}(\psi, -)$, where $\frac{dM}{dH}(\psi, +)$ ($\frac{dM}{dH}(\psi, -)$, resp.) carries the interpretation of the derivative of M with respect to H when H is being increased (decreased, resp). For $\psi \in \Psi$, Let $(\bar{H}, \bar{H})$ be the point where ψ intersects with the line $\alpha = \beta$. Define (see Figure 3.6 for illustration)

$$\bar{H}_\beta \stackrel{\triangle}{=} \inf_\beta \{\beta : (\beta, \bar{H}) \in \text{ graph of } \psi\},$$

and

$$\bar{H}_\alpha \stackrel{\triangle}{=} \sup_\alpha \{\alpha : (\bar{H}, \alpha) \in \text{ graph of } \psi\}.$$

Note usually either $\bar{H}_\beta$ or $\bar{H}_\alpha$ is equal to $\bar{H}$.

We let

$$\frac{dM}{dH}(\psi, +) = \lim_{\triangle H \to 0^+} \frac{\triangle M^+}{\triangle H}, \tag{3.39}$$

$$\frac{dM}{dH}(\psi, -) = \lim_{\triangle H \to 0^+} \frac{\triangle M^-}{\triangle H} \tag{3.40}$$

if the limits in (3.39) and (3.40) exist, where $\triangle M^+$ and $\triangle M^-$ represent contribu-

tions from the shaded areas in Figure 3.6(a) and (b), respectively:

$$\triangle M^+ = 2\int_{\bar{H}}^{\bar{H}+\triangle H}\int_{\bar{H}_\beta}^{\alpha}\mu(\beta,\alpha)d\beta d\alpha,$$
$$\triangle M^- = 2\int_{\bar{H}-\triangle H}^{\bar{H}}\int_{\beta}^{\bar{H}_\alpha}\mu(\beta,\alpha)d\alpha d\beta.$$

If μ is continuous, $\frac{dM}{dH}(\psi,+)$ and $\frac{dM}{dH}(\psi,-)$ are well defined and given by

$$\frac{dM}{dH}(\psi,+) = 2\int_{\bar{H}_\beta}^{\bar{H}}\mu(\beta,\bar{H})d\beta, \tag{3.41}$$
$$\frac{dM}{dH}(\psi,-) = 2\int_{\bar{H}}^{\bar{H}_\alpha}\mu(\bar{H},\alpha)d\alpha. \tag{3.42}$$

It turns out that our stability result is independent of the metric we use.

Proposition 3.4.1 *Assume that the Preisach measure is nonnegative and non-singular, and that the density function is piecewise continuous. Then each $\psi \in \Psi_0$ is a stable but not asymptotically stable equilibrium of (3.35).*

Proof Consider $\psi^* \in \Psi_0$. Denote ψ_t the memory curve at time $t > 0$ when the system starts from $\psi_0 \in \Psi$ at $t = 0$. We claim

$$\| \psi_t - \psi^* \| \leq \| \psi_0 - \psi^* \|, \forall\, t \geq 0, \tag{3.43}$$

where $\| \cdot \|$ is any of the three metrics we defined above.

We first show if $H(0)$ corresponding to ψ_0 is not zero, then $H(t) \to 0$ *monotonically*. By the assumptions of the proposition and the implicit assumption that μ has a compact support, $\frac{dM}{dH}(\psi_t, sgn(\dot{H}))$ is well defined a.e., and

$$0 \leq \frac{dM}{dH}(\psi_t, sgn(\dot{H})) \leq C, \tag{3.44}$$

for some $C > 0$. Then the first equation in (3.35) is of the form

$$\dot{H} = -\frac{c_1}{c_0(1+g(t))}H, \tag{3.45}$$

where $g(t) = \frac{dM}{dH}(\psi_t, sgn(\dot{H}))$, and $0 \leq g(t) \leq C$. From (3.45), we can see $H(t) \to 0$ monotonically. This implies that for $\psi_0 \in \Psi$ with $H(0) \neq 0$, $\psi_t \to \psi_\infty$ as illustrated in Figure 3.5 (b) and (c). If $H(0) = 0$, i.e., $\psi_0 \in \Psi_0$, then $\psi_t \equiv \psi_0$. Therefore (3.43) holds and any $\psi \in \Psi_0$ is stable. Any $\psi \in \Psi_0$ is not asymptotically stable due to that Ψ_0 forms a continuum. ■

Remark 3.4.2 *Although any individual equilibrium $\psi \in \Psi_0$ is not asymptotically stable, Ψ_0 is "globally asymptotically stable", in the sense that, starting from any $\psi_0 \in \Psi$, $\lim_{t\to\infty} \inf_{\psi\in\Psi_0} \parallel \psi_t - \psi \parallel = 0$.*

3.4.2 Input-output stability

For each $\psi_0 \in \Psi$, (3.2) defines a mapping from the input $I(\cdot)$ to the output $H(\cdot)$ and $M(\cdot)$. Here we discuss the question of *finite gain stability* for this mapping.

Definition 3.4.3 *A mapping $\mathcal{M}$ is finite gain $\mathcal{L}$ stable if there exist $\gamma \geq 0$ and b_0, such that for all u in the input space,*

$$\parallel \mathcal{M}u \parallel_{\mathcal{L}} \leq \gamma \parallel u \parallel_{\mathcal{L}} + b_0, \tag{3.46}$$

where $\parallel \cdot \parallel_{\mathcal{L}}$ denotes the signal space norm. We say $\mathcal{M}$ has an $\mathcal{L}$ gain less than or equal to γ, and call b_0 the bias term.

We study the finite gain L_∞ stability and the finite gain L_2 stability of (3.2). Accordingly, we define two input spaces

$$U_\infty \triangleq \{I(\cdot) : I(\cdot) \text{ is piecewise continuous and } \sup_{t\geq 0} |I(t)| < \infty\},$$
$$U_2 \triangleq \{I(\cdot) : I(\cdot) \text{ is piecewise continuous and } \int_0^\infty I^2(t)dt < \infty\},$$

and we write

$$\| I(\cdot) \|_\infty = \sup_{t \geq 0} |I(t)|, \ \forall I(\cdot) \in U_\infty,$$
$$\| I(\cdot) \|_2 = \sqrt{\int_0^\infty I^2(t) dt}, \ \forall I(\cdot) \in U_2.$$

Finite gain L_∞ stability

Since the Preisach measure is assumed to be finite, $|M(t)| \leq M_s, \forall t \geq 0$ for any input $I(\cdot)$, where M_s stands for the saturation magnetization. Therefore the mapping from $I(\cdot)$ to $M(\cdot)$ is finite gain L_∞ stable with $\gamma = 0$ and $b_0 = M_s$.

For the mapping from $I(\cdot)$ to $H(\cdot)$, we have the following:

Proposition 3.4.4 *Let the Preisach measure be nonnegative and nonsingular. Then $\forall \psi_0 \in \Psi$, $\forall I(\cdot) \in U_\infty$, we have*

$$\| H(\cdot) \|_\infty \leq \max\{|H(0)|, c_0 \| I(\cdot) \|_\infty\}. \tag{3.47}$$

Proof The proposition follows from the observation that, due to the piecewise monotonicity of the Preisach operator, (3.2) gives

$$\dot{H} \geq 0 \text{ if } I(t) \geq \frac{H(t)}{c_0},$$
$$\dot{H} \leq 0 \text{ if } I(t) \leq \frac{H(t)}{c_0}.$$

■

Finite gain L_2 stability

The mapping from $I(\cdot)$ to $M(\cdot)$ is not L_2 stable in general. To see this, consider an example: Let the initial memory curve $\psi_0 \in \Psi$ be such that the corresponding

$H(0) = 0$ (i.e. $\psi_0 \in \Psi_0$) and $M(0) \neq 0$, and let $I \equiv 0$. Then $M \equiv M(0)$ and hence not square integrable although $\| I(\cdot) \|_2 = 0$.

The mapping from $I(\cdot)$ to $H(\cdot)$ is finite gain L_2 stable:

Proposition 3.4.5 *Let the Preisach measure be nonnegative and nonsingular with a piecewise continuous density μ. Then $\forall \psi_0 \in \Psi$, $\forall I(\cdot) \in U_2$, we have*

$$\| H(\cdot) \|_2 \leq \bar{\gamma} \| I(\cdot) \|_2 + \bar{b}_0, \tag{3.48}$$

where

$$\bar{\gamma} = \sup_{\omega} \frac{c_1}{|j\omega + \frac{c_1}{c_0(1+C)}|},$$
$$\bar{b}_0 = \sqrt{\frac{c_0(1+C)}{2c_1}} |H(0)|,$$

and $C > 0$ is the constant in (3.44).

Proof For each $\psi_0 \in \Psi$, we can rewrite (3.2) as

$$\dot{H}(t) = -\frac{c_1}{c_0(1+g(t))} H(t) + \frac{c_1}{1+g(t)} I(t), \tag{3.49}$$

where $g(t)$ is as defined in the proof of Proposition 3.4.1. Eq. (3.49) is a linear time-varying ODE and its solution is given by [61]: $H(t) = H_0(t) + H_1(t)$, where

$$H_0(t) = e^{-\int_0^t \frac{c_1}{c_0(1+g(\sigma))} d\sigma} H(0), \tag{3.50}$$

$$H_1(t) = \int_0^t e^{-\int_\tau^t \frac{c_1}{c_0(1+g(\sigma))} d\sigma} \frac{c_1}{1+g(\tau)} I(\tau) d\tau. \tag{3.51}$$

From (3.44), one obtains $\| H_0(\cdot) \|_2 \leq \bar{b}_0$. Again from (3.44),

$$|H_1(t)| \leq H_2(t) \stackrel{\triangle}{=} e^{-\frac{c_1}{c_0(1+C)} t} \otimes c_1 |I(t)|, \tag{3.52}$$

where "$\otimes$" denotes the convolution. Note H_2 is just the output of a linear time invariant system

$$G_0(s) = \frac{c_1}{s + \frac{c_1}{c_0(1+C)}}$$

when the input is $|I(\cdot)|$. Denote Fourier transforms of H_2, I and $|I|$ by $\widehat{H}_2(j\omega)$, $\widehat{I}(j\omega)$ and $\widehat{I}'(j\omega)$, respectively. Then

$$\begin{aligned} \| H_1(\cdot) \|_2^2 &\leq \| H_2(\cdot) \|_2^2 && (3.53)\\ &= \frac{1}{2\pi}\int_{-\infty}^{\infty} |G_0(j\omega)\widehat{I}'(j\omega)|^2 d\omega && (3.54)\\ &\leq \bar{\gamma}^2 \frac{1}{2\pi}\int_{-\infty}^{\infty} |\widehat{I}'(j\omega)|^2 d\omega && (3.55)\\ &= \bar{\gamma}^2 \frac{1}{2\pi}\int_{-\infty}^{\infty} |\widehat{I}(j\omega)|^2 d\omega && (3.56)\\ &= \bar{\gamma}^2 \| I(\cdot) \|_2^2, && (3.57) \end{aligned}$$

where we have used the Parseval's identity [39] in (3.54), (3.56) and (3.57). Eq. (3.48) now follows by using the triangular inequality. ■

Remark 3.4.6 *The bound $\bar{\gamma}$ is just the $\mathcal{H}_\infty$ norm [39] of the system $G_0(s)$.*

3.4.3 Reachability

In this subsection and next subsection, we will adapt the notions of *reachability* and *observability* [74] to the Preisach operator Γ and the system (3.2).

Let $H \in C([0,T])$ be the input to the Preisach operator and let $\psi[t]$ be the memory curve at time t. It's easy to check that $\psi[\cdot]$ is continuous on [0,T] under any of the three metrics on Ψ defined in Subsection 3.4.1, and we write

$$\psi[\cdot] \in C([0,T],\Psi).$$

Let $\Xi : C([0,T]) \times \Psi \to C([0,T],\Psi)$ be the evolution map of the memory curve (c.f. Section 2.3 for the definition of Ξ_d in the discrete-time case), i.e., for the input $H \in C([0,T])$ and the initial memory curve $\psi_0 \in \Psi$,

$$\psi[t] = \Xi[H,\psi_0](t).$$

Definition 3.4.7 (Reachability for the Preisach operator) *Let $\psi_1, \psi_2 \in \Psi$. We say ψ_2 is reachable from ψ_1 if there exists a finite $T > 0$, and $H \in C([0,T])$, such that $\psi_2 = \Xi[H, \psi_1](T)$. The state space Ψ is called reachable if any state is reachable from any other state.*

Definition 3.4.8 (Approximate reachability for the Preisach operator) *Let $d(\cdot,\cdot)$ be one of the three metrics in Ψ defined in Subsection 3.4.1. We say $\psi_2 \in \Psi$ is approximately reachable from $\psi_1 \in \Psi$ if for any $\epsilon > 0$, there exists $\psi_\epsilon \in \Psi$, such that ψ_ϵ is reachable from ψ_1 and $d(\psi_\epsilon, \psi_2) \leq \epsilon$. The state space Ψ is called approximately reachable if any state is approximately reachable from any other state.*

Remark 3.4.9 *The definition of approximate reachability above is adapted from that in [37].*

Proposition 3.4.10 *[37] For the Preisach operator Γ, the state space Ψ is not reachable, but approximately reachable.*

Proof Denote $\Psi_r \subset \Psi$ the set of memory curves composed of segments with slope ± 1 in (r, s) coordinates. It's easy to check that Ψ_r is a dense subset of Ψ, and any $\psi_r \in \Psi_r$ is reachable from any $\psi \in \Psi$. ∎

Now for the system (3.2), for any input $I \in PC([0,T])$ (the space of piecewise continuous functions), the corresponding trajectory $\psi[\cdot] \in C([0,T], \Psi)$ by Theorem 3.2.2. Denote $\Xi_D : PC([0,T]) \times \Psi \to C([0,T], \Psi)$ the state evolution map for (3.2).

Definition 3.4.11 (Reachability and approximate reachability for (3.2)) *Same as Definition 3.4.7 and Definition 3.4.8, except we replace $H \in C([0,T])$ and Ξ by $I \in PC([0,T])$ and Ξ_D, respectively.*

Proposition 3.4.12 *Let the Preisach measure be nonnegative and nonsingular. The state space Ψ for (3.2) is not reachable, but approximately reachable.*

Proof Ψ is not reachable since the state space for the Preisach operator is not reachable. We now show Ψ is approximately reachable, i.e., given $\psi_1, \psi_2 \in \Psi$, $\epsilon > 0$, there exists $I \in PC([0,T])$, such that

$$\Xi_D[I, \psi_1](T) = \psi_r \in \Psi_r, \tag{3.58}$$

with $d(\psi_r, \psi_2) \leq \epsilon$. Indeed, from the rate-independence property of the Preisach operator and Proposition 3.4.10, we can find $\widetilde{H} \in C^1([0,T])$ (the space of continuously differentiable functions), such that $\Xi[\widetilde{H}, \psi_1](T) = \psi_r \in \Psi_r$ with $d(\psi_r, \psi_2) \leq \epsilon$. By the hypothesis, $\widetilde{M} = \Gamma[\widetilde{H}, \psi_1] \in C([0,T])$ and it is a.e. differentiable. Then by the uniqueness of the solution to (3.2), the input

$$I = \frac{\dot{\widetilde{H}} + \dot{\widetilde{M}}}{c_1} + \frac{\widetilde{H}}{c_0}$$

satisfies (3.58).

■

3.4.4 Observability

Definition 3.4.13 (Observability for the Preisach operator) *We say $\psi_1 \in \Psi$ is distinguishable from $\psi_2 \in \Psi$, if there exists a finite $T > 0$ and $H \in C([0,T])$, such that $M_1(t') \neq M_2(t')$ for some $t' \in [0,T]$, where $M_i = \Gamma[H, \psi_i]$, $i = 1, 2$. The Preisach operator is observable if any state $\psi \in \Psi$ is distinguishable from any other state.*

Proposition 3.4.14 *Recall the definition of ζ_ψ (Subsection 2.1.1). Let the Preisach measure be nonnegative, and nonsingular with density μ. The Preisach operator is*

observable if and only if $\forall \psi_1, \psi_2 \in \Psi$ *and* $\psi_1 \neq \psi_2$,

$$\int \int_P \mu(\beta, \alpha) |\zeta_{\psi_1}(\beta, \alpha) - \zeta_{\psi_2}(\beta, \alpha)| d\beta d\alpha > 0. \tag{3.59}$$

Proof If (3.59) holds, straightforward analysis on the Preisach plane shows any state can be distinguished from any other state. Conversely, if (3.59) is violated for some pair ψ_1, ψ_2, then one can find $\psi_1' \neq \psi_2'$ both intersecting the line $\alpha = \beta$ at the same point and

$$\int \int_P \mu(\beta, \alpha) |\zeta_{\psi_1'}(\beta, \alpha) - \zeta_{\psi_2'}(\beta, \alpha)| d\beta d\alpha = 0. \tag{3.60}$$

It's obvious that ψ_1' is not distinguishable from ψ_2'. ■

As in Subsection 3.4.2, we take $I(\cdot)$ as the input and $\{H(\cdot), M(\cdot)\}$ as the output of the system (3.2).

Definition 3.4.15 (Observability for (3.2)) *Let* $\psi_1, \psi_2 \in \Psi$. *We say* ψ_1 *is distinguishable from* ψ_2, *if there exists a finite* $T > 0$ *and* $I \in PC([0, T])$, *such that* $H_1(t') \neq H_2(t')$ *or* $M_1(t') \neq M_2(t')$ *for some* $t' \in [0, T]$. *The system (3.2) is observable if any state* $\psi \in \Psi$ *is distinguishable from any other state.*

Proposition 3.4.16 *Let the Preisach measure be nonnegative, and nonsingular with density* μ. *The system (3.2) is observable if and only if* $\forall \psi_1, \psi_2 \in \Psi$ *and* $\psi_1 \neq \psi_2$,*(3.59) holds.*

Proof We first show if (3.59) holds, (3.2) is observable. Let's consider $\psi_1, \psi_2 \in \Psi$ such that $H_1(0) = H_2(0)$ and $M_1(0) = M_2(0)$ (otherwise ψ_1 is already distinguished from ψ_2 by taking $t' = 0$). From (3.59),

$$M_1(0) - M_2(0) = 2 \int \int_{D_1} \omega(r, s) ds dr - 2 \int \int_{D_2} \omega(r, s) ds dr + \nu_\infty = 0, \tag{3.61}$$

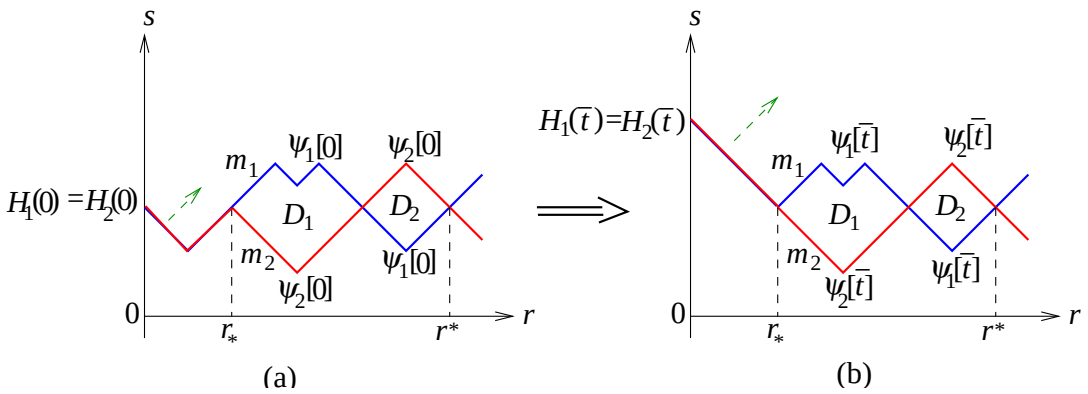

Figure 3.7: Illustration of the proof of Proposition 3.4.16.

where D_1 and D_2 are regions as illustrated in Figure 3.7(a) and ν_∞ represents the contribution from the region $r > r^*$. Applying a monotonically increasing (or decreasing, resp.) input I with $I(0) \geq \frac{H_1(0)}{c_0}$ ($I(0) \leq \frac{H_1(0)}{c_0}$, resp.). Then

$$\{H_1(t), M_1(t)\} = \{H_2(t), M_2(t)\}$$

until at some time $\bar{t}$, the segment m_2 (m_1, resp.) is touched and the area D_1 starts to change (Figure 3.7 (b)). This breaks the balance in (3.61) and we will observe $M_1(t') \neq M_2(t')$ for some $t' > \bar{t}$.

Conversely, if (3.59) is violated for some $\psi_1, \psi_2 \in \Psi$. Then as in the proof of Proposition 3.4.14, we can find $\psi_1' \neq \psi_2'$ and they satisfy (3.60) and the corresponding $H_1'(0) = H_2'(0)$. Then we can show (using, e.g., the Euler polygon method), for any $I(\cdot) \in PC([0,T])$, $\{H_1', M_1'\} \equiv \{H_2', M_2'\}$. ■

3.5 Existence of Periodic Solutions under Periodic Forcing

We observe a periodic motion of the actuator head when a periodic input is applied (Figure 3.1). We want to investigate whether the model (3.2), (3.3) has this same property. Eq. (3.3) is a linear system when we treat $M^2(t)$ as its input, and it's easy to show it has an *asymptotically orbitally stable* periodic solution [54] when M^2 is periodic. Therefore we need only study whether (3.2) has periodic solutions when the input I is periodic.

Brokate and Pokrovskii studied asymptotic stability of oscillations in nonlinear ODE systems with small hysteretic perturbations [19], where the hysteresis nonlinearity is required to satisfy certain contraction property. Studies on oscillations in systems with hysteresis can also be found in [56, 14, 66]. Techniques from these papers can not be directly applied to (3.2), but the key idea of finding a fixed point of some operator in these papers proves to be useful in our following result:

Theorem 3.5.1 *Let the Preisach measure be nonnegative and nonsingular. Define* $J_I = [\frac{H_{min}}{c_0}, \frac{H_{max}}{c_0}]$. *Let* $I \in C_{J_I}([0,\infty))$ *be T-periodic, i.e.,*

$$I(t+T) = I(t),\ \forall t \geq 0.$$

Let $\Xi_D : C([0,\infty)) \times \Psi \to C([0,\infty), \Psi)$ *be the state evolution map for (3.2). Then there exists* $\psi_0 \in \Psi$, *such that* $\Xi_D[I,\psi_0](t+T) = \Xi_D[I,\psi_0](t),\ \forall t \geq 0$.

Proof We will use the Schauder fixed point theorem (Appendix A). Recall Definition 2.1.1 and Figure 2.4. It's obvious that Ψ is a convex set. Denote $L_1([0,r_0])$ the Banach space of integrable functions on $[0,r_0]$. First we show Ψ is a

closed subset of $L_1([0, r_0])$, where we borrow some ideas from the proof of Theorem 3.3 in [37].

In (r, s) coordinates, any $\psi \in \Psi$ is a continuous function of r on $[0, r_0]$, and thus $\psi \in L_1([0, r_0])$. Let $\{\psi_n \in \Psi\}$ be a sequence that converges to $\widetilde{\psi} \in L_1([0, r_0])$ (in the L_1 norm). By definition of Ψ, $\{\psi_n\}$ is equicontinuous and equibounded. Therefore by the Ascoli-Arzelá Theorem, a subsequence $\psi_{n_k} \to \bar{\psi} \in \Psi$ uniformly on $[0, r_0]$, which implies $\{\psi_{n_k}\}$ converges to $\bar{\psi}$ in the L_1 norm. Therefore $\widetilde{\psi} = \bar{\psi}$ and Ψ is closed.

Given $\psi_0 \in \Psi$ and a T-periodic $I \in C_{J_I}([0, \infty))$, we have

$$\Xi_D[I, \psi_0](t) \in \Psi, \, \forall t \geq 0,$$

from Proposition 3.4.4. We then define the map $\Xi_D^T : \Psi \to \Psi$ by

$$\Xi_D^T(\psi_0) = \Xi_D[I, \psi_0](T), \; \forall \psi_0 \in \Psi. \tag{3.62}$$

The metric of $L_1([0, r_0])$ on Ψ is equivalent to the metric (3.36), which is further equivalent to the metric (3.37) under the assumptions on the Preisach measure. Hence Ξ_D^T is continuous by Theorem 3.2.8. Also Ξ_D^T is a compact mapping since Ψ itself is compact. Therefore Ξ_D^T has a fixed point by Schauder's fixed point theorem, and this completes the proof. ■

Remark 3.5.2 *Theorem 3.5.1 implies that the corresponding solution* $\{H(\cdot), M(\cdot)\}$ *is also periodic.*

3.5.1 Existence of recurrent solutions

Pokrovskii and his colleagues studied existence of so called *recurrent oscillations* in the differential-operator equation of the form [64, 65]:

$$\begin{cases} \dot{x}(t) = f(t, x(t), z(t)) \\ z(t) = \Lambda[x(\cdot), z(t_0)](t) \end{cases}, \tag{3.63}$$

where $\forall t$, $x(t) \in \mathbb{R}^d$, $z(t)$ typically represents the internal state of some hysteresis operator and belongs to an infinite dimensional metric space $\mathcal{Z}$ with the metric $d_{\mathcal{Z}}$, and $\Lambda[\cdot, \cdot]$ is the evolution map for the state z. For instance, for the case of the Preisach operator Γ, $\mathcal{Z} = \Psi$ and $\Lambda = \Xi$.

Roughly speaking, a function $u(t)$ with $-\infty < t < \infty$ is *recurrent* if, given $\epsilon > 0$, $T > 0$, there exists $A > 0$, such that $\forall \tau \in (-\infty, \infty)$, any interval longer than A contains σ such that the function $t \to u(t + \tau)$ is "ϵ-close" to the function $t \to u(t+\sigma)$, $t \in [-T, T]$. The class of recurrent functions includes periodic, quasi-periodic, almost-periodic functions and many more [65]. It was shown in [64, 65] that (3.63) has at least a recurrent solution, if $f(t, x, z)$ is recurrent in t and (3.63) has a uniformly bounded solution. One can adapt the proof of this result to get the following: when I is recurrent, (3.19) (and thus (3.2)) has at least a recurrent solution.

Remark 3.5.3 *One should not say the result of existence of recurrent solutions is stronger or weaker than that of existence of periodic solutions (Theorem 3.5.1). In some sense, the result of existence of recurrent solutions is more general but it does not imply Theorem 3.5.1.*

3.6 Numerical Simulation of the Model

Numerically solving (3.2) helps predict behaviors of the model, verify theoretical analysis, and validate the model by comparing the simulation result to the experimental measurement. It will also prove useful in parameter identification for the model.

3.6.1 Explicit Euler algorithm

The Euler polygon method was used in establishing the well-posedness of (3.2) in the proof of Theorem 3.2.2. Here we use the Euler method to obtain an approximate solution to (3.2). Given the memory curve $\psi[t_0]$ at time t_0 and the input $I(\cdot)$, approximate values of H and M at $t_0 + h$ are computed via

$$\begin{cases} \frac{\widetilde{H}(t_0+h)-H(t_0)}{h} + \frac{\widetilde{M}(t_0+h)-M(t_0)}{h} = c_1(I(t_0) - \frac{H(t_0)}{c_0}) \\ \widetilde{M}(t_0+h) = \Gamma[\widetilde{H}(t_0+h), \psi[t_0]] \end{cases}, \tag{3.64}$$

where h is the time step size (see the comments in the proof of Theorem 3.2.2 for proper understanding of the notation in (3.64)). We call (3.64) the *explicit Euler* scheme since $\widetilde{H}(t_0 + h)$ is not involved in the right-hand side of the first equation in (3.64), following the terminology in the ODE literature [40].

As noted in the proof of Theorem 3.2.2, (3.64) has a unique solution if the Preisach measure is nonnegative and nonsingular. Eq. (3.64) can be solved by adapting the inversion algorithms for Γ discussed in Subsection 2.3.2. Denote the right-hand side of the first equation in (3.64) as g_0. We consider the case $g_0 > 0$ and the other case can be dealt with similarly.

If the Preisach measure satisfies the assumptions of Proposition 2.3.4, the fol-

lowing algorithm can be used to solve (3.64):

$$\begin{cases} H^{(n+1)} = H^{(n)} + \frac{l^{(n)}}{1+\bar{\nu}} \\ M^{(n+1)} = \Gamma[H^{(n+1)}, \psi^{(n)}] \\ l^{(n+1)} = l^{(n)} - (H^{(n+1)} - H^{(n)}) - (M^{(n+1)} - M^{(n)}), \end{cases} \tag{3.65}$$

with $\bar{\nu}$ as defined in (2.20), $H^{(0)} = H(t_0)$, $M^{(0)} = M(t_0)$, $l^{(0)} = hg_0$.

If the density μ is piecewise uniform, obtained from the collection of identified weighting masses as discussed in Subsection 2.3.2, the algorithm (2.22) can be modified to solve (3.64). At iteration n, evaluate $d_1^{(n)}$, $d_2^{(n)}$, $a_1^{(n)}$ and $a_2^{(n)}$ as in Subsection 2.3.2. Then solve

$$a_2^{(n)}(d_0^{(n)})^2 + (1 + a_1^{(n)})d_0^n = l^{(n)}$$

for $d_0^{(n)}$, where $l^{(0)} = hg_0$, and

$$l^{(n+1)} = l^{(n)} - (H^{(n+1)} - H^{(n)}) - (M^{(n+1)} - M^{(n)}), \forall n \geq 0.$$

Then iteration of (2.22) will yield the solution to (3.64).

3.6.2 Accuracy of the Euler algorithm

We have the following result about accuracy of the algorithm (3.64):

Proposition 3.6.1 *Assume that the Preisach measure is nonnegative, and non-singular with a piecewise continuous density. Assume that the input $I(\cdot)$ is continuous and bounded. Consider the algorithm (3.64). Let the true solution to (3.2) be $\{H(\cdot), M(\cdot)\}$. Assume $\frac{dM}{dH}(\psi[t_0], \pm)$ and the derivatives of $H(t)$ and $M(t)$ at t_0 exist. Then*

$$|\widetilde{H}(t_0 + h) - H(t_0 + h)| = \mathcal{O}(h^2), \tag{3.66}$$

$$|\widetilde{M}(t_0 + h) - M(t_0 + h)| = \mathcal{O}(h^2). \tag{3.67}$$

Proof Denote g_0 the right-hand side of the first equation in (3.64). Taylor series expansion of H and M at t_0 gives us

$$H(t_0+h) = H(t_0) + \dot{H}(t_0)h + \mathcal{O}(h^2), \tag{3.68}$$

$$M(t_0+h) = M(t_0) + \dot{M}(t_0)h + \mathcal{O}(h^2), \tag{3.69}$$

where

$$\dot{H}(t_0) = \frac{g_0}{1+\frac{dM}{dH}(\psi[t_0], sgn(g_0))},$$

and

$$\dot{M}(t_0) = \frac{dM}{dH}(\psi[t_0], sgn(g_0))\dot{H}(t_0).$$

From (3.64) and the piecewise monotonicity property of Γ,

$$|\widetilde{H}(t_0+h) - H(t_0)| \le h|g_0| \le hC, \tag{3.70}$$

for some constant $C > 0$. From this we have

$$\begin{aligned} & \widetilde{M}(t_0+h) - M(t_0) \\ = \; & \frac{dM}{dH}(\psi[t_0], sgn(g_0))(\widetilde{H}(t_0+h) - H(t_0)) + \mathcal{O}(|\widetilde{H}(t_0+h) - H(t_0)|^2) \\ = \; & \frac{dM}{dH}(\psi[t_0], sgn(g_0))(\widetilde{H}(t_0+h) - H(t_0)) + \mathcal{O}(h^2). \end{aligned} \tag{3.71}$$

Combining (3.64) and (3.71), we have

$$\widetilde{H}(t_0+h) = H(t_0) + \frac{hg_0}{1+\frac{dM}{dH}(\psi[t_0], sgn(g_0))} + \mathcal{O}(h^2). \tag{3.72}$$

Then (3.68) and (3.72) lead to the estimate (3.66), while (3.69), (3.71) and (3.72) lead to (3.67). ■

We have seen the local error (the error in one step) for the algorithm (3.64) is $\mathcal{O}(h^2)$ and thus the global error is $\mathcal{O}(h)$. This is consistent with the accuracy order of the Euler method in numerical integration of usual ODEs.

A natural question to ask is whether we can obtain algorithms of high order accuracy for solving (3.2) by properly adapting high order integration methods for ODEs, e.g.,the mid-point rule and other Runge-Kutta methods. From our preliminary investigation, the answer appears to be "no". One of the difficulties is due to the dependence of "$\frac{dM}{dH}$" on the sign of $\dot{H}$.

3.6.3 Implicit Euler algorithm

Implicit methods perform better than explicit ones for many problems, especially for stiff problems [41]. Existence of fast transient dynamics in a system is a typical cause of stiffness. Eq. (3.2) is stiff, which one can see easily after it is rewritten as (3.49). Therefore we propose an implicit Euler algorithm to solve (3.2):

$$\begin{cases} \frac{\widetilde{H}(t_0+h)-H(t_0)}{h} + \frac{\widetilde{M}(t_0+h)-M(t_0)}{h} = c_1(I(t_0+h) - \frac{\widetilde{H}(t_0+h)}{c_0}) \\ \widetilde{M}(t_0+h) = \Gamma[\widetilde{H}(t_0+h), \psi[t_0]] \end{cases} . \tag{3.73}$$

Solving (3.73) does not require more effort than solving (3.64) since (3.73) can be rewritten as

$$\begin{cases} (\frac{1}{h} + \frac{c_1}{c_0})(\widetilde{H}(t_0+h) - H(t_0)) + \frac{\widetilde{M}(t_0+h)-M(t_0)}{h} = c_1(I(t_0+h) - \frac{H(t_0)}{c_0}) \\ \widetilde{M}(t_0+h) = \Gamma[\widetilde{H}(t_0+h), \psi[t_0]] \end{cases} , \tag{3.74}$$

which carries the same structure of (3.64). Figure 3.8 compares the performance of the explicit scheme (3.64) and the implicit scheme (3.73). Same input I is applied. The step size $h = 8 \times 10^{-5}$ second. We can see that the implicit algorithm is much more stable and it can provide meaningful solutions even if h is not very small.

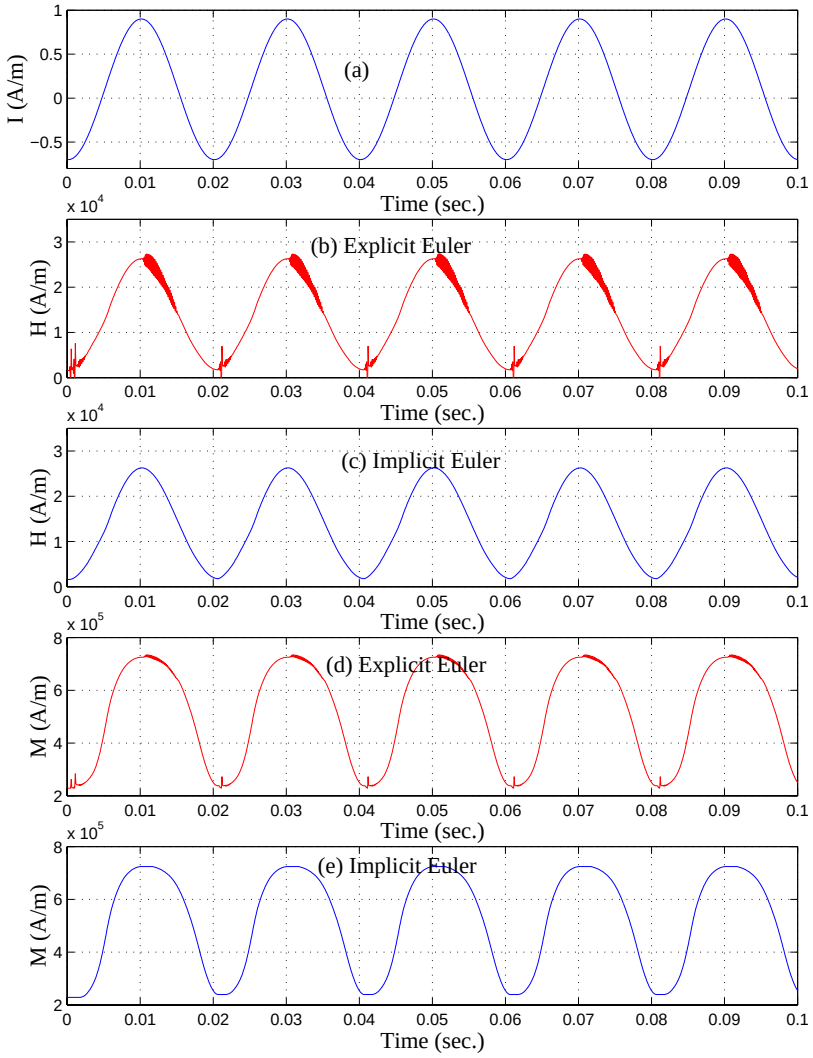

Figure 3.8: Comparison of the implicit Euler scheme with the explicit Euler scheme. (a): the input current; (b), (d): trajectories of H, M computed by the explicit scheme; (c), (e): trajectories of H, M computed by the implicit scheme.

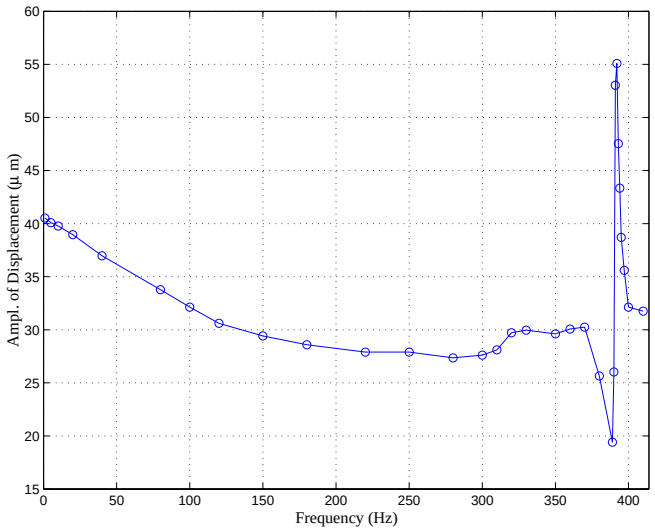

Figure 3.9: Displacement amplitude vs. input frequency.

3.7 Parameter Identification

In this section we discuss how to identify parameters involved in the model (3.2) and (3.3). The Preisach measure is identified as described in Section 2.2. The following parameters are provided by the manufacturer (some of them presented already in Section 2.2): $N_m = 1300$, $A_m = 2.83 \times 10^{-5}\text{m}^2$, $l_{rod} = 5.13 \times 10^{-2}\text{m}$, $M_s = 7.87 \times 10^5\text{A/m}$, $c_0 = 1.54 \times 10^4/\text{m}$. The saturation magnetostriction λ_s is identified to be 0.001313. To estimate the first resonant frequency, we apply sinusoidal inputs of the same amplitude but different frequencies and measure the amplitudes of the displacement. Figure 3.9 displays the displacement amplitudes at different frequencies and we determine the first resonant frequency to be 392 Hz.

We are now left with identification of R_{eddy} and ξ. Generally it's impossible to write down the explicit solution of (3.2) in terms of R_{eddy}, therefore we can not identify R_{eddy} directly. A theoretical value of R_{eddy} can be computed with the

formula $R_{eddy} = \frac{8\pi\rho N_m^2(b^2-a^2)}{l_{rod}(b^2+a^2)}$ [82], where ρ is the resistivity of the magnetostrictive material, b and a are the outer and inner radii of the magnetostrictive rod. We use this formula to obtain an upper bound $\bar{R}$ of R_{eddy} by letting $a = 0$. Plugging in $\rho = 5.8 \times 10^{-7}\Omega$/m for Terfenol-D, we get $\bar{R} = 480.2\Omega$. We then discretize $[0, \bar{R}]$ and denote the mesh points by $R_{eddy}^{(i)}$, $i = 1, \cdots, N$. The discretization need not be uniform and we make it finer in the region where the dynamics of (3.2) is more sensitive to R_{eddy}.

We observe a periodic motion of the actuator head when a periodic input is applied. We have also shown (3.2) and (3.3) have periodic solutions if $I(\cdot)$ is periodic (Section 3.5) . These observations motivate the following scheme to identify R_{eddy} and ξ:

- **Step 1.** We apply a sinusoidal current (with some dc shift if necessary) $I(\cdot)$ with frequency f to the actuator and measure the phase lag $\theta_{y,I}$ between the fundamental frequency component of the displacement and the current;

- **Step 2.** For each $R_{eddy}^{(i)}$, we numerically integrate (3.2) with $I(\cdot)$ as the input, and calculate the phase lag $\theta_{M^2,I}$ between the fundamental frequency component of $M^2(\cdot)$ (in its steady state) and $I(\cdot)$.

- **Step 3.** The difference $\theta_{y,I} - \theta_{M^2,I}$ is considered to be the phase lag between the fundamental frequency component of $y(\cdot)$ and that of $M^2(\cdot)$ in (3.3), from which we can compute $\xi^{(i)}$.

Remark 3.7.1 *The idea of relating the phase shift between the output and the input to hysteresis can also be found in [28]. We note that in general, the phase lag depends highly nonlinearly on the initial condition, and the amplitude and the*

frequency of $I(\cdot)$, so we should make sure that the initial condition in simulation is consistent with the condition in the experiment.

We repeat the above experiment (Step 1 to Step 3) K times with different input frequencies and denote the damping coefficients as $\{\xi_k^{(i)}\}_{k=1}^K$ for $R_{eddy}^{(i)}$. If $R_{eddy}^{(i)}$ is close to the true parameter R_{eddy}, $\xi_k^{(i)}$ should not vary much with k. Therefore we pick $i^* \in \{1, \cdots, N\}$ such that $\{\xi_k^{(i^*)}\}_{k=1}^K$ has the minimum variance, and estimate R_{eddy} via $R_{eddy} = R_{eddy}^{(i^*)}$ and let ξ be the mean of $\{\xi_k^{(i^*)}\}$.

Figure 3.10 shows the variation of ξ with respect to frequency for different $R_{eddy}^{(i)}$'s. The parameters are determined to be $R_{eddy} = 70\Omega$, $\xi = 0.7783$. Figure 3.11 compares the rate-dependent hysteresis loops measured in experiments to those obtained through simulation based on the identified parameters. We see that the simulation results agree with the experimental results reasonably well up to 200 Hz. Since the depth of eddy current penetration depends on the frequency, so does R_{eddy}. This explains why the comparison in Figure 3.11 goes worse when the frequency is beyond 200 Hz. In practice, one can identify R_{eddy} according to the operating frequency range of the specific application.

3.8 An Inverse Control Scheme

In this section we propose an inverse control scheme for the dynamic hysteresis model (3.2) and (3.3). We first formally describe the scheme to highlight the idea, then we discuss how to implement it.

Given a desired displacement trajectory $\bar{y}(\cdot) \in C^2([0,T])$, we compute for every t, $\bar{u}(t) = \frac{M_s^2}{\omega_0^2 l_{rod} \lambda_s}(\ddot{\bar{y}}(t) + 2\xi\omega_0\dot{\bar{y}}(t) + \omega_0^2\bar{y}(t))$ and then let $\bar{M}(t) = \sqrt{u(t)}$. Next we obtain $\bar{H}(\cdot)$ from $\bar{M}(\cdot)$ by inverting the Preisach operator Γ. We then (formally)

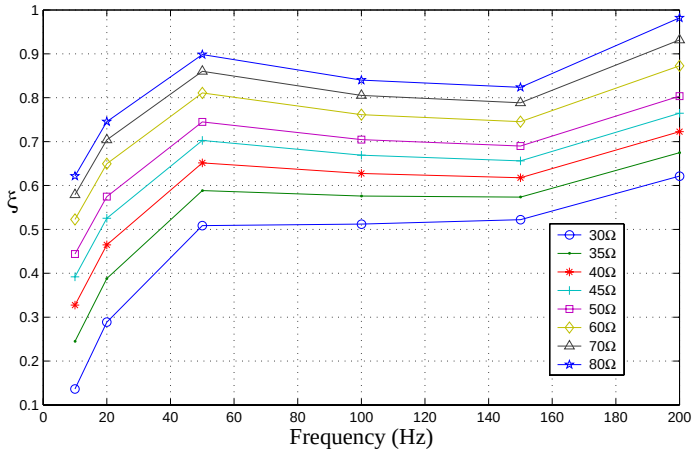

Figure 3.10: Identification of R_{eddy} and ξ.

let

$$I(t) = \frac{1}{c_1}(\dot{\bar{H}}(t) + \dot{\bar{M}}(t) + \frac{\bar{H}(t)}{c_0}). \tag{3.75}$$

Due to the uniqueness of the solution to (3.2) and (3.3), we expect the output $y(\cdot)$ under $I(\cdot)$ to agree with $\bar{y}(\cdot)$.

All we have just said is the ideal case. Several issues need to be taken care of in implementing the scheme.

First of all, the desired trajectory $\bar{y}(\cdot)$ may not be twice differentiable. For (3.3), let $D([0,T])$ be the space of attainable $y(\cdot)$ under some control $u(\cdot) \in C([0,T])$ and $0 \leq u(t) \leq M_s^2$, $\forall t \in [0,T]$ (u plays the role of M^2 in (3.3)). In general, we need first find $y^*(\cdot) \in D([0,T])$ which is closest to $\bar{y}(\cdot)$ in the sup norm (i.e., the projection of $\bar{y}(\cdot)$ on $D([0,T])$) and then work with $y^*(\cdot)$. In our experiments below, however, $\bar{y}$ is picked from $D([0,T])$ since our main objective is to validate the model.

Since (3.3) is a linear system, sometimes $\bar{u}(\cdot)$ (and therefore $\bar{M}(\cdot)$) is available as the output of some linear controller. In such cases, the inverse problem becomes how to get I from $\bar{M}$ and the solution to it is just (3.75).

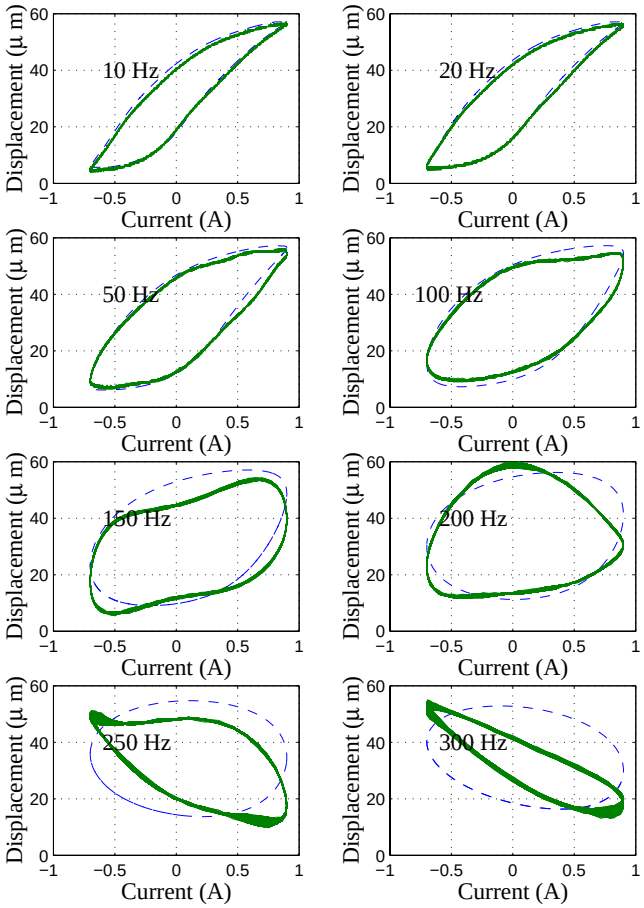

Figure 3.11: Model validation. Solid line: experimental measurement; Dashed line: numerical prediction.

Another question is that $\bar{M}(\cdot)$ or $\bar{H}(\cdot)$ may not be differentiable. In general this should not bother us because we work in the discrete-time setting (for digital computer control) and the derivatives are approximated by the finite difference method.

Three inverse control schemes have been implemented to track a desired displacement trajectory. The first one is based on the dynamic hysteresis model, the second one is based on the Preisach model alone (c.f. Section 2.3), and the third one is based on the non-hysteretic model described in Subsection 2.4.3. The

sampling period used is 0.05 ms. Experimental results are shown in Figure 3.12 - 3.14. In each figure, the displacement trajectories (both the desired and the measured), the tracking error and the input current are displayed. We can see that the performance of the first scheme is very satisfactory. This shows that the dynamic hysteresis model can capture high frequency effects in the actuator, and that our identification and inverse control schemes are effective.

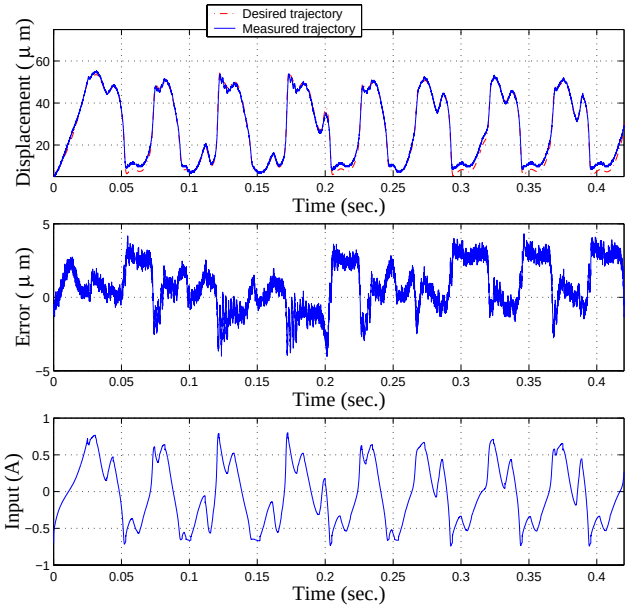

Figure 3.12: Trajectory tracking based on the dynamical hysteresis model.

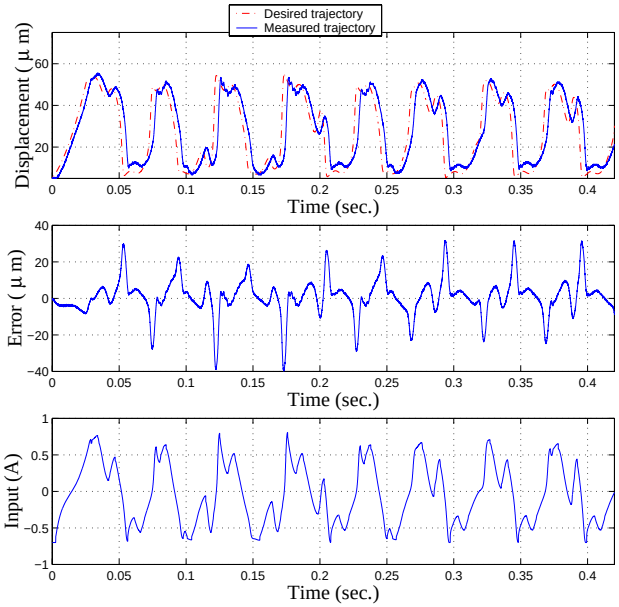

Figure 3.13: Trajectory tracking based on the Preisach model alone.

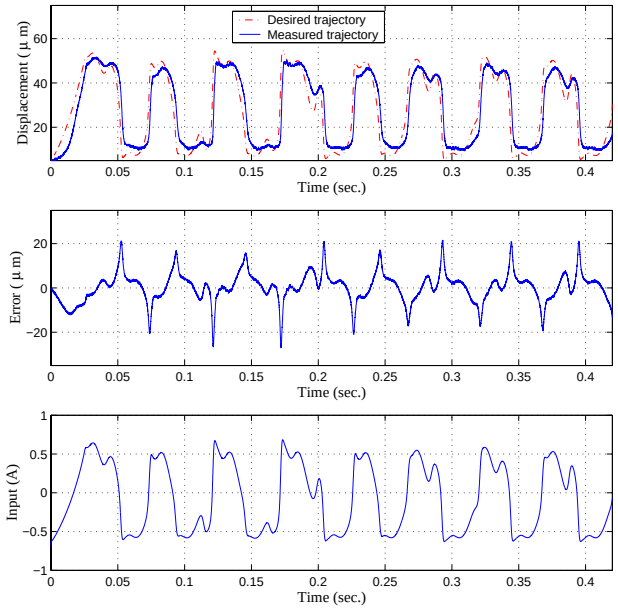

Figure 3.14: Trajectory tracking based on the non-hysteretic model.

Chapter 4

A Robust Control Framework for Smart Actuators

Due to the open loop nature of inverse compensation, its performance is susceptible to model uncertainties and to errors introduced by the inverse schemes. In this chapter we address this problem by combining inverse control with robust control techniques. Appendix C provides the background (and notation) on robust control necessary for development of results in this chapter.

Figure 4.1 illustrates the idea underlying the robust controller design method for smart actuators. We consider the discrete-time setting in the interest of digital control. W and $\widehat{G}_a(\lambda)$ represent the nonlinear part and the linear part of the actuator model, respectively. W could be a Preisach operator (rate-independent hysteresis), or a rate-dependent hysteretic operator, like (3.2), together with other nonlinearities, e.g., the square operator in Figure 3.2. We recall (see Appendix C) that λ-transform $\widehat{G}(\lambda)$ of a LTI system G is essentially the usual z-transform of G with $\lambda = z^{-1}$. $\widehat{G}_0(\lambda)$ denotes the plant we want to control. An approximate (right) inverse $\widetilde{W}^{-1}$ is connected in series to W, to approximately cancel out the

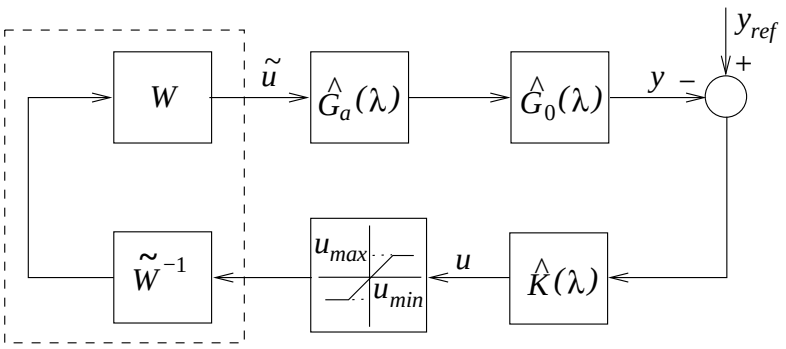

Figure 4.1: A robust control framework for smart actuators.

nonlinearity W. Then a linear controller $\widehat{K}(\lambda)$ is designed for the composite plant $\widehat{G}_0\widehat{G}_a$. In addition, actuator saturation is also considered in Figure 4.1.

As an example, we study the robust trajectory tracking problem. The requirements for the controller can be roughly stated as: in the presence of the inversion error $e_u \stackrel{\triangle}{=} \widetilde{u} - u$ and the model uncertainties in $\widehat{G}_a$ and $\widehat{G}_0$, for all desired trajectories in a certain class,

- the closed-loop system is stable,
- the tracking error is minimized, and
- the output of $\widehat{K}$ does not exceed the saturation limits.

A more precise formulation of the robust control problem will be presented in Section 4.2.

Remark 4.0.1 *We take the saturation limits into account in the design of $\widehat{K}$ to ensure that the overall system operates in the linear region and thus predictions based on the linear design are credible. We will see, however, that strictly enforcing the saturation constraint at the stage of controller design compromises the tracking*

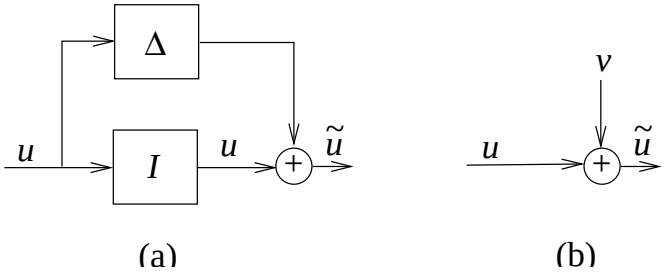

Figure 4.2: Two ways to represent the inversion error.

performance. Further discussions on how to incorporate the saturation nonlinearity into controller design will be provided in Section 4.4.

A first step toward the robust controller design is to quantify the inversion error e_u.

4.1 Quantification of the Inversion Error

In general $\widetilde{W}^{-1}$ is not an exact inverse of W (Figure 4.1) and two factors may contribute to the inversion error: parameter uncertainties and non-existence of exact inverse schemes.

There are two possible ways to model e_u. The first one is to model it as the output of some uncertainty block Δ (Figure 4.2(a)) and the other one is to simply model it as an exogenous disturbance v (Figure 4.2(b)). As we will see shortly, e_u is independent of u and it is possible that $e_u \neq 0$ for $u = 0$. Therefore there exists no stable Δ such that $e_u = \Delta u$, and we will treat $e_u = v$ as an external noise.

We need specify the signal spaces for quantification of the inversion error. The inversion error for the Preisach operator is bounded in magnitude instead of in energy. Hence a natural choice for the signal spaces is l_∞ and not l_2. Also it is more appropriate to use l_∞ for the desired trajectory and the tracking error. Another

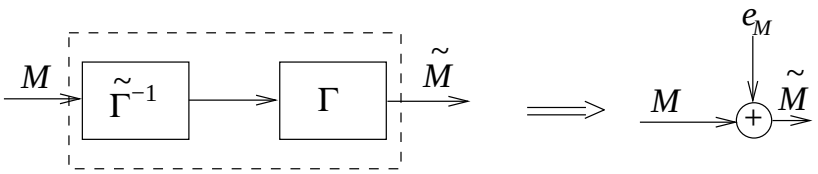

Figure 4.3: The error in inversion of the Preisach operator.

advantage of using l_∞ for signals is that the actuator saturation constraint can be easily handled in the corresponding l_1 robust control theory, while it's very hard to be formulated in $\mathcal{H}_\infty$ control theory.

We first quantify the error in inversion of the Preisach operator, and then consider a new inversion scheme for the dynamic hysteresis model (3.2) and quantify the error introduced by this scheme. In both cases we are concerned with quantification of $e_M = \widetilde{M} - M$, where $\widetilde{M}$ and M denote the trajectories of achieved magnetization and desired magnetization, respectively. Finally we indicate how to obtain e_u from e_M when a square nonlinearity is included in W.

4.1.1 Error in inversion of the Preisach operator

Consider Figure 4.3, where Γ is a Preisach operator with nonsingular Preisach measure ν.

Error due to an inversion scheme

Assume we are given the Preisach measure. Consider the inversion algorithm (2.21) with the stopping criterion $|M^{(n)} - \bar{M}| \leq \epsilon$. Then it's straightforward that $\| e_M \|_\infty \leq \epsilon$ for any $M \in l_\infty$.

Error due to the parameter uncertainty

If the Preisach measure is not given, we can discretize the Preisach plane and identify a collection of weighting masses, as discussed in Subsection 2.2.2. We can then obtain a nonsingular Preisach measure ν_p with a piecewise uniform density μ_p by distributing each weighting mass uniformly over the corresponding cell in the discretization grid. We have presented an exact inversion scheme (2.22) for the Preisach operator $\widetilde{\Gamma}$ with measure ν_p (Subsection 2.3.2). For the inverse algorithm (2.22), e_M can be attributed to the measure uncertainty $|\nu_p - \nu|$. We now quantify e_M in terms of the identification error and the discretization level.

Proposition 4.1.1 *Let the true Preisach measure ν be nonnegative, and nonsingular with density μ. Assume $\mu(\beta, \alpha) \leq \bar{\mu}$, for any (β, α) in the Preisach plane, where $\bar{\mu} > 0$ is a constant. Let $H_r = \alpha_0 - \beta_0$, where $[\beta_0, \alpha_0]$ is the input range of the Preisach operator. Given a discretization of level L, denote the integral of μ over a cell i (either square or triangular) as ν_i^0, $1 \leq i \leq N_c$, where N_c is the total number of cells. Consider the measure identification scheme in Subsection 2.2.2 and denote by ν_i the identified mass for cell i, $1 \leq i \leq N_c$. Assume that the relative error in identification is δ_I, i.e.,*

$$\frac{|\nu_i - \nu_i^0|}{\nu_i^0} \leq \delta_I, \ 1 \leq i \leq N_c.$$

Assume that the initial memory curve $\psi_0 \in \Psi$ is given. Then for any $M \in l_\infty$, any $\psi_0 \in \Psi$,

$$\| e_M \|_\infty < \delta_I M_s + \frac{2\bar{\mu} H_r^2}{L}, \tag{4.1}$$

where M_s is the positive saturation corresponding to ν.

Proof Define μ_p as discussed earlier. We obtain another Preisach measure with a piecewise constant density μ_p^0 by distributing ν_i^0 uniformly over the cell i,

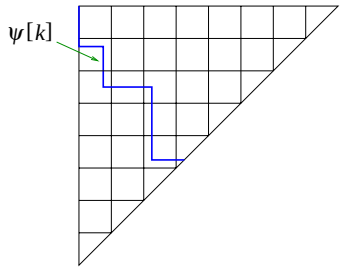

Figure 4.4: Illustration of the proof of Proposition 4.1.1 ($L = 8$).

$1 \leq i \leq N_c$. To distinguish the Preisach operators, we will put the corresponding density as the subscript of Γ, e.g., Γ_μ means the Preisach operator with the density μ.

Given $M \in l_\infty$ and ψ_0, we denote the output of $\widetilde{\Gamma}^{-1}$ in Figure 4.3 as H. Then, $\forall k \geq 0$,

$$\begin{aligned} & |e_M[k]| = |\Gamma_\mu[H, \psi_0][k] - \Gamma_{\mu_p}[H, \psi_0][k]| \\ \leq \; & |\Gamma_\mu[H, \psi_0][k] - \Gamma_{\mu_p^0}[H, \psi_0][k]| + |\Gamma_{\mu_p^0}[H, \psi_0][k] - \Gamma_{\mu_p}[H, \psi_0][k]|. \end{aligned} \quad (4.2)$$

All three Preisach operators involved in (4.2) share the same memory curve $\psi[k]$, $\forall k \geq 0$. It's obvious that the second term of (4.2) is bounded by $\delta_I M_s$. To bound the first term, we note that for any $k \geq 0$, the memory curve $\psi[k]$ spans $L - 1$ square cells and one triangular cell (Figure 4.4). Any cell not touched by $\psi[k]$ will contribute the same amount to $\Gamma_\mu[H, \psi_0][k]$ and $\Gamma_{\mu_p^0}[H, \psi_0][k]$. Hence the first term of (4.2) is bounded by twice the interal of μ over cells spanned by $\psi[k]$, which is further bounded by

$$\frac{2\bar{\mu}H_r^2(L - \frac{1}{2})}{L^2} < \frac{2\bar{\mu}H_r^2}{L}.$$

This completes the proof. ■

Remark 4.1.2 *From Proposition 4.1.1, the bound on the inversion error consists*

of two parts: the first part is proportional to the relative identification error, and the second part is inversely proportional to the level L of discretization.

Remark 4.1.3 *The assumption that ψ_0 is known is not very restrictive since in many cases we have the choice to initialize the system. On the other hand, if ψ_0 is not known exactly, we can easily include a term in $\| e_M \|_\infty$ which takes care of the uncertainty in ψ_0.*

4.1.2 Error in inversion of the dynamic hysteresis model

Given a desired trajectory of magnetization, we proposed an inverse control scheme (3.75) for the model (3.2) in Section 3.8. But if there is uncertainty in the model parameters, it is very hard (if not impossible) to derive a bound for the inversion error. Here we will present another inversion algorithm. This algorithm leads to an inversion error even if the exact parameters are known, but it will allow us to quantify the inversion error when model uncertainty is considered.

One way to rewrite (3.2) is:

$$\begin{cases} \dot{H}(t) = \frac{c_1}{1+g(t)}(I(t) - \frac{H(t)}{c_0}) \\ M(t) = \Gamma[H, \psi_0](t) \end{cases}, \tag{4.3}$$

where $g(t) = \frac{dM}{dH}(\psi_t, sgn(\dot{H}(t)))$ and $0 \leq g(t) \leq C$ (c.f.(3.45)). We can treat the first equation in (4.3) as a linear time-varying ODE of H, and regard (4.3) as perturbed from the following decoupled system:

$$\begin{cases} \dot{H}(t) = \frac{c_1}{1+\bar{g}}(I(t) - \frac{H(t)}{c_0}) \\ M(t) = \Gamma[H, \psi_0](t) \end{cases}, \tag{4.4}$$

where $\bar{g} \in [0, C]$ is some constant. Based on (4.4), an approximate inversion scheme

for (4.3) is given formally by

$$\begin{cases} H(t) = \Gamma^{-1}[M, \psi_0](t) \\ I(t) = \frac{1+\bar{g}}{c_1}\dot{H}(t) + \frac{H(t)}{c_0} \end{cases}. \tag{4.5}$$

When implementing (4.5) in the discrete time, we have two ways of writing $I[\cdot]$, which correspond to the explicit Euler scheme and the implicit Euler scheme in discretizing the first equation in (4.4), respectively: for $k \geq 0$,

$$I[k] = \frac{1+\bar{g}}{c_1 h}(H[k] - H[k-1]) + \frac{H[k-1]}{c_0}, \tag{4.6}$$

$$I[k] = \frac{1+\bar{g}}{c_1 h}(H[k] - H[k-1]) + \frac{H[k]}{c_0}, \tag{4.7}$$

where h is the time step size, $H[-1] = H[0]$.

Remark 4.1.4 *Direct discretization of the first equation in (4.4) by the explicit Euler scheme (a similar remark applies to the implicit Euler scheme) gives:*

$$I[k] = \frac{1+\bar{g}}{c_1 h}(H[k+1] - H[k]) + \frac{H[k]}{c_0},$$

but this is not a causal system and thus not realizable. An intrinsic delay is introduced in the inversion due to the dynamics in the rate-dependent hysteresis model.

We now want to study the errors caused exclusively by the inversion algorithms, i.e., we assume that we have exact values of parameters. For the inversion algorithm (4.6), the discrete time version of the first equation in (4.3) is obtained by the explicit Euler scheme:

$$\frac{\widetilde{H}[k+1] - \widetilde{H}[k]}{h} = \frac{c_1}{1+g[k]}(I[k] - \frac{\widetilde{H}[k]}{c_0}), \tag{4.8}$$

where $g[k] \stackrel{\triangle}{=} g(kh)$. Similarly, if the inversion algorithm (4.7) is used, we will use the corresponding discrete-time model obtained by the implicit Euler scheme. Figure 4.5(a) shows the problem setup for the explicit Euler case.

For the purpose of deriving the bound on the inversion error, we will not need the exact values of $g[k]$.

Due to the delay caused by the inversion, the error e_M is now defined as (Figure 4.5(d)):

$$e_M[k] \stackrel{\triangle}{=} \widetilde{M}[k] - M[k-1].$$

Proposition 4.1.5 *Let the Preisach measure be nonnegative, and nonsingular with a piecewise continuous density μ. Let the Preisach operator Γ be Lipschitz continuous with Lipschitz constant L_μ. Let $H_m \stackrel{\triangle}{=} \max\{|\beta_0|, |\alpha_0|\}$ where $[\beta_0, \alpha_0]$ is the input range of Γ. Consider the inversion algorithm obtained from the explicit Euler method (Figure 4.5(a)). Let $H[-1] = H[0] = \widetilde{H}[0]$. Pick $\bar{g} \in [0, C]$, where C is the constant as defined in (3.44). Then for any $M \in l_\infty$, for any $\psi_0 \in \Psi$,*

$$\| e_M \|_\infty \leq 2L_\mu \bar{\gamma}_e H_m, \tag{4.9}$$

where

$$\bar{\gamma}_e = \frac{\max\{\bar{g}, \frac{C-\bar{g}}{1+C}\}}{1 - \max\{\frac{hc_1}{c_0} - 1, 1 - \frac{hc_1}{c_0(1+C)}\}}.$$

The optimal $\bar{g}$ to minimize $\bar{\gamma}_e$ is $\frac{C}{C+2}$.

Proof We first derive a bound for e_H, defined by $e_H[k] = \widetilde{H}[k] - H[k-1]$, $k \geq 0$. Substituting (4.6) into (4.8), we have

$$e_H[k+1] = a[k]e_H[k] + b[k](H[k] - H[k-1]), \tag{4.10}$$

where

$$a[k] \stackrel{\triangle}{=} 1 - \frac{hc_1}{c_0(1+g[k])}, \quad b[k] \stackrel{\triangle}{=} \frac{\bar{g} - g[k]}{1+g[k]}.$$

From (4.10), we compute

$$e_H[k+1] = (\prod_{i=0}^{k} a[i])e_H[0] + \sum_{i=0}^{k}(\prod_{j=i+1}^{k} a[j])b[i](H[i] - H[i-1]). \tag{4.11}$$

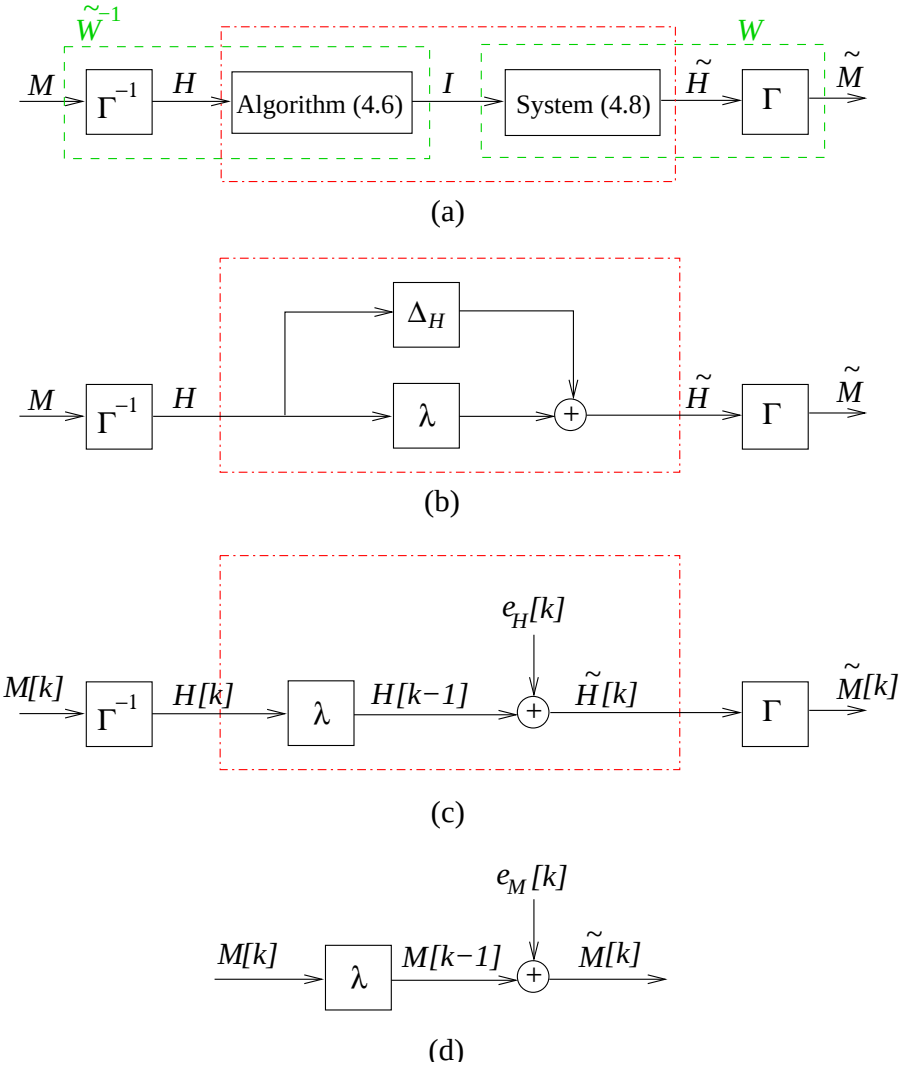

Figure 4.5: The error in inversion of the rate-dependent hysteresis model.

Since $e_H[0] = 0$,

$$\begin{aligned} |e_H[k+1]| &\leq 2(\sum_{i=0}^{k} \bar{a}^i)\bar{b} \parallel H \parallel_\infty \\ &\leq \frac{2\bar{b}}{1-\bar{a}} \parallel H \parallel_\infty, \end{aligned} \tag{4.12}$$

where

$$\bar{a} \stackrel{\triangle}{=} \max_{x\in[0,C]} |1 - \frac{hc_1}{c_0(1+x)}|, \quad \bar{b} \stackrel{\triangle}{=} \max_{x\in[0,C]} |\frac{\bar{g}-x}{1+x}|.$$

It's easy to verify that

$$\bar{a} = \max\{\frac{hc_1}{c_0} - 1, 1 - \frac{hc_1}{c_0(1+C)}\}, \quad \bar{b} = \max\{\bar{g}, \frac{C-\bar{g}}{1+C}\}.$$

Therefore $\parallel e_H \parallel_\infty \leq 2\bar{\gamma}_e \parallel H \parallel_\infty$. The error e_H can be thought of as the output of some uncertainty block Δ_H with the induced gain less than or equal to $2\bar{\gamma}_e$ (Figure 4.5(b)). But since Γ, Γ^{-1} sit outside the dashed box in Figure 4.5(b), we can not carry Δ_H along further. Instead we represent e_H as an exogenous disturbance with magnitude bounded by $2\bar{\gamma}_e H_m$ (Figure 4.5(c)). Eq. (4.9) now follows using the Lipschitz continuity and the time invariance properties of Γ. It's easy to see that the optimal $\bar{g}$ minimizing the error bound is $\frac{C}{C+2}$. ■

Similarly we can derive the error bound for the implicit Euler algorithm (4.7):

Proposition 4.1.6 *Let the assumptions in Proposition 4.1.5 hold. Consider the implicit Euler algorithm (4.7). Then for any $M \in l_\infty$, for any $\psi_0 \in \Psi$,*

$$\parallel e_M \parallel_\infty \leq 2L_\mu \bar{\gamma}_i H_m, \tag{4.13}$$

where

$$\bar{\gamma}_i = \max\{\frac{\bar{g}}{1+\frac{c_1 h}{c_0}}, \frac{C-\bar{g}}{1+C+\frac{c_1 h}{c_0}}\} \frac{c_0(1+C)+c_1 h}{c_1 h}.$$

The optimal $\bar{g}$ to minimize $\bar{\gamma}_i$ is $\frac{(c_0+c_1 h)C}{2(c_0+c_1 h)+c_0 C}$.

Remark 4.1.7 *For the explicit algorithm, the step size h has to be chosen small enough to ensure stability of (4.8) and (4.10). The implicit algorithm, however, is stable $\forall h > 0$. Therefore the implicit algorithm is preferred in general.*

Propositions 4.1.5 and 4.1.6 quantify the errors solely due to inversion algorithms (4.6) and (4.7). It's straightforward to extend the error estimates to the case that there are parametric uncertainties in c_0 and c_1, e.g., when R_{eddy} in (3.2) is not exactly known. The error due to inversion of the Preisach operator and the uncertainty in the Preisach measure can also be included as done in Subsection 4.1.1.

When the square operator is present, like in the case of a magnetostrictive actuator, the estimate of e_u can be derived from that of e_M. Let $u \in [u_{min}, u_{max}]$ (recall Figure 4.1). One can easily verify that

$$\| e_u \|_\infty \leq \| e_M \|_\infty^2 + 2 \| e_M \|_\infty \sqrt{u_{max}}.$$

4.2 Formulation of the Robust Control Problem

We formulate the robust control problem precisely in this section. For simplicity of presentation, we consider $\widehat{G}_0(\lambda)$ to be the identity operator, i.e., we are interested in trajectory tracking of the actuator head itself. We aim to convey the essential ideas for robust control of general smart actuators through the example of controlling the magnetostrictive actuator.

Figure 4.6 shows the closed-loop system after the inverse compensation is done, where the exogenous noise v represents the inversion error. From Section 4.1, $\| v \|_\infty \leq \bar{v}$ where the bound $\bar{v}$ is quantifiable in terms of inverse schemes and parametric uncertainties. $\widehat{G}_a(\lambda)$ stands for the discretized version of the second

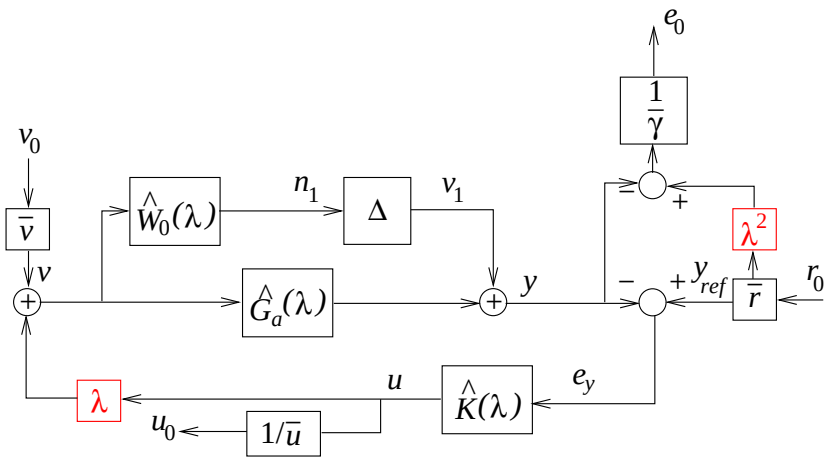

Figure 4.6: Robust control of a magnetostrictive actuator.

order system (3.3). The composition $\Delta \circ \widehat{W}_0(\lambda)$ represents the deviation of the actual plant from the nominal plant $\widehat{G}_a(\lambda)$. We assume that Δ can be any nonlinear operator with $\| \Delta \|_{l_\infty - ind} < 1$. $\widehat{W}_0(\lambda)$ is a weighting function and it reflects that at a higher frequency the model uncertainty is larger.

Let $\| y_{ref} \|_\infty \leq \bar{r}$, where y_{ref} is the reference trajectory. The error $e_y \stackrel{\triangle}{=} y_{ref} - y$ is fed into the controller $\widehat{K}(\lambda)$. The delay λ following $\widehat{K}(\lambda)$ is due to inversion of the dynamic hysteresis model.

Let the saturation limits of the actuator be $-\bar{u}$ and $\bar{u}$ respectively. Then the saturation constraint translates into $\| u_0 \|_\infty \leq 1$, where u_0 is as defined in Figure 4.6. The case $u_{min} \neq -u_{max}$ will be discussed in Section 4.4.

There are two delays in the loop since $\widehat{G}_a(\lambda)$ contains a pure delay. This motivates us to define the tracking error e_0 as

$$e_0[k] = \frac{y_{ref}[k-2] - y[k]}{\gamma}, \tag{4.14}$$

where $\gamma > 0$ is the desired disturbance attenuation level. To ease the formulation, we normalize signals v and y_{ref}, and regard v_0 and r_0 as inputs to the system with

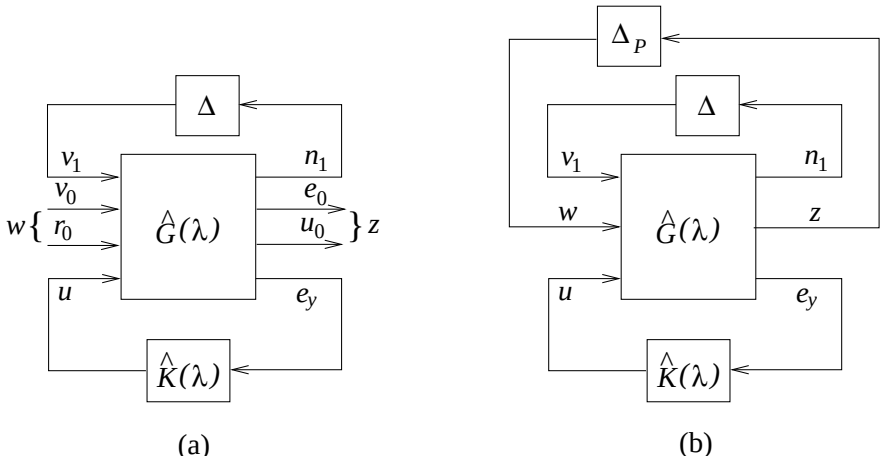

Figure 4.7: Formulation of the robust control problem.

$\| v_0 \|_\infty \leq 1$, $\| r_0 \|_\infty \leq 1$ (Figure 4.6).

The transfer function $\widehat{G}(\lambda)$ of the open-loop system is

$$\begin{pmatrix} n_1 \\ e_0 \\ u_0 \\ \hline e_y \end{pmatrix} = \underbrace{\left(\begin{array}{ccc|c} 0 & \bar{v}\widehat{W}_0(\lambda) & 0 & \lambda\widehat{W}_0(\lambda) \\ -\frac{1}{\gamma} & -\frac{\bar{v}}{\gamma}\widehat{G}_a(\lambda) & \frac{\bar{r}\lambda^2}{\gamma} & -\frac{\lambda}{\gamma}\widehat{G}_a(\lambda) \\ 0 & 0 & 0 & \frac{1}{\bar{u}} \\ \hline -1 & -\bar{v}\widehat{G}_a(\lambda) & \bar{r} & -\lambda\widehat{G}_a(\lambda) \end{array}\right)}_{\widehat{G}(\lambda)} \begin{pmatrix} v_1 \\ v_0 \\ r_0 \\ \hline u \end{pmatrix}. \tag{4.15}$$

In terms of $\widehat{G}$, the closed-loop system in Figure 4.6 can be simplified as in Figure 4.7(a).

The control objective is: find the smallest γ and a stabilizing controller $\widehat{K}(\lambda)$, such that

1. the closed-loop system is stable for any Δ with $\| \Delta \|_{l_\infty - ind} < 1$,
2. $\| e_0 \|_\infty \leq 1$ if $\Delta = 0$, for all v_0, r_0 with $\| v_0 \|_\infty \leq 1$ and $\| r_0 \|_\infty \leq 1$, and
3. $\| u_0 \|_\infty \leq 1$ if $\Delta = 0$, for all v_0, r_0 with $\| v_0 \|_\infty \leq 1$ and $\| r_0 \|_\infty \leq 1$.

If we define the exogenous input w and the regulated output z as

$$w \triangleq \begin{pmatrix} v_0 \\ r_0 \end{pmatrix}, \quad z \triangleq \begin{pmatrix} e_0 \\ u_0 \end{pmatrix},$$

items 2 and 3 above are equivalent to the following:

$$\| \Phi_{zw} \|_1 \leq 1, \tag{4.16}$$

where Φ_{zw} is the mapping from w to z.

By the small gain theorem (Appendix C), (4.16) is equivalent to requiring robust stability of the system when we wrap a nonlinear uncertainty block Δ_P from z to w with $\| \Delta_P \|_{l_\infty - ind} < 1$, as shown in Figure 4.7 (b). Therefore the control problem can be reformulated as: find the smallest γ and a stabilizing controller $\widehat{K}(\lambda)$, such that the closed-loop system in Figure 4.7 (b) is robustly stable for all $\widetilde{\Delta} \in \widetilde{\mathbf{\Delta}}$, where $\widetilde{\mathbf{\Delta}} \triangleq \{\widetilde{\Delta} = diag(\Delta, \Delta_P) : \Delta$ is nonlinear and of dimension 1×1, Δ_P is nonlinear and of dimension 2×2, $\| \widetilde{\Delta} \|_{l_\infty - ind} < 1\}$.

4.3 Solving the Robust Control Problem

To solve the robust control problem, we need determine, for a fixed $\gamma > 0$, whether we can find a stabilizing $\widehat{K}(\lambda)$, such that the closed-loop system is stable, $\forall \widetilde{\Delta} \in \widetilde{\mathbf{\Delta}}$. This will be called *the robust control problem with disturbance attenuation level* γ. From Theorems C.3.2 and C.3.4, the robust control problem with attenuation level γ is solvable if and only if

$$\inf_{\text{stabilizing } \widehat{K}} \inf_{D \in \mathbf{D}} \| D^{-1} F_l(\widehat{G}, \widehat{K}) D \|_1 \leq 1, \tag{4.17}$$

where

$$\mathbf{D} \stackrel{\triangle}{=} \left\{ D = \begin{pmatrix} d_1 & & \\ & d_2 & \\ & & d_2 \end{pmatrix} : d_1, d_2 > 0 \right\},$$

and $F_l(\cdot,\cdot)$ denotes the lower Linear Fractional Transformation (c.f. Section C.2). We will restrict ourselves to finite dimensional LTI (FDLTI) controllers. Eq. (4.17) is a l_1 model matching problem and it can be solved as discussed in Section C.4. First one can use the $D-K$ iteration method to decompose the joint optimization problem (4.17) into a sequence of decoupled optimization problems.

In Step 1 of the $D-K$ iteration (Section C.4), for a fixed $D \in \mathbf{D}$, we want to solve

$$\inf_{\text{stabilizing } \widehat{K}} \| D^{-1} F_l(\widehat{G}, \widehat{K}) D \|_1 . \tag{4.18}$$

Partition $\widehat{G}$ into a 2×2 block matrix as shown in (4.15) and denote it as

$$\widehat{G} = \begin{pmatrix} \widehat{G}_{11} & \widehat{G}_{12} \\ \widehat{G}_{21} & \widehat{G}_{22} \end{pmatrix}.$$

Since $\widehat{G}_{22}$ is stable, the set of stabilizing FDLTI controllers $\widehat{K}$ is parametrized by (see Corollary C.2.5):

$$\widehat{K}(\lambda) = -\frac{Q}{1 - \widehat{G}_{22} Q}, \; Q \in \mathcal{RH}_\infty^{1\times 1}, \tag{4.19}$$

and the scaled achievable closed-loop maps is parametrized by

$$D^{-1} F_l(\widehat{G}, \widehat{K}) D = E - UQV, \; Q \in \mathcal{RH}_\infty^{1\times 1}, \tag{4.20}$$

where $E \stackrel{\triangle}{=} D^{-1}\widehat{G}_{11}D$, $U \stackrel{\triangle}{=} D^{-1}\widehat{G}_{12}$ and $V \stackrel{\triangle}{=} \widehat{G}_{21}D$. Therefore (4.17) is transformed into

$$\inf_{Q \in \mathcal{RH}_\infty^{1\times 1}} \| E - UQV \|_1 . \tag{4.21}$$

Problem (4.21) is a multi-block l_1 model matching problem (Appendix C). We can approximate it by a one-block l_1 model matching problem through delay augmentation (DA) (c.f. Subsection C.4.3). The latter problem is then solved using linear programming (c.f. Subsection C.4.2). Re-ordering input and output variables of $\widehat{G}$ if necessary, the lower bound $\underline{\eta}_N$ and the upper bound $\bar{\eta}_N$ both converge to the minimum l_1 norm ν^0 (see Theorem C.4.11 for notation) as the number of augmented delays $N \to \infty$. We also obtain a sub-optimal controller for (4.20) from the DA method.

Remark 4.3.1 *For the system we consider, the only zeros that the delay augmented matrices U_N and V_N (c.f. Subsection C.4.3) have inside the unit disk are 0's. This has two pleasant consequences:*

1. *In computation of null chains (c.f. Subsection C.4.2) and evaluation of the zero interpolation conditions, relevant coefficients can be obtained directly from the impulse responses and we thus avoid expensive symbolic calculation of high order derivatives.*

2. *From the zero interpolation conditions (C.17) in Theorem C.4.10, the upper bound on the (finite) length of the impulse response Φ is explicitly known.*

Since there are only two blocks in the structured uncertainty class $\widetilde{\mathbf{\Delta}}$, an analytical expresssion for the optimal D^* exists in Step 2 of the $D-K$ iteration.

We now present some computation results on how the optimal attenuation level γ^* is affected by the following factors: the magnitude of uncertainty, the magnitude $\bar{v}$ of the inversion error and the saturation limit $\bar{u}$.

The sampling frequency we use is 2000 Hz. The corresponding $\widehat{G}_a(\lambda)$ is

$$\widehat{G}_a(\lambda) = \frac{2.23 \times 10^{-11}\lambda^2 + 4.28 \times 10^{-11}\lambda}{0.147\lambda^2 - 0.549\lambda + 1}.$$

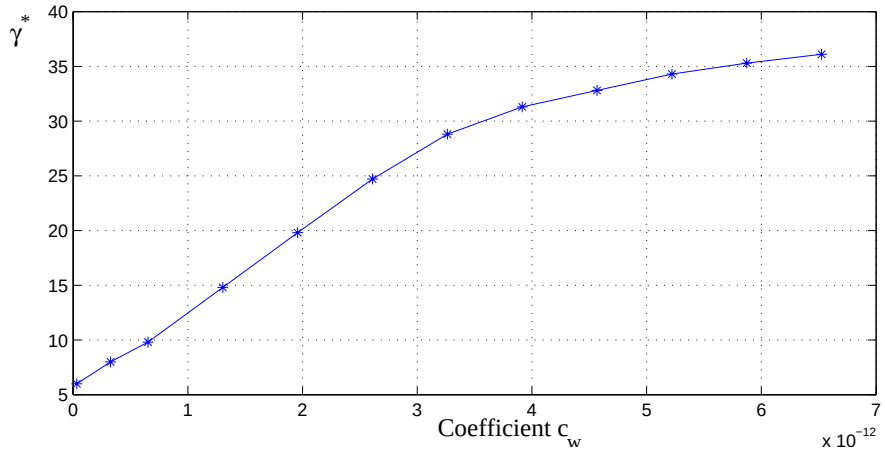

Figure 4.8: Effect of the model uncertainty on γ^*.

We choose the continuous time weighting function to be $W_0(s) = \frac{c_w(s+1)}{s+300}$, where $c_w > 0$ determines the magnitude of the uncertainty in the plant. Discretizing $W_0(s)$ gives

$$\widehat{W_0}(\lambda) = \frac{1.1759c_w(\lambda - 1.0005)}{\lambda - 1.1765}.$$

We let $\bar{r} = 30$.

Figure 4.8 shows the effect of the uncertainty magnitude on γ^*. Other parameters used are $\bar{v} = 0.1M_s^2$, $\bar{u} = 7.5M_s^2$, where M_s is the saturation magnetization. Since the range of u for the magnetostrictive actuator is $[0, M_s^2]$, expressing $\bar{v}$ and $\bar{u}$ in terms of M_s^2 allows one to make more concrete sense out of these numbers. From Figure 4.8, we see that the higher the uncertainty, the bigger γ^*.

Figure 4.9 displays how γ^* varies with the magnitude $\bar{v}$ of the inversion error, where we have fixed $c_w = 6.53 \times 10^{-13}$ and $\bar{u} = 1.25M_s^2$. As one expects, the optimal attenuation level γ^* increases as $\bar{v}$ increases.

Figure 4.10 shows how γ^* is affected by the saturation constraint. We have used $c_w = 6.53 \times 10^{-13}$ and $\bar{v} = 0.1M_s^2$. γ^* drops when $\bar{u}$ increases, but γ^* becomes a constant when $\bar{u}$ hits $4.5M_s^2$, beyond which the saturation constraint no longer

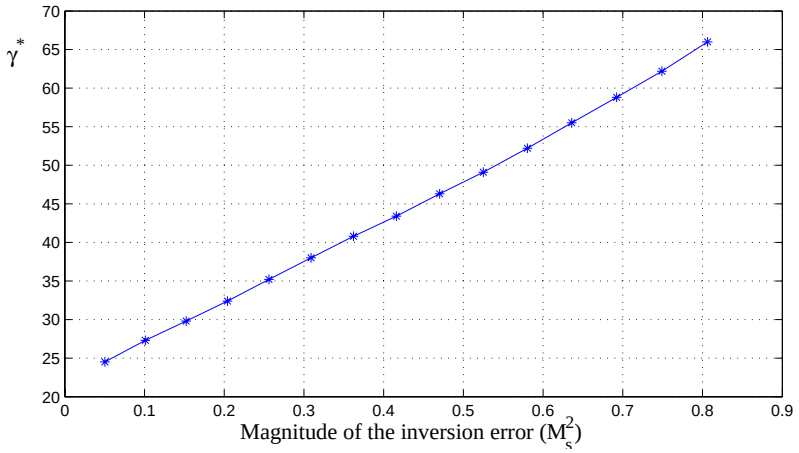

Figure 4.9: Effect of the inversion error on γ^*.

plays a role.

4.4 Simulation and Experimental Results

In this section we conduct simulation and experiments to examine the effectiveness of the robust controller design method.

The saturation constraint considered so far is of the form $|u| \leq \bar{u}$. But for real actuators, the saturation limits may be asymmetric, i.e., $u_{min} \neq -u_{max}$. For example, for the magnetostrictive actuators, $u \in [0, M_s^2]$. To handle the general constraint $u \in [u_{min}, u_{max}]$, we let $\bar{u} = \frac{u_{max}-u_{min}}{2}$ and $u_b = \frac{u_{max}+u_{min}}{2}$. The quantity $\bar{u}$ is the saturation limit to be used in the controller design, while u_b is a bias input to be injected into the system. Then the actual control will be $u = u_c + u_b$ with $|u_c| \leq \bar{u}$.

Since the gain of $\widehat{W}_0$ is close to 0 for a dc signal, we can ignore the contribution of u_b to the actuator output y through the $\Delta \circ \widehat{W}_0$ branch. Its contribution through

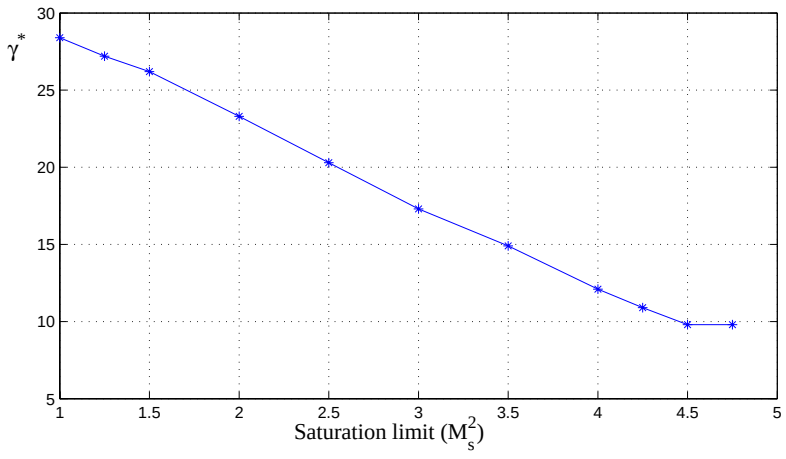

Figure 4.10: Effect of the saturation limit on γ^*.

the $\widehat{G}_a$ branch can be calculated as

$$y_b = \frac{\lambda \widehat{G}_a(\lambda)}{1 + \lambda \widehat{K}(\lambda)\widehat{G}_a(\lambda)} u_b.$$

The previous robust control framework applies if we add y_b to the reference trajectory y_{ref} (or alternatively, taking y_b off from y). Figure 4.11 shows the flow diagram for simulation of trajectory tracking.

As we have seen from Figure 4.10, the tracking performance deteriorates as the saturation constraint $\bar{u}$ is tightened. For the magnetostrictive actuator, $\bar{u} = 0.5M_s^2$ and strictly enforcing this constraint will lead to large tracking errors. This reveals the limitation of pure linear design for an intrinsically nonlinear plant. Hence a practical approach would be to properly relax the constraint.

Figures 4.12 and 4.13 show the simulation results of tracking two desired trajectories: a sinusoidal signal and an irregular signal generated via a Van del Pol oscillator. In the figures, the desired signals are intentionally delayed by two time steps (recall our definition of tracking error (4.14)). The current I applied is also displayed. The controller $\widehat{K}(\lambda)$ is designed based on $c_w = 3.3 \times 10^{-13}$, $\bar{v} = 0.1M_s^2$,

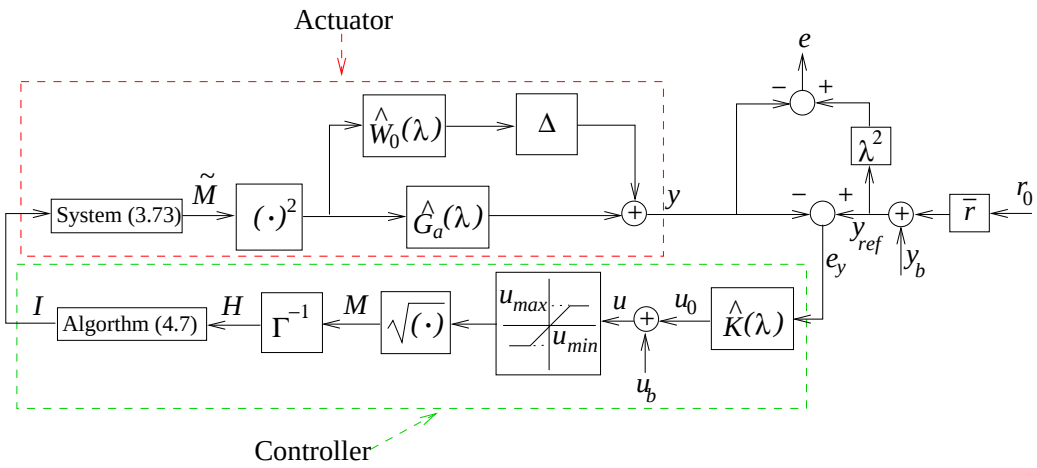

Figure 4.11: The flow diagram of the closed-loop system.

and $\bar{u} = 3.25M_s^2$.

Figure 4.14 shows the inversion error $\widetilde{M}[k+1] - M[k]$ during simulation of tracking the sinusoidal signal. Figure 4.15 shows the control output u_c of $\widehat{K}(\lambda)$, and we see that although we set $\bar{u} = 3.25M_s^2$ in the controller design, the output u_c stays in the (true) unsaturated region $[-0.5M_s^2, 0.5M_s^2]$ except during the transient period at the beginning.

Our composite controller (the linear robust controller plus the inverse algorithm) is compuation efficient and we can implement it in real-time. Figures 4.16 and 4.17 show the experimental results of trajectory tracking based on the same controller as used in the simulation. We can see that the experimental results match well with the simulation ones and the overall performance is satisfactory.

The saturation limit $\bar{u}$ can not be "over-relaxed". For example, we design another controller based on $\bar{r} = 25$, $c_w = 3.3 \times 10^{-13}$, $\bar{v} = 0.05M_s^2$, and $\bar{u} = 5M_s^2$. The simulation result (Figures 4.18) based on this new controller is better than that in Figure 4.12. But in the experiment the tracking performance suffers from the persistant saturation (Figure 4.19).

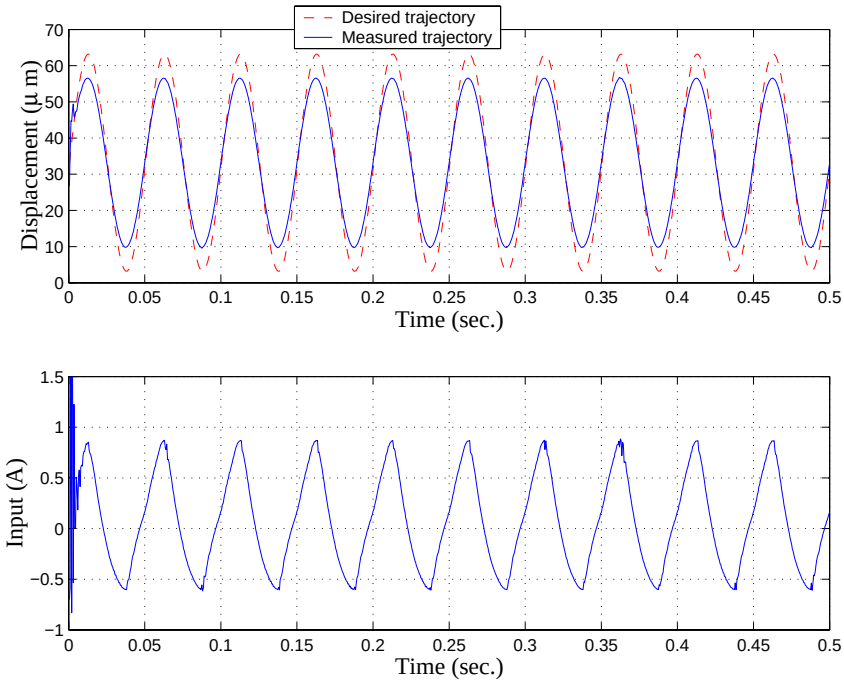

Figure 4.12: Simulation result of tracking a sinusoidal signal.

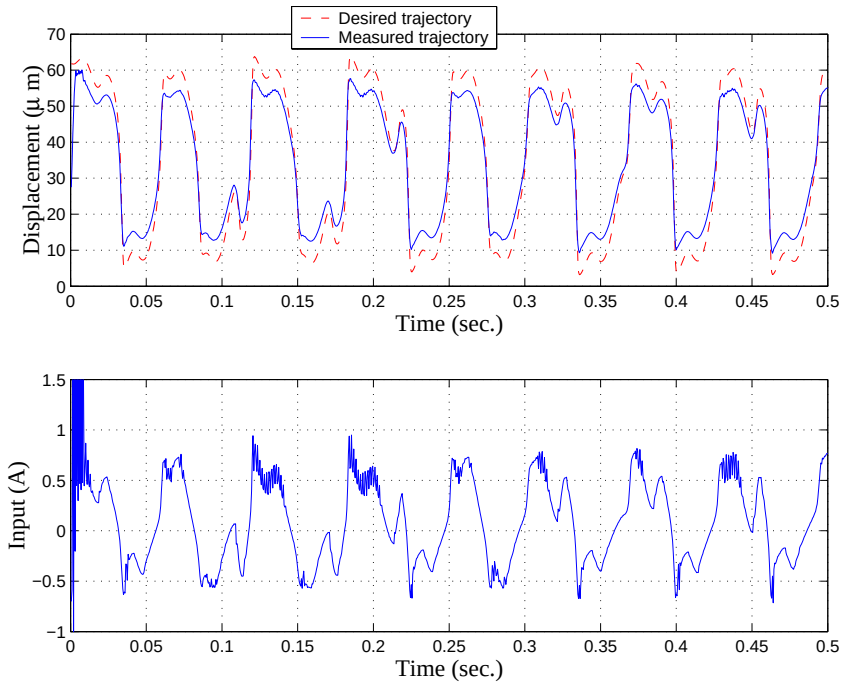

Figure 4.13: Simulation result of tracking an irregular signal.

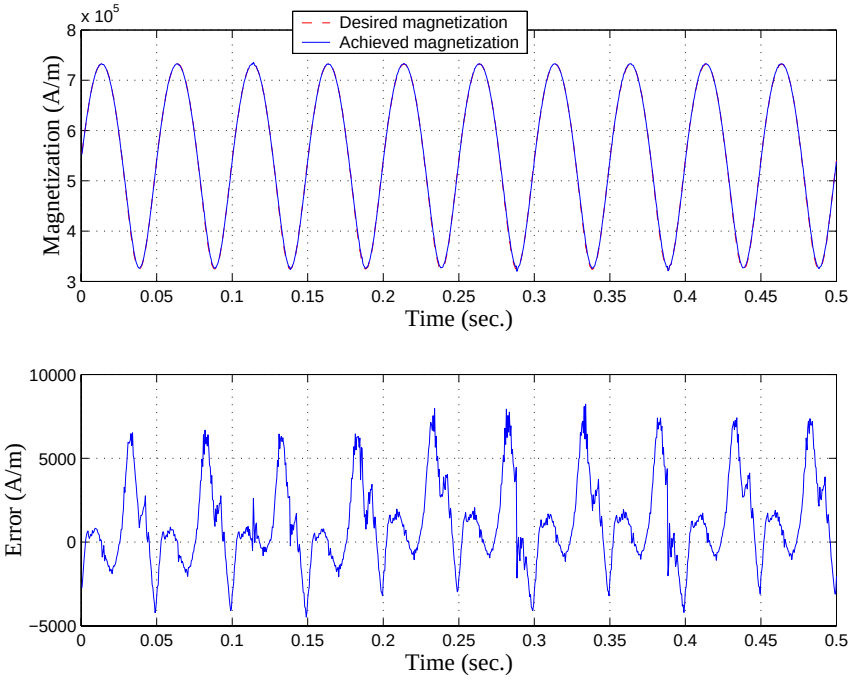

Figure 4.14: The inversion error e_M.

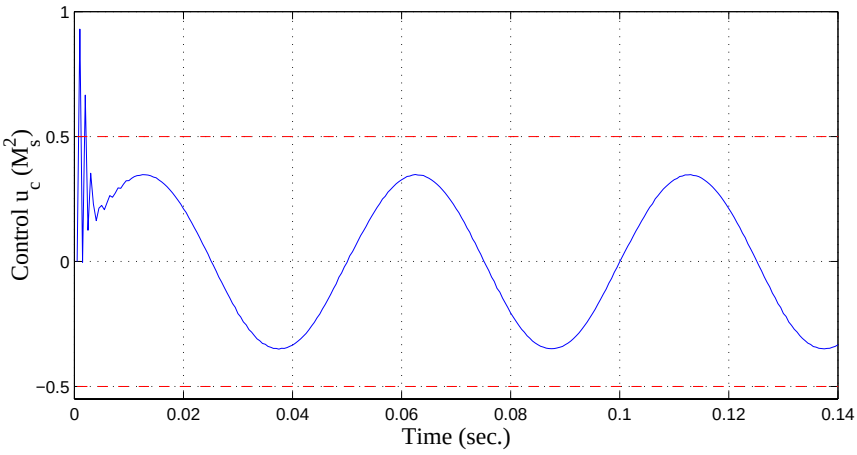

Figure 4.15: The control output u_c.

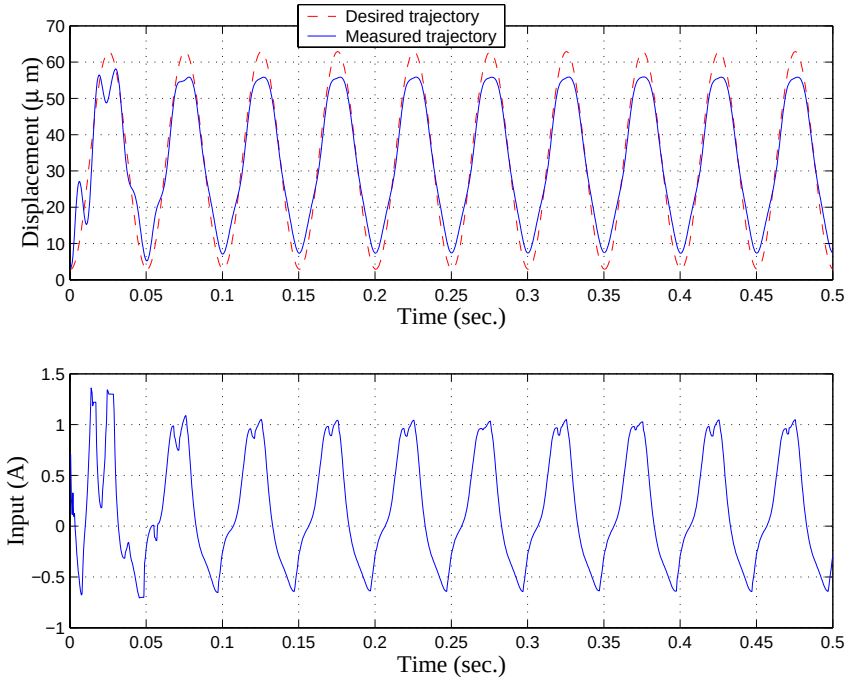

Figure 4.16: Experimental result of tracking a sinusoidal signal.

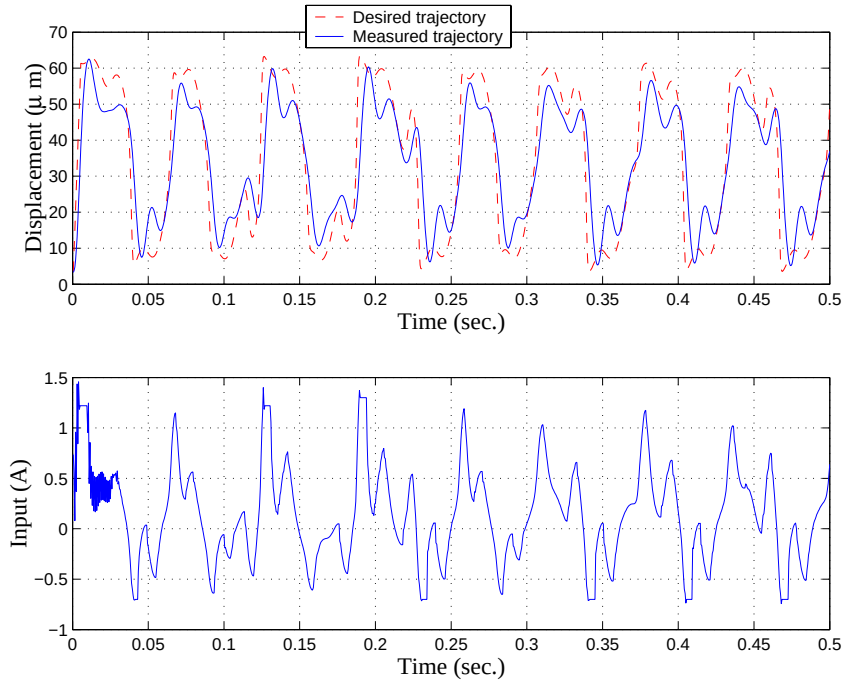

Figure 4.17: Experimental result of tracking an irregular signal.

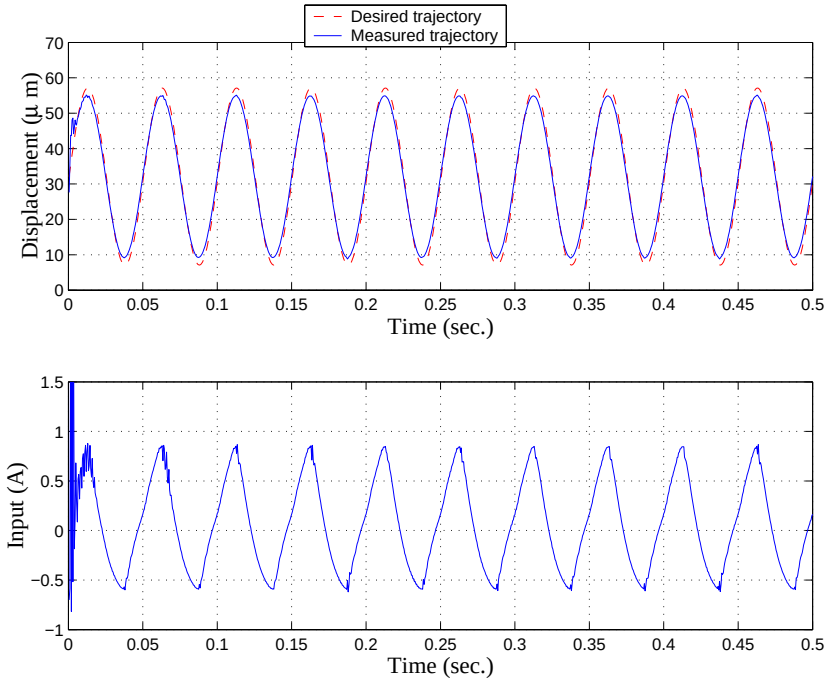

Figure 4.18: Simulation result of trajectory tracking based on an "over-relaxed" controller.

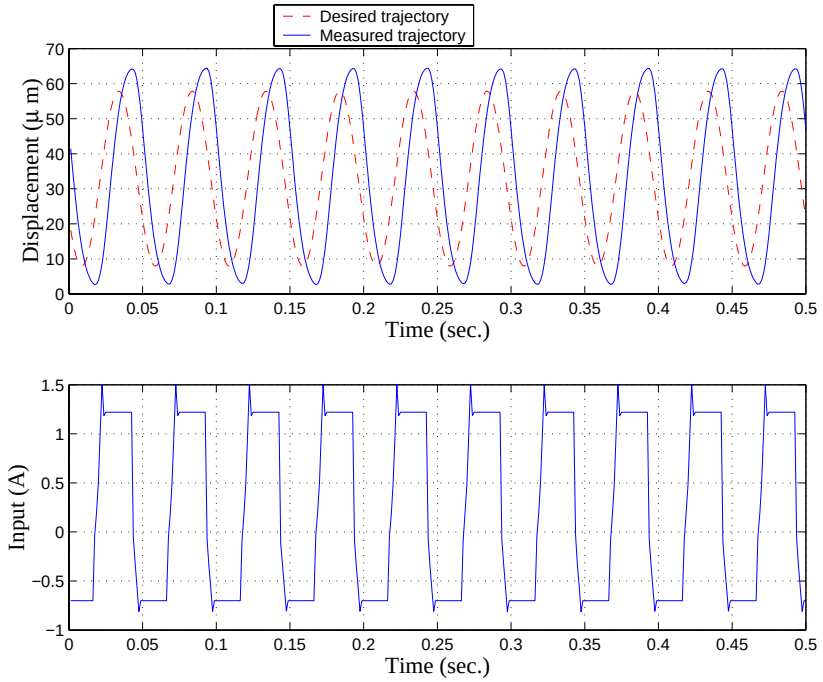

Figure 4.19: Experimental result of trajectory tracking based on an "over-relaxed" controller.

Chapter 5

Optimal Control of Hysteresis: A Viscosity Solutions Approach

In this chapter we study optimal control of hysteresis in smart actuators. Optimal control of dynamical systems with various hysteretic nonlinearities has been studied in [18, 2, 3, 4, 11, 12]. Dynamic programming is one of the most important tools in the optimal control theory. All the work mentioned earlier except [18] took the dynamic programming approach, while in [18] the author aimed to seek the necessary conditions (the Pontryagin Maximum Principle) for optimality.

When the value function of the control problem is smooth, we can derive the Hamilton-Jacobi-Bellman (HJB) equation from the Dynamic Programming Principle (DPP), and in many cases, solving the HJB equation amounts to solving the optimal control problem. The value function however, in general, is not smooth even for smooth systems, not to mention for a hysteretic system. Crandall and Lions [26] introduced the notion of viscosity solutions to Hamilton-Jacobi equations. This turned out to be a very useful concept for optimal control since value functions of many optimal control problems do satisfy the HJB equation in the viscosity

sense; and under mild assumptions, uniqueness results for viscosity solutions hold. For references on application of the viscosity solutions theory to optimal control problems, please see [32, 9], where [32] mainly deals with stochastic optimal control problems while [9] is devoted to deterministic problems.

The viscosity solutions approach was taken in [2, 3, 4, 12]. We will explore this approach for control of hysteresis in smart actuators. We will first discuss control problems based on a low dimensional hysteresis model [78]. The model is a hybrid system with both controlled switching and autonomous switching. It belongs to the class of Duhem hysteresis models and can be rewritten as a system involving both continuous control and switching control. Then we will consider an optimal control problem based on the dynamic hysteresis model proposed in Chapter 3.

Lots of work has been done in control of hybrid systems. Witsenhausen formulated a class of hybrid-state continuous-time dynamical systems and studied an optimal control problem back in 1966 [89]. Yong studied the optimal control problem for a system with continuous, switching and impulse controls in [91]. The Pontryagin Maximum Principle or its variant was used in optimal control for hybrid systems in [63, 68]. By solving the Bellman inequality, a lower bound on the value function and an approximation to the optimal control law were obtained in [42, 67]. With a unified model for hybrid control, Branicky, Borkar and Mitter proposed generalized quasi-variational inequalities (GQVIs) satisfied by the value function [17].

This chapter will be organized as follows. First we introduce the low dimensional hysteresis model in Section 5.1. Based on this model we then formulate and solve an infinite time horizon control problem using the viscosity solutions approach in Section 5.2. The approach is extended to other control problems of

practical interest in Section 5.3. Finally we discuss an optimal control problem based on the dynamic hysteresis model (3.2) in Section 5.4.

5.1 The Low Dimensional Ferromagnetic Hysteresis Model

As we introduced in Chapter 2, when the input frequency is low, the magnetostrictive hysteresis is rate-independent. Furthermore, we can relate the magnetostriction to the magnetization M by a square law and relate the input current I to the magnetic field H by a proportional law. Hence in this case the magnetostrictive hysteresis is fully captured by the ferromagnetic hysteresis between M and H.

Jiles and Atherton proposed a low dimensional model for ferromagnetic hysteresis, based upon the quantification of energy losses due to domain wall intersections with inclusions or pinning sites within the material [51]. A modification to the Jiles-Atherton model was made by Venkataraman and Krishnaprasad with rigorous use of the energy balancing principle [84]. The resulting model, named the *bulk ferromagnetic hysteresis model,* has a slightly different form from the Jiles-Atherton model. Also based on the energy balancing principle, they derived a bulk magnetostrictive hysteresis model [83], where high frequency effects are considered.

Here we will restrict ourselves to the low frequency case to highlight the methodology of hysteresis control. Extension to the high frequency case is straightforward. We now briefly outline the bulk ferromagnetic hysteresis model.

For an external magnetic field H and a bulk magnetization M, we define

$$H_{\mathrm{e}} = H + \alpha M$$

to be the effective field, where α is a mean field parameter representing inter-

domain coupling. Through thermodynamic considerations, the *anhysteretic magnetization* $M_{\rm an}$ can be expressed as

$$M_{\rm an}(H_{\rm e}) = M_{\rm s}(\coth(\frac{H_{\rm e}}{a}) - \frac{a}{H_{\rm e}}) = M_{\rm s}\mathcal{L}(z), \tag{5.1}$$

where $\mathcal{L}(\cdot)$ is the Langevin function, $\mathcal{L}(z) = \coth(z) - \frac{1}{z}$, with $z = \frac{H_{\rm e}}{a}$, $M_{\rm s}$ is the saturation magnetization of the material and a is a parameter characterizing the shape of the $M_{\rm an}$ curve.

Define

$$\begin{aligned}
f_1(H,M) &= c\frac{M_{\rm s}\frac{\partial \mathcal{L}(z)}{\partial z}}{a - \alpha c M_{\rm s}\frac{\partial \mathcal{L}(z)}{\partial z}},\\
f_2(H,M) &= \frac{ckM_{\rm s}\frac{\partial \mathcal{L}(z)}{\partial z} - \mu_0 a(M_{\rm an}(H_{\rm e}) - M)}{k(a - \alpha c M_{\rm s}\frac{\partial \mathcal{L}(z)}{\partial z}) + \mu_0\alpha a(M_{\rm an}(H_{\rm e}) - M)},\\
f_3(H,M) &= \frac{ckM_{\rm s}\frac{\partial \mathcal{L}(z)}{\partial z} + \mu_0 a(M_{\rm an}(H_{\rm e}) - M)}{k(a - \alpha c M_{\rm s}\frac{\partial \mathcal{L}(z)}{\partial z}) - \mu_0\alpha a(M_{\rm an}(H_{\rm e}) - M)},
\end{aligned}$$

where c is the reversibility constant, μ_0 is the permeability of vacuum, k is a measure for the average energy required to break a pinning site. Note each f_i is smooth in H and M.

The bulk ferromagnetic hysteresis model is as follows [84]:

$$\frac{dM}{dH} = f_i(H,M), \quad \text{where } i = \begin{cases} 1, & dH < 0,\ M < M_{\rm an}(H_{\rm e}) \text{ or} \\ & dH \geq 0,\ M \geq M_{\rm an}(H_e) \\ 2, & dH < 0,\ M \geq M_{\rm an}(H_{\rm e}) \\ 3, & dH \geq 0,\ M < M_{\rm an}(H_{\rm e}) \end{cases}.$$

If we define a control $u = \dot{H}$, the model is rewritten as

$$\begin{pmatrix} \dot{H} \\ \dot{M} \end{pmatrix} = \begin{pmatrix} 1 \\ f_i(H,M) \end{pmatrix} u, \text{ where } i = \begin{cases} 1, & u < 0,\ M < M_{\text{an}}(H_{\text{e}}) \text{ or} \\ & u \geq 0,\ M \geq M_{\text{an}}(H_{\text{e}}) \\ 2, & u < 0,\ M \geq M_{an}(H_{\text{e}}) \\ 3, & u \geq 0,\ M < M_{an}(H_{\text{e}}) \end{cases}. \tag{5.3}$$

Remark 5.1.1 *Note that the control u defined above is different from the physical current I we apply to the actuator. The current I is related to the state component H by a constant c_0 (the coil factor): $H = c_0 I$. Therefore from the control u, the current we will apply is $I(t) = I(0) + \frac{1}{c_0}\int_0^t u(s)ds$.*

Remark 5.1.2 *The switching in (5.3) depends on both (the sign of) the continuous control u and the state (H, M), therefore the model (5.3) is a hybrid system with both controlled switching and autonomous switching [16, 17].*

We can represent (5.3) in a more compact way. Letting

$$\Omega_1=\{(H,M) : M < M_{\text{an}}(H_{\text{e}})\},\ \ \Omega_2=\{(H,M) : M \geq M_{\text{an}}(H_{\text{e}})\},$$

and $x = (H, M)$, we define

$$f_+(x) = \begin{cases} \begin{pmatrix} 1 \\ f_1(x) \end{pmatrix} & \text{if } x \in \Omega_2 \\ \begin{pmatrix} 1 \\ f_3(x) \end{pmatrix} & \text{if } x \in \Omega_1 \end{cases}, \text{ and } f_-(x) = \begin{cases} \begin{pmatrix} 1 \\ f_1(x) \end{pmatrix} & \text{if } x \in \Omega_1 \\ \begin{pmatrix} 1 \\ f_2(x) \end{pmatrix} & \text{if } x \in \Omega_2 \end{cases}.$$

Since $f_i, 1 \leq i \leq 3$, coincide on $\Gamma \stackrel{\triangle}{=} \{(H,M) : M = M_{\text{an}}(H_{\text{e}})\}$, f_+ and f_- are continuous. We define two continuous control sets

$$U_+ = \{u : u_{\text{c}} \geq u \geq 0\}, \quad U_- = \{u : -u_{\text{c}} \leq u \leq 0\},$$

where $u_c > 0$ represents the operating bandwidth constraint of the actuator (recall $u = c_0\dot{I}$). To ease the presentation, we make the dependence of switching on u explicit by introducing a discrete control set $D = \{1, 2\}$.

Now the model (5.3) can be represented as a system with both a continuous control u and a discrete mode (switching) control d:

$$\dot{x} = f(x, u, d) \triangleq \begin{cases} f_+(x)u, & u \in U_+, \text{ if } d = 1 \\ f_-(x)u, & u \in U_-, \text{ if } d = 2 \end{cases}. \tag{5.4}$$

The (state-dependent) autonomous switching has now been incorporated into the definitions of f_+, f_-, thanks to the nice structure of the physical model. Note the model (5.4) belongs to the category of *Duhem* hysteresis model [86].

5.1.1 Properties of the model

We first present a lemma which will be useful in the proof of Proposition 5.1.4.

Lemma 5.1.3 *[77]* $\mathcal{L}(z)$ *satisfies:*

$$0 < \frac{\partial \mathcal{L}(z)}{\partial z} \leq \frac{1}{3}, \tag{5.5}$$

$$|\mathcal{L}(z)| \leq 1. \tag{5.6}$$

Proof

$$\begin{aligned} \frac{\partial \mathcal{L}(z)}{\partial z} &= \frac{1}{z^2} - csch^2(z) \\ &= \frac{1}{z^2} - \frac{1}{(\frac{e^z - e^{-z}}{2})^2} \\ &= \frac{1}{z^2} - \frac{1}{(z + \frac{z^3}{3!} + \frac{z^5}{5!} + \cdots)^2}. \end{aligned} \tag{5.7}$$

Therefore

$$\frac{\partial \mathcal{L}(z)}{\partial z} > 0, \ \forall z \neq 0. \tag{5.8}$$

Further manipulation on (5.7) yields

$$\frac{\partial \mathcal{L}(z)}{\partial z} = \frac{(2 + \frac{z^2}{3!} + \frac{z^4}{5!} + \cdots)(\frac{1}{3!} + \frac{z^2}{5!} + \cdots)}{(1 + \frac{z^2}{3!} + \frac{z^4}{5!} + \cdots)^2},$$

from which we obtain

$$\frac{\partial \mathcal{L}}{\partial z}(0) = \frac{1}{3}. \tag{5.10}$$

Combining (5.8) and (5.10) we have

$$\frac{\partial \mathcal{L}(z)}{\partial z} > 0. \tag{5.11}$$

Since in addition,

$$\lim_{z \to \infty} \mathcal{L}(\mathrm{z}) = 1, \quad \lim_{z \to -\infty} \mathcal{L}(\mathrm{z}) = -1,$$

we have (5.6).

To prove $\frac{\partial \mathcal{L}(z)}{\partial z} \leq \frac{1}{3}$, it suffices to show

$$\frac{\partial^2 \mathcal{L}(z)}{\partial z^2} > 0 \ \forall z < 0,$$
$$\frac{\partial^2 \mathcal{L}(z)}{\partial z^2} < 0 \ \forall z > 0.$$

But

$$\begin{aligned} \frac{\partial^2 \mathcal{L}(z)}{\partial z^2} &= \frac{8(e^z + e^{-z})}{(e^z - e^{-z})^3} - \frac{2}{z^3} \\ &= 2\frac{(1 + \frac{z^2}{2!} + \frac{z^4}{4!} + \cdots) - (1 + \frac{z^2}{3!} + \frac{z^4}{5!} + \cdots)^3}{z^3(1 + \frac{z^2}{3!} + \frac{z^4}{5!} + \cdots)^3}, \end{aligned} \tag{5.13}$$

so we need only to show that the numerator of (5.13) is always less than 0, $\forall z \neq 0$.

We first note that the coefficient of $z^{2k}, k > 1$ in the second term is

$$\begin{aligned} 3(\frac{1}{(2k+1)!} + \frac{1}{(2k-1)!3!} + \cdots) &> 3\frac{1}{(2k-1)!3!} \\ &> \frac{1}{(2k)!}(\frac{3(2k)}{3!}) \\ &> \frac{1}{(2k)!}, \end{aligned}$$

while $\frac{1}{(2k)!}$ is the coefficient of z^{2k} in the first term. For $k = 0, 1$, the coefficients of both terms cancel out. The proof is now complete. ■

Proposition 5.1.4 (Boundedness of f_i) *If the parameters satisfy:*

$$T_1 \stackrel{\triangle}{=} a - \frac{\alpha c M_{\rm s}}{3} > 0, \tag{5.14}$$

$$T_2 \stackrel{\triangle}{=} k(a - \frac{\alpha c M_{\rm s}}{3}) - 2\mu_0 \alpha a M_{\rm s} > 0, \tag{5.15}$$

then $0 < f_i \leq C_{\rm f}, i = 1, 2, 3$, *for some constant* $C_{\rm f} > 0$.

Proof By (5.5) and (5.14)

$$0 < T_1 = a - \frac{\alpha c M_s}{3} \leq a - \alpha c M_s \frac{\partial \mathcal{L}(z)}{\partial z} < a.$$

We rewrite f_1 as

$$f_1 = -\frac{1}{\alpha} + \frac{a}{\alpha(a - \alpha c M_s \frac{\partial \mathcal{L}(z)}{\partial z})},$$

and note that it is a nondecreasing function of $\frac{\partial \mathcal{L}(z)}{\partial z}$. Since

$$\begin{aligned} f_1 &= 0 \text{ when } \tfrac{\partial \mathcal{L}(z)}{\partial z} = 0, \\ f_1 &= \frac{c M_s}{3a - \alpha c M_s} =: C_1 \text{ when } \tfrac{\partial \mathcal{L}(z)}{\partial z} = \tfrac{1}{3}, \end{aligned}$$

we get

$$0 < f_1 \leq C_1.$$

The function f_2 can be written as

$$f_2 = -\frac{1}{\alpha} + \frac{ka}{\alpha} \underbrace{\frac{1}{k(a - \alpha c M_s \frac{\partial \mathcal{L}(z)}{\partial z}) + \mu_0 \alpha a (M_{an} - M)}}_{=:T}$$

From the model (5.3), when f_2 is selected, $M_{an} - M \leq 0$. Since magnitudes of both M_{an} and M must be less than M_s, $M_{an} - M \geq -2M_s$. These facts together with (5.5) yield

$$0 < T_2 \leq T \leq ka.$$

Therefore

$$0 < f_2 \leq \frac{ka - T_2}{\alpha T_2} =: C_2.$$

Similarly we can show $0 < f_3 < C_2$. Picking $C_f = \max\{C_1, C_2\}$, we have $0 < f_i \leq C_f$ for $i = 1, 2, 3$. ■

Remark 5.1.5 *Conditions (5.14) and (5.15) are satisfied for typical parameters. For example, taking the parameters identified in [82],* $\alpha = 1.9 \times 10^{-4}$, $a = 190$, $k = 48$ *Gauss,* $c = 0.3$, $M_s = 9.89 \times 10^3$ *Gauss and* $\mu_0 = 1$, *we calculate* $T_1 = 189.8$, $T_2 = 8.40 \times 10^3$.

Proposition 5.1.6 (Lipschitz continuity) *Functions* $f_+(x)$ *and* $f_-(x)$ *are Lipschitz continuous with some Lipschitz constant* L, *and* $f(x, u, d)$ *is Lipschitz continuous with respect to* x *with Lipschitz constant* $L_0 = Lu_c$.

Proof We first prove f_- is Lipschitz continuous with some Lipschitz constant L_-. We discuss three cases:

- Case I: Both $x_1, x_2 \in \Omega_1$. In this case, mode 1 is active, and thus

$$\frac{\partial f_-(x)}{\partial x} = \begin{pmatrix} 0 & 0 \\ \frac{\partial f_1(H,M)}{\partial H} & \frac{\partial f_1(H,M)}{\partial M} \end{pmatrix}. \tag{5.16}$$

  It can be shown that $|\frac{\partial f_1(H,M)}{\partial H}| \leq C_1$, $|\frac{\partial f_1(H,M)}{\partial M}| \leq \alpha C_1$ for some $C_1 > 0$. Therefore $|\frac{\partial f_-(x)}{\partial x}| \leq L_1$ for some $L_1 > 0$, and the following holds:

$$|f_-(x_1) - f_-(x_2)| \leq L_1 |x_1 - x_2|.$$

- Case II: Both $x_1, x_2 \in \Omega_2$. In this case, mode 2 is active. Following similar steps as in Case I, we can show $|\frac{\partial f_-(x)}{\partial x}| \leq C_2$ for some $L_2 > 0$ and therefore

$$|f_-(x_1) - f_-(x_2)| \leq L_2 |x_1 - x_2|.$$

- Case III: $x_1 \in \Omega_1, x_2 \in \Omega_2$. Then there exists $x_0 \in \Gamma$, such that the line segment connecting x_1 and x_2 intersects Γ at x_0. We express $x_0 = \theta x_1 + (1-\theta)x_2$ with $0 \leq \theta \leq 1$. Thus

$$\begin{aligned} |f_-(x_1) - f_-(x_2)| &= |f_-(x_1) - f_-(x_0) + f_-(x_0) - f_-(x_2)| \\ &\leq L_1|x_1 - x_0| + L_2|x_0 - x_2| \\ &= L_1(1-\theta)|x_1 - x_2| + L_2\theta|x_1 - x_2| \\ &\leq L_-|x_1 - x_2|, \end{aligned}$$

  with $L_- = \max\{L_1, L_2\}$.

Following exactly the same arguments, we can show, there exists $L_+ \geq 0$, such that

$$|f_+(x_1) - f_+(x_2)| \leq L_+|x_1 - x_2|, \ \forall x_1, x_2.$$

We conclude the first part by taking $L = \max\{L_-, L_+\}$. The rest of the proposition follows trivially. ■

5.2 The Infinite Time Horizon Optimal Control Problem

We first formulate an infinite time horizon optimal control problem for the system (5.4). Define the cost functional with an initial condition x and a control pair $\alpha(\cdot) = \{d(\cdot), u(\cdot)\}$ as

$$J(x, \alpha(\cdot)) = \int_0^\infty l(x(t), u(t))e^{-\lambda t}dt, \tag{5.17}$$

where the *discount factor* $\lambda \geq 0$. Note the *running cost* $l(\cdot,\cdot)$ is defined to be independent of the switching control d, since this makes sense in the context of

smart actuator control. We require $u(\cdot)$ to be measurable. This together with Proposition 5.1.6 guarantees that (5.4) has a unique solution $x(\cdot)$ (the dependence of $x(\cdot)$ on x and $\alpha(\cdot)$ is suppressed when no confusion arises).

The optimal control problem is to find the value function

$$V(x) = \inf_{\alpha(\cdot)} J(x, \alpha(\cdot)),$$

and if $V(x)$ is achievable, find the optimal control $\alpha^*(\cdot)$.

We make the following assumptions about $l(\cdot, \cdot)$:

- (A_1): $l(x, u)$ continuous with respect to x and u, $l(x, u) \geq 0$, $\forall x, u$;
- (A_2): $l(0, 0) = 0$, $|l(x_1, u) - l(x_2, u)| \leq C_l(1 + |x_1| + |x_2|)|x_1 - x_2|$, $\forall u$, for some $C_l > 0$.

Note (A_2) includes the case of quadratic cost.

5.2.1 Properties of the value function

We can show the value function is locally bounded and locally Lipschitz continuous.

Proposition 5.2.1 (Local boundedness) *Under assumptions* (A_1) *and* (A_2), $\forall \lambda > 0$, $V(x)$ *is locally bounded, i.e.,* $\forall R > 0, \exists\, C_{\mathrm{R}} \geq 0$, *such that*

$$|V(x)| \leq C_{\mathrm{R}},\ \forall x \in \bar{B}(0, R) \stackrel{\triangle}{=} \{x : |x| \leq R\}.$$

Proof First note that since $l(\cdot, \cdot)$ is nonnegative, $V(x) \geq 0$, $\forall x$. Take $u(t) \equiv 0$, then $x(t) \equiv x$. Letting $\alpha(t) = \{d(t), u(t)\}$ where $d(t) \equiv 1$, we have

$$\begin{aligned} V(x) \leq J(x, \alpha(\cdot)) &= \int_0^\infty l(x, 0) e^{-\lambda t} dt \\ &= \frac{l(x, 0)}{\lambda}. \end{aligned}$$

By (A_2), $l(x,0) \leq C_l(1+R)R$, and the proof is complete with $C_{\mathrm{R}} \stackrel{\triangle}{=} \frac{C_l(1+R)R}{\lambda}$. ■

To prove the local Lipschitz continuity of the value function, we will need the following lemma:

Lemma 5.2.2 *Let $x_1(\cdot), x_2(\cdot)$ be solutions to (5.4) under some admissible control $\alpha(\cdot) = \{d(\cdot), u(\cdot)\}$ with initial condition x_1, x_2 respectively. Then*

$$|x_1(t) - x_2(t)| \leq e^{L_0 t}|x_1 - x_2|, \tag{5.18}$$

$$|x_1(t)| \leq |x_1|e^{L_0 t} + \frac{C}{L_0}(e^{L_0 t} - 1), \tag{5.19}$$

where $C = \max_d |f(0, u_c, d)|$, and L_0 is as defined in Proposition 5.1.6.

Proof 1. We first show (5.18). Denote the sequence of mode switching times as $\{t_i, i = 0, 1, \cdots\}$ with $t_0 = 0$, and the mode during $[t_i, t_{i+1})$ as d_i. Then $\forall t \in [0, t_1)$,

$$\begin{aligned} \frac{d}{dt}|x_1(t) - x_2(t)|^2 &= 2(x_1(t) - x_2(t)) \cdot (f(x_1(t), u(t), d_0) - f(x_2(t), u(t), d_0) \\ &\leq 2L_0|x_1(t) - x_2(t)|^2, \end{aligned}$$

where the inequality comes from Proposition 5.1.6. Integrating both sides from 0 to t and applying the Gronwall inequality, we get

$$|x_1(t) - x_2(t)|^2 \leq |x_1 - x_2|^2 e^{2L_0 t},$$

from which (5.18) follows. Now $\forall t \in [t_1, t_2)$, taking $x_1(t_1), x_2(t_1)$ as initial conditions, we follow the above procedures and get

$$\begin{aligned} |x_1(t) - x_2(t)| &\leq |x_1(t_1) - x_2(t_1)|e^{L_0(t-t_1)} \\ &\leq |x_1 - x_2|e^{L_0(t-t_1)}e^{L_0(t_1-0)} = |x_1 - x_2|e^{L_0 t}. \end{aligned}$$

Using the same argument successively, we can show that (5.18) holds $\forall t \geq 0$.

2. Now we show (5.19). $\forall x_1(t) \neq 0$, we can write

$$\begin{aligned} |x_1(t)|\frac{d}{dt}|x_1(t)| &= \frac{1}{2}\frac{d}{dt}|x_1(t)|^2 = x_1(t)\cdot f(x_1(t),u(t),d(t)) \\ &= x_1(t)\cdot(f(0,u(t),d(t))+f(x_1(t),u(t),d(t))-f(0,u(t),d(t))) \\ &\leq C|x_1(t)|+L_0|x_1(t)|^2, \end{aligned}$$

from which we obtain

$$\frac{d}{dt}|x_1(t)| \leq C + L_0|x_1(t)|.$$

Integrating it from 0 to t and then using the Gronwall inequality, we have (5.19).

■

Proposition 5.2.3 (Local Lipschitz continuity) *Under assumptions* (A_1) *and* (A_2), $\forall\lambda > 2L_0$ *with* L_0 *as defined in Proposition 5.1.6,* $V(x)$ *is locally Lipschitz, i.e.,* $\forall R > 0, \exists\, L_{\mathrm{R}} \geq 0$, *such that* $|V(x_1)-V(x_2)| \leq L_{\mathrm{R}}|x_1-x_2|$, $\forall x_1, x_2 \in \bar{B}(0,R)$. *In addition,* L_{R} *can be chosen to be* $C(1+R)$ *for some* $C > 0$.

Proof For $\epsilon > 0$, let $\alpha^\epsilon(\cdot) = \{d^\epsilon(\cdot), u^\epsilon(\cdot)\}$ be $\epsilon-$optimal for x_2, i.e.,

$$V(x_2) \geq J(x_2, \alpha^\epsilon(\cdot)) - \epsilon.$$

Since $V(x_1) \leq J(x_1, \alpha^\epsilon(\cdot))$, we have

$$\begin{aligned} V(x_1)-V(x_2) &\leq J(x_1,\alpha^\epsilon(\cdot)) - J(x_2,\alpha^\epsilon(\cdot)) \\ &\leq \int_0^\infty e^{-\lambda t}|l(x_1(t),u^\epsilon(t)) - l(x_2(t),u^\epsilon(t))|dt + \epsilon \\ &\leq \int_0^\infty e^{-\lambda t}C_l(1+|x_1(t)|+|x_2(t)|)|x_1(t)-x_2(t)|dt + \epsilon, \end{aligned}$$

where the last inequality is from (A_2). Using Lemma 5.2.2, we get

$$V(x_1) - V(x_2) \leq L_R|x_1 - x_2| + \epsilon,$$

where $L_R = (C_0 + \frac{2R}{\lambda - 2L_0})C_l$ and C_0 is a constant independent of R. Since ϵ is arbitrary, we have

$$V(x_1) - V(x_2) \leq L_R|x_1 - x_2|.$$

The proof is complete by noting that x_1 and x_2 are symmetric. ■

Remark 5.2.4 *One can get a sharper estimate for $|x_1(t)|$ (linear growth) by exploiting Proposition 5.1.4. This can be used to weaken the condition $\lambda > 2L_0$ to $\lambda > L_0$ in Proposition 5.2.3 and anywhere else it appears.*

5.2.2 The Dynamic Programming Principle and the Hamilton-Jacobi-Bellman equation

The value function satisfies the Dynamic Programming Principle (DPP):

Proposition 5.2.5 (DPP) *Assume (A_1) and (A_2), $\lambda > 0$. We have*

$$V(x) = \inf_{\alpha(\cdot)}\{\int_0^t e^{-\lambda s} l(x(s), u(s))ds + e^{-\lambda t}V(x(t))\},\ \forall t \geq 0,\ \forall x. \tag{5.20}$$

The proof is omitted since the argument is standard, see, e.g., [9].

Based on the DPP, we can show that the value function $V(\cdot)$ satisfies a Hamilton-Jacobi-Bellman equation (HJB) of a hybrid type in the viscosity sense. Viscosity solutions to Hamilton-Jacobi equations were first introduced by Crandall and Lions [26]. Here we use one of the three equivalent definitions [25]:

Definition 5.2.6 (Viscosity solutions) *[9] Let W be a continuous function from an open set $O \subset \mathbb{R}^n$ into $\mathbb{R}$ and let DW denote the gradient of W (when W is*

differentiable). We call W a viscosity solution to a nonlinear first order partial differential equation

$$F(x, W(x), DW(x)) = 0,\ x \in O, \tag{5.21}$$

where $F : O \times \mathbb{R} \times \mathbb{R}^n \to \mathbb{R}$ is continuous, if W is both a viscosity subsolution and viscosity supersolution; and by viscosity subsolution (supersolution, resp.), we mean: $\forall \phi \in C^1(O)$, if $W - \phi$ attains a local maximum (minimum, resp.) at $x_0 \in O$, then $F(x_0, W(x_0), D\phi(x_0)) \leq 0$ (≥ 0, resp.).

Viscosity solutions have a couple of nice properties [25, 26]. We mention one elementary property here, *consistency with the notion of classical solution*, that is: 1) any classical solution to (5.21) is a viscosity solution; 2) the viscosity solution satisfies (5.21) in the classical sense at any point where it is differentiable.

Theorem 5.2.7 (HJB) *Assume (A_1) and (A_2), $\lambda > 2L_0$. $V(x)$ is a viscosity solution of:*

$$\begin{aligned} \lambda W(x) + \max\{ \quad & \max_{u \in U_+}\{-u f_+(x) \cdot DW(x) - l(x,u)\}, \\ & \max_{u \in U_-}\{-u f_-(x) \cdot DW(x) - l(x,u)\}\} = 0,\ x \in \mathbb{R}^2. \end{aligned} \tag{5.22}$$

Proof 1. We first show $V(\cdot)$ is a viscosity subsolution. For any $u \in U_-$, take $\alpha(\cdot) = \{d(\cdot), u(\cdot)\}$ with $d(t) \equiv 2,\ u(t) \equiv u$. From (5.20), for any $t \geq 0$,

$$V(x) \leq \int_0^t l(x(s), u) e^{-\lambda s} ds + e^{-\lambda t} V(x(t)),$$

which we rewrite as

$$V(x(t)) - V(x) + \int_0^t l(x(s), u) e^{-\lambda s} ds + V(x(t))(e^{-\lambda t} - 1) \geq 0. \tag{5.23}$$

Now suppose that $V - \phi$ with $\phi \in C^1(\mathbb{R}^2)$ has a local maximum at x, then

$$V(x(t)) - \phi(x(t)) \leq V(x) - \phi(x),$$

for t sufficiently small. This together with (5.23) implies

$$\phi(x(t)) - \phi(x) + \int_0^t l(x(s), u)e^{-\lambda s}ds + V(x(t))(e^{-\lambda t} - 1) \geq 0. \tag{5.24}$$

Divide (5.24) by t and let $t \to 0$, we obtain

$$uf_-(x) \cdot D\phi(x) + l(x, u) - \lambda V(x) \geq 0, \ \forall u \in U_-,$$

i.e.,

$$\lambda V(x) + \max_{u \in U_-}\{-uf_-(x) \cdot D\phi(x) - l(x, u)\} \leq 0.$$

Similarly, we have

$$\lambda V(x) + \max_{u \in U_+}\{-uf_+(x) \cdot D\phi(x) - l(x, u)\} \leq 0.$$

Therefore

$$\begin{aligned} \lambda V(x) + \max\{&\max_{u \in U_-}\{-uf_-(x) \cdot D\phi(x) - l(x, u)\}, \\ &\max_{u \in U_+}\{-uf_+(x) \cdot D\phi(x) - l(x, u)\}\} \leq 0. \end{aligned} \tag{5.25}$$

2. The proof of supersolution is much more technically involved and therefore omitted here. It can be found in [77]. ■

5.2.3 Uniqueness of the solution to the HJB equation

We would like to characterize the value function V as a unique solution to the HJB equation. The uniqueness result basically follows from Theorem 1.5 in [47].

In [47], the author gave only a sketch of proof. For completeness, we will provide the full proof here.

Before stating the theorem, we first identify structural properties of the HJB equation. We rewrite (5.22) as:

$$\lambda W(x) + H(x, DW(x)) = 0,\ x \in \mathbb{R}^2, \tag{5.26}$$

where

$$H(x,p) \stackrel{\triangle}{=} \max\{\max_{u\in U_+}\{-uf_+(x)\cdot p - l(x,u)\}, \max_{u\in U_-}\{-uf_-(x)\cdot p - l(x,u)\}\},$$

is called the *Hamiltonian* of (5.26).

Proposition 5.2.8 *Assume* (A_2). $H(x,p)$ *satisfies the following:*

$$|H(x_1,p) - H(x_2,p)| \leq C_{\mathrm{R}}(1+|p|)|x_1 - x_2|,\ \forall x_1, x_2 \in \bar{B}(0,R),\ \forall p, \tag{5.27}$$

$$|H(x,p_1) - H(x,p_2)| \leq C_0|p_1 - p_2|, \forall x,\ \forall p_1, p_2, \tag{5.28}$$

for some $C_{\mathrm{R}} > 0, C_0 > 0$, *with* C_{R} *dependent on* R.

Proof We will only prove (5.27), since proof of (5.28) is analogous.

Without loss of generality, suppose $u_1 \in U_-$ attains the maximum in $H(x_1,p)$. Since $H(x_2,p) \geq -u_1 f_-(x_2)\cdot p - l(x_2,u_1)$,

$$\begin{aligned} H(x_1,p) - H(x_2,p) &\leq -u_1 f_-(x_1)\cdot p - l(x_1,u_1) + u_1 f_-(x_2)\cdot p + l(x_2,u_1) \\ &\leq |p|L_0|x_1 - x_2| + C_l(1+|x_1|+|x_2|)|x_1 - x_2| \\ &\leq C_{\mathrm{R}}(1+|p|)|x_1 - x_2|, \end{aligned}$$

where C_{R} is a constant dependent on R. By symmetry, we conclude. ∎

Remark 5.2.9 *As we have seen above, despite the hybrid structure of our physical model,* $H(x,p)$ *enjoys nice structural properties, which enables us to prove the uniqueness result.*

From Proposition 5.2.3, we know that the value function $V(\cdot)$ belongs to the class

$$\mathcal{P}(\mathbb{R}^2) = \{W(\cdot): \quad |W(x_1) - W(x_2)| \leq C(1+R)|x_1 - x_2|, \forall x_1, x_2 \in \bar{B}(0,R), \\ \forall\, R > 0, \text{for some } C > 0\}.$$

The following theorem is adapted from Theorem 1.5 in [47].

Theorem 5.2.10 *If (5.26) has a viscosity solution in $\mathcal{P}(\mathbb{R}^2)$, it is unique.*

Proof Without loss of generality, we take $\lambda = 1$. Let $W(\cdot), V(\cdot) \in \mathcal{P}(\mathbb{R}^2)$ be viscosity solutions to (5.26). For $\epsilon > 0, \alpha > 0, m > 2$, define

$$\Phi(x,y) = W(x) - V(y) - \frac{|x-y|^2}{\epsilon} - \alpha(< x >^m + < y >^m),$$

with $< x > \stackrel{\triangle}{=} \sqrt{1+|x|^2}$. Since $W(\cdot), V(\cdot) \in \mathcal{P}(\mathbb{R}^2)$, $\lim_{|x|+|y|\to\infty} \Phi(x,y) = -\infty$. By continuity of $\Phi(\cdot,\cdot)$, there exists (x_0, y_0) where Φ attains the global maximum. First we want to obtain bounds for $|x_0|, |y_0|$ and $|x_0 - y_0|$.

From $\Phi(0,0) \leq \Phi(x_0, y_0)$, and $W(\cdot), V(\cdot) \in \mathcal{P}(\mathbb{R}^2)$, we can get

$$< x_0 >^m + < y_0 >^m \leq C_\alpha(1 + < x_0 >^2 + < y_0 >^2),$$

where C_α is a constant independent of ϵ (but dependent on α). Since $m > 2$, there exists $R_\alpha > 0$ (independent of ϵ), such that $|x_0| \leq R_\alpha$, $|y_0| \leq R_\alpha$.

From $\Phi(x_0, x_0) + \Phi(y_0, y_0) \leq 2\, \Phi(x_0, y_0)$, we can derive

$$|x_0 - y_0| \leq \epsilon C'_\alpha, \tag{5.29}$$

with C'_α depending on α only.

Define

$$\phi(x) = V(y_0) + \frac{1}{\epsilon}|x - y_0|^2 + \alpha(< x >^m + < y_0 >^m),$$
$$\psi(y) = W(x_0) - \frac{1}{\epsilon}|x_0 - y|^2 - \alpha(< x_0 >^m + < y >^m).$$

Since $W-\phi$ achieves maximum at x_0, and $V-\psi$ achieves minimum at y_0,

$$W(x_0) + H(x_0, D\phi(x_0)) \leq 0, \tag{5.30}$$

$$V(y_0) + H(y_0, D\psi(y_0)) \geq 0. \tag{5.31}$$

Subtracting (5.31) from (5.30) and using Proposition 5.2.8, we have

$$\begin{aligned} W(x_0) - V(y_0) \leq \quad & C_{R_\alpha}(1 + \frac{2}{\epsilon}|x_0 - y_0|)|x_0 - y_0| \\ & + \alpha C_0 m(< x_0 >^{m-1} + < y_0 >^{m-1}). \end{aligned}$$

Now fix α, construct a sequence $\{\epsilon_k\}$ with $\lim_{k\to\infty} \epsilon_k = 0$. We denote the corresponding maximizers of Φ as (x_{0k}, y_{0k}). Since $\forall k, (x_{0k}, y_{0k}) \in \bar{B}(0, R_\alpha)$, by extracting a subsequence if necessary, we get

$$\lim_{k\to\infty} (x_{0k}, y_{0k}) \to (x_\alpha, y_\alpha) \in \bar{B}(0, R_\alpha). \tag{5.32}$$

From (5.29), we have $x_\alpha = y_\alpha$. For each ϵ_k, from $\Phi(x, x) \leq \Phi(x_{0k}, y_{0k})$, we can get

$$\begin{aligned} W(x) \quad - \quad & V(x) - 2\alpha < x >^m \leq C_{R_\alpha}(1 + \frac{2}{\epsilon_k}|x_{0k} - y_{0k}|)|x_{0k} - y_{0k}| \\ + \quad & \alpha C_0 m(< x_{0k} >^{m-1} + < y_{0k} >^{m-1}) - \alpha(< x_{0k} >^m + < y_{0k} >^m), \end{aligned}$$

and letting $k \to \infty$,

$$W(x) - V(x) \leq 2\alpha(C_0 m < x_\alpha >^{m-1} - < x_\alpha >^m) + 2\alpha < x >^m .$$

Since $C_0 m < x_\alpha >^{m-1} - < x_\alpha >^m \leq C''$ for some $C'' > 0$,

$$W(x) - V(x) \leq 2\alpha(C'' + < x >^m).$$

Letting $\alpha \to 0$, we get $W(x) - V(x) \leq 0$, $\forall x$. We conclude by noting W and V are symmetric. ∎

From Theorem 5.2.10, if we can solve for a solution to (5.26) in $\mathcal{P}(\mathbb{R}^2)$, it must be the value function. One way to solve it is by the discrete-time approximation.

5.2.4 The discrete approximation scheme

The approximation will be accomplished in two steps. First we approximate the continuous time optimal control problem by a discrete time problem, derive the hybrid discrete Bellman equation (DBE), and show the value function of the discrete time problem converges to that of the continuous time problem locally uniformly. Following [9], we call this step "semi-discrete" approximation. Then we indicate how to further discretize (DBE) in the spatial variable, which is called "fully-discrete" approximation. The approaches we take here follow closely those in [9](Chapter VI and Appendix A).

Consider a discrete time problem obtained by discretizing the original continuous time one with time step $h \in (0, \frac{1}{\lambda})$. The dynamics is given by

$$x[n] = x[n-1] + hf(x[n-1], u[n-1], d[n-1]),\ x[0] = x, \tag{5.33}$$

and the cost is given by

$$J_h(x, \alpha[\cdot]) = \sum_{n=0}^{\infty} hl(x[n], u[n])(1-\lambda h)^n, \tag{5.34}$$

where $\alpha[\cdot] = \{d[\cdot], u[\cdot]\}$ is the control. The value function is defined to be

$$V_h(x) = \inf_{\alpha[\cdot]} J_h(x, \alpha[\cdot]). \tag{5.35}$$

It's not hard to show:

Proposition 5.2.11 *Assume A_1 and A_2, $\lambda > 2L_0$. Then $V_h(\cdot) \in \mathcal{P}(\mathbb{R}^2)$, and the coefficient C in defining $\mathcal{P}(\mathbb{R}^2)$ can be made independent of h.*

Following standard arguments, one can show:

Proposition 5.2.12 (DBE) *$V_h(\cdot)$ satisfies:*

$$\begin{aligned} V_h(x) = \quad & \min\{\min_{u\in U_+}\{(1-\lambda h)V_h(x+huf_+(x))+hl(x,u)\}, \\ & \min_{u\in U_-}\{(1-\lambda h)V_h(x+huf_-(x))+hl(x,u)\}\},\ x\in\mathbb{R}^2. \end{aligned} \tag{5.36}$$

It's of interest to know whether (5.36) characterizes the value function $V_h(x)$. Unlike in [9](Chapter VI), where a bounded value function was considered, we have V_h unbounded. But it turns out that with a little bit additional assumption, (5.36) has a unique solution.

Proposition 5.2.13 *There exists a unique solution in $\mathcal{P}(\mathbb{R}^2)$ to (5.36), if*

$$\frac{(1-\lambda h)(\sqrt{C_0^2+4}+C_0)}{\sqrt{C_0^2+4}-C_0}<1, \tag{5.37}$$

where $C_0 = hu_{\mathrm{c}}\left|\begin{array}{c}1\\ C_{\mathrm{f}}\end{array}\right|$ and C_{f} is as defined in Proposition 5.1.4.

Proof Let $\widetilde{V}_h(x) = V_h(x) < x >^{-m}, m > 2$, where $< x > \stackrel{\triangle}{=} \sqrt{1+|x|^2}$. Since $V_h \in \mathcal{P}(\mathbb{R}^2)$, $\widetilde{V}_h$ is bounded. In terms of $\widetilde{V}_h$, (5.36) is rewritten as

$$\begin{aligned} & \widetilde{V}_h(x) = (\mathcal{G}(\widetilde{V}_h))(x) \stackrel{\triangle}{=} \min\{ \\ & \min_{u\in U_+}\{(1-\lambda h)\widetilde{V}_h(x+huf_+(x))\frac{< x+huf_+(x) >^m}{< x >^m} + hl(x,u) < x >^{-m}\}, \\ & \min_{u\in U_-}\{(1-\lambda h))\widetilde{V}_h(x+huf_-(x))\frac{< x+huf_-(x) >^m}{< x >^m} + hl(x,u) < x >^{-m}\}\}. \end{aligned} \tag{5.38}$$

It suffices to show (5.38) has a unique solution. It's clear that the operator $\mathcal{G}(\cdot)$ maps any $\widetilde{W} \in BC(\mathbb{R}^2)$ into $BC(\mathbb{R}^2)$, where $BC(\mathbb{R}^2)$ denotes the set of bounded continuous functions. When (5.37) is satisfied, one can show that $\mathcal{G}(\cdot)$ is a contraction mapping. Hence we conclude using the contraction mapping theorem. ■

The following theorem asserts that $V_h(\cdot)$ converges to $V(\cdot)$ as $h \to 0$. The proof can be found in [9](Chapter VI)(with minor modification).

Theorem 5.2.14 *Assume A_1 and A_2, $\lambda > 2L_0$, and (5.37). Then*

$$\sup_{x \in \mathcal{K}} |V_h(x) - V(x)| \to 0 \ \ as \ \ h \to 0, \tag{5.39}$$

for every compact $\mathcal{K} \subset \mathbb{R}^2$.

It was also shown in [9] that one can obtain a sub-optimal control for the continuous time problem when solving the DBE. Theoretically the solution to (5.36) can be obtained by successive approximation. A practical approximation scheme for solving the DBE is described in [9] (Appendix A, by Falcone). It was shown there that when space discretization gets finer and finer, the solution obtained via solving a finite system of equations converges to $V_h(\cdot)$.

5.3 Other Control Problems

In this section, we briefly discuss how to extend the viscosity solutions approach to other control problems of practical interest. Since key ideas have been studied in details in Section 5.2, we will just state the results without proof.

In some optimal control problems or dynamical games, the value functions may be discontinuous. To handle this problem, we introduce the notion of *non-continuous viscosity solutions*.

We recall that a function $f : E \subset \mathbb{R}^n \to \mathbb{R}$ is *upper* (*lower,* resp.) *semicontinuous* if for any $x \in E$ and $\epsilon > 0$, there exists $\delta > 0$, such that $f(y) < f(x) + \epsilon$ ($f(y) > f(x) - \epsilon$, resp.) for all $y \in E$ and $|y - x| < \delta$. An upper (lower, resp.) semicontinuous function achieves its maximum (minimum, resp.) value on any compact subset of E.

Definition 5.3.1 (Semicontinuous semisolutions) *[9] Let W be an upper (lower, resp.) semicontinuous function from an open set $O \subset \mathbb{R}^n$ into $\mathbb{R}$. W is called a viscosity subsolution (supersolution, resp.) to (5.21), provided $\forall \phi \in C^1(O)$, if $W - \phi$ attains a local maximum (minimum, resp.) at $x_0 \in O$, then*

$$F(x_0, W(x_0), D\phi(x_0)) \leq 0 \ (\geq 0, \ resp.).$$

Definition 5.3.2 (Semicontinuous envelopes) *[9] For a locally bounded function $V : E \subset \mathbb{R}^n \to R$, its upper semicontinuous envelope V^* is defined by*

$$V^*(x) = \limsup_{y \to x} V(y) \stackrel{\triangle}{=} \lim_{r \to 0^+} \sup\{V(y) : y \in E, |y - x| \leq r\},$$

and its lower semicontinuous envelope V_* is defined by

$$V_*(x) = \liminf_{y \to x} V(y) \stackrel{\triangle}{=} \lim_{r \to 0^+} \inf\{V(y) : y \in E, |y - x| \leq r\}.$$

It's easy to check that V^* is upper semicontinuous and V_* is lower semicontinuous.

Definition 5.3.3 (Non-continuous viscosity solutions) *A locally bounded function V is a non-continuous viscosity solution of (5.21) if V^* is a subsolution of (5.21) and V_* is a supersolution of (5.21) according to Definition 5.3.1.*

We note that Definition 5.3.3 coincides with Definition 5.2.6 if the function is continuous. Hence from now on, whenever we say a viscosity solution, it should be understood in the sense of Definition 5.3.3.

5.3.1 The finite time horizon optimal control problem

We define the cost functional for the finite time horizon problem: starting from x at time t,

$$J(x,t,\alpha(\cdot)) = \int_t^T l(x(\tau),u(\tau),\tau)e^{-\lambda\tau}d\tau + g(x(T)), \tag{5.40}$$

where $T > 0$, $0 \le t \le T$, $x \in \mathbb{R}^2$, $\lambda \ge 0$, and g is the *terminal cost*. The value function $V(x,t)$ is defined as

$$V(x,t) = \inf_{\alpha(\cdot)} J(x,t,\alpha(\cdot)).$$

We assume:

- (A_3): $l(\cdot,\cdot,\cdot)$ is continuous, $l \ge 0$;
- (A_4): $|l(x_1,u,t) - l(x_2,u,t)| \le C_l(1+|x_1|+|x_2|)|x_1-x_2|$, $\forall u, \forall\, x_1, x_2, \forall\, t \in [0,T]$, for some $C_l > 0$;
- (A_5): $|g(x_1) - g(x_2)| \le C_{\mathrm{g}}(1+|x_1|+|x_2|)|x_1-x_2|, \forall\, x_1, x_2$.

Example 5.3.4 *A trajectory tracking problem on a finite interval can be formulated as above with $\lambda = 0$, $g \equiv 0$, and*

$$l(x,u(t),t) = q(t)(x_2 - \bar{x}_2(t))^2 + u^2(t),$$

where $q(t) > 0, \forall\, t$, x_2 denotes the M component of x and $\bar{x}_2(\cdot)$ is a bounded, desired trajectory of M.

We can show the value function has some nice properties.

Proposition 5.3.5 *Under assumptions $(A_3) - (A_5)$, $V(x,t)$ is locally bounded.*

Proposition 5.3.6 *Under assumptions* $(A_3)-(A_5)$, $V(x,t)$ *is locally Lipshitz continuous, i.e.,* $\forall\, R>0$,

$$|V(x_1,t)-V(x_2,s)|\le L_{\mathrm{R}}(|x_1-x_2|+|t-s|), \forall\, x_1,x_2\in\bar{B}(0,R),\ \forall\, t,s\in[0,T], \tag{5.41}$$

and L_{R} *can be written as* $L_{\mathrm{R}}=C(1+R)$ *for some* $C>0$.

Therefore V belongs to the following class of functions on $\mathbb{R}^2\times(0,T)$:

$$\mathcal{P}_1(\mathbb{R}^2\times(0,T))=\{W(\cdot,\cdot): |W(x_1,t)-W(x_2,s)|\le C(1+R)(|x_1-x_2|+|t-s|),$$
$$\forall\, x_1,x_2\in\bar{B}(0,R), \forall\, R>0, \forall\, t,s\in(0,T),\ \text{for some } C>0\}.$$

We can prove:

Proposition 5.3.7 *The value function* V *is a viscosity solution of the following evolutive HJB equation:*

$$-W_t(x,t)+\lambda W(x,t)+H(x,DW(x,t),t)=0,\ x\in\mathbb{R}^2,\ t\in(0,T), \tag{5.42}$$

$$W(x,T)=g(x),\ x\in\mathbb{R}^2, \tag{5.43}$$

where the Hamiltonian

$$H(x,p,t)\stackrel{\triangle}{=}\max\{\max_{u\in U_+}\{-uf_+(x)\cdot p-l(x,u,t)\},\max_{u\in U_-}\{-uf_-(x)\cdot p-l(x,u,t)\}\},$$

W_t *denotes the partial derivative with respect to* t, *and* DW *denotes the partial derivative with respect to* x.

The Hamiltonian in (5.42) enjoys nice regularity properties, similar to those in Proposition 5.2.8. Based on this, we can prove:

Proposition 5.3.8 *If the HJB equation (5.42) with the terminal condition (5.43) has a viscosity solution in* $\mathcal{P}_1(\mathbb{R}^2\times(0,T))$, *it is unique.*

The proof can be found in [47, 60].

5.3.2 The time-optimal control problem

Time-optimal control is important in applications, like micro-positioning. Since only the M component of x is related to the displacement output, we consider the target set $\mathcal{T}$ to be

$$\mathcal{T} \stackrel{\triangle}{=} \{(H, M) \in \mathbb{R}^2 : H_{min} \leq H \leq H_{max}, M = M_0\}, \tag{5.44}$$

where $M_0 \in [-M_s, M_s]$ is the magnetization corresponding to, say, the desired displacement.

Remark 5.3.9 *The constraint $H \in [H_{min}, H_{max}]$ in (5.44) reflects the limitation on the input current of the actuator. Also without this constraint, the time-optimal control problem would be uninteresting: since $f_i > 0$, $i = 1, 2, 3$, in the model (5.3), the optimal control would be $u = u_c$ if $M < M_0$, $u = -u_c$ if $M > M_0$ and $u = 0$ if $M = M_0$.*

For any control pair $\alpha(\cdot)$, $x \in \mathbb{R}^2$, define

$$t_x(\alpha) = \begin{cases} \infty \text{ if } \{t : x(t) \in \mathcal{T}\} = \emptyset \\ \min\{t : x(t) \in \mathcal{T}\} \text{ otherwise} \end{cases}. \tag{5.45}$$

Then the minimum-time function, the value function for the time-optimal problem, is defined as

$$T(x) = \inf_{\alpha(\cdot)} t_x(\alpha). \tag{5.46}$$

Let $\partial\mathcal{T}$ denote the boundary of $\mathcal{T}$, and $\mathcal{T}^c$ denote the complement of $\mathcal{T}$ in $\mathbb{R}^2$. In the case of (5.44), $\partial\mathcal{T} = \mathcal{T}$. The continuity of $T(x)$ is closely related to the *small-time controllability* on $\mathcal{T}$ [9]. Due to lack of controllability in (5.4), we are unable to establish the small-time controllability of (5.4) at $\mathcal{T}$, and therefore we have to take $T(x)$ to be a non-continuous (not necessarily continuous) function.

It's often more convenient to study the *Kružkov transform* of $T(x)$ [9]:

$$V(x) \triangleq \begin{cases} 1 - e^{-T(x)} & \text{if } T(x) < \infty \\ 1 & \text{if } T(x) = \infty \end{cases} . \tag{5.47}$$

We note that $V(x)$ is the value function for the optimal control problem with cost functional

$$J(x, \alpha(\cdot)) = \inf_{\alpha(\cdot)} \int_0^{t_x(\alpha)} e^{-t} dt, \tag{5.48}$$

and the optimal control for (5.48) coincides with the time-optimal control.

One can show that $V(x)$ is a non-continuous viscosity solution of

$$W(x) + H(x, DW(x)) = 0, \ x \in \mathcal{T}^c, \tag{5.49}$$

$$W(x) = 0, \ x \in \partial\mathcal{T}, \tag{5.50}$$

where the Hamiltonian

$$H(x, p) \triangleq \max\{\max_{u \in U_+}\{-u f_+(x) \cdot p\}, \max_{u \in U_-}\{-u f_-(x) \cdot p\}\} - 1.$$

It is very hard to characterize the value function as the unique solution of the Dirichlet problem (5.49),(5.50) in the class of non-continuous functions. To proceed toward that direction, we introduce a generalized solution, the *envelope solution*, of the Dirichlet problem.

Consider the Dirichlet boundary value problem:

$$\begin{cases} F(x, W(x), DW(x)) = 0, \ x \in O \\ W(x) = g(x), \ x \in \partial O \end{cases} , \tag{5.51}$$

where $O \subset \mathbb{R}^n$ is open, $F : O \times \mathbb{R} \times \mathbb{R}^n \to \mathbb{R}$ continuous, $g : \partial O \to \mathbb{R}$. Let $\bar{O}$ denote the closure of O. We say that a bounded upper (lower, resp.) semicontinuous function $W : \bar{O} \to \mathbb{R}$ is a *subsolution* (*supersolution,* resp.) of (5.51) if it is

a viscosity subsolution (supersolution, resp.) of $F(x, W(x), DW(x)) = 0$ on O (Definition 5.3.1) and is $\leq g$ ($\geq g$, resp.) on ∂O.

Now denote

$$\mathcal{S} \triangleq \{\text{subsolutions of (5.51)}\}, \quad \mathcal{Z} \triangleq \{\text{supersolutions of (5.51)}\}.$$

Definition 5.3.10 (Envelope solutions) *[9] Let $W : \bar{O} \to \mathbb{R}$ be locally bounded.*

1. *W is an envelope viscosity subsolution of (5.51), briefly, e-subsolution, if there exists $\mathcal{S}(W) \subset \mathcal{S}$, $\mathcal{S} \neq \emptyset$, such that*

$$W(x) = \sup_{w \in \mathcal{S}(W)} w(x), \ x \in \bar{O};$$

2. *W is an e-supersolution of (5.51), if there exists $\mathcal{Z}(W) \subset \mathcal{Z}$, $\mathcal{Z} \neq \emptyset$, such that*

$$W(x) = \inf_{w \in \mathcal{Z}(W)} w(x), \ x \in \bar{O};$$

3. *W is an e-solution of (5.51) if it is an e-subsolution and e-supersolution.*

We can show:

Proposition 5.3.11 *$V_*(x)$ (recall Definition 5.3.2) is the unique e-solution of the Dirichlet problem (5.49),(5.50).*

The proof can be found in [9].

5.3.3 The exit problem

It's natural to consider problems with the restricted state space for control of a magnetostrictive actuator. Let

$$\Omega \triangleq \{(H, M) \in \mathbb{R}^2 : H_{min} < H < H_{max}, -M_s < M < M_s\},$$

and let $\bar{\Omega}$, Ω^c be its closure and complement in $\mathbb{R}^2$, respectively. The constraint on H has been explained in Subsection 5.3.2, while the constraint on M is from the physics.

For a control problem with state space constraint, in which any admissible control has to keep the state within certain domain throughout the time period of interest, the value function, if it's continuous, is a *constrained viscosity solution* of the corresponding HJB equation [73]. As in the case of time-optimal control, the continuity of the value function depends on the controllability of the system at the domain boundary.

In this subsection we study an exit problem for the model (5.4). For any $x \in \mathbb{R}^2$, any measurable control pair $\alpha(\cdot)$, we denote by $t_x(\alpha)$ the first exit time of $x(t)$ from the open set Ω. Clearly, if $x \in \Omega$, $t_x(\alpha) = 0$ for any $\alpha(\cdot)$. The cost functional is defined as

$$J(x, \alpha(\cdot)) = \begin{cases} \int_0^{t_x(\alpha)} l(x(t), u(t)) e^{-t} dt + e^{-t_x(\alpha)} g(x(t_x(\alpha))) & \text{if } t_x(\alpha) < \infty \\ \int_0^{\infty} l(x(t), u(t)) e^{-t} dt & \text{if } t_x(\alpha) = \infty \end{cases}, \tag{5.52}$$

where for simplicity, we have let the discount factor $\lambda = 1$. The running cost l is assumed to be bounded, continuous with respect to x and u, and Lipschitz continuous with respect to x. The terminal cost g is assumed to be bounded, continuous, and satisfies a global principle of sub-optimality:

$$g(x) \leq \inf_{\alpha(\cdot)} \{ \int_0^t l(x(s), u(s)) e^{-s} ds + e^{-t} g(x(t)) \}, \ \forall x \in \mathbb{R}^2, \ \forall\, t > 0. \tag{5.53}$$

Eq. (5.53) plays a role of a compatibility condition.

Remark 5.3.12 *If we let $\Omega = \mathcal{T}^c$, $g \equiv 0$, $l \equiv 1$, we recover the time-optimal control problem. Hence the result of this subsection applies to the time-optimal problem as well.*

We can't prove the continuity of the value function $V(x) = \inf_{\alpha(\cdot)} J(x, \alpha(\cdot))$, again due to lack of controllability. $V(x)$ is a (non-continuous) viscosity solution of the HJB equation. As discussed in Subsection 5.3.2, we need some additional tools to single out the value function from all viscosity solutions of the HJB equation. In Subsection 5.3.2, we used the notion of e-solutions, here we will make use of another concept, the *bilateral supersolutions* of Dirichlet problems.

The HJB equation associated with the exit problem is

$$\begin{cases} W(x) + H(x, DW(x)) = 0, \ x \in \Omega \\ W(x) = g(x), \ x \in \partial\Omega \end{cases}, \tag{5.54}$$

where the Hamiltonian

$$H(x,p) \stackrel{\triangle}{=} \max\{\max_{u\in U_+}\{-uf_+(x)\cdot p - l(x,u)\}, \max_{u\in U_-}\{-uf_-(x)\cdot p - l(x,u)\}\}.$$

Consider the first equation in (5.54):

$$W(x) + H(x, DW(x)) = 0, \ x \in \Omega. \tag{5.55}$$

Definition 5.3.13 (Bilateral supersolutions of (5.55)) *[9] A lower semicontinuous function $W : \Omega \to \mathbb{R}$ is a bilateral (non-continuous viscosity) supersolution of (5.55) if it is both a supersolution of (5.55) and*

$$-W(x) - H(x, DW(x)) = 0, \ x \in \Omega.$$

Definition 5.3.14 (Bilateral supersolutions of (5.54)) *[9] Given a lower semicontinuous function $g : \mathbb{R}^2 \to \mathbb{R}$, a lower semicontinuous function $W : \mathbb{R}^2 \to \mathbb{R}$ is a bilateral supersolution of (5.54) if it is a bilateral supersolution of (5.55), $W(x) = g(x)$, $\forall\, x \in \Omega^c$, and it is a supersolution of*

$$-W(x) - H(x, DW(x)) = 0, \ x \in \mathbb{R}^2.$$

The following result is adapted from [9]:

Proposition 5.3.15 *$V_*(x)$ is the unique bounded bilateral supersolution of (5.54).*

5.3.4 The nonlinear $\mathcal{H}_\infty$ control problem

In this subsection, we consider the nonlinear $\mathcal{H}_\infty$ control problem. For that we introduce an exogenous disturbance w into the model (5.4) and define a regulated output z:

$$\begin{cases} \dot{x}(t) = f(x(t), u(t), d(t)) + g(x(t))w(t) \\ z(t) = h(x(t), u(t)) \end{cases}, \tag{5.56}$$

where g is a continuous function taking values in $\mathbb{R}^{2\times p}$, $p > 0$, w takes values in $W_0 \subset \mathbb{R}^p$, z takes values in $\mathbb{R}^q$, $q > 0$, and h is continuous. We will assume that $w(\cdot) \in L^2_{loc}(\mathbb{R}, W_0)$, i.e.,

$$\int_0^T |w(t)|^2 dt < \infty, \forall\, T < \infty, \text{ and } w(t) \in W_0, \forall\, t.$$

Definition 5.3.16 *The (state feedback) sub-optimal $\mathcal{H}_\infty$ control problem with disturbance attenuation level $\gamma > 0$ is solvable if there is a state feedback controller $K(\cdot)$, such that:*

1. **(Dissipativity)** the closed-loop system is dissipative with level γ, i.e., there exists some finite function $U(x) \geq 0$ and $U(0) = 0$, such that starting from $x \in \mathbb{R}^2$,

$$\int_0^T |z(t)|^2 - \gamma^2 |w(t)|^2 dt \leq U(x),\ \forall x, \forall T \geq 0, \forall w(\cdot) \in L^2_{loc}(\mathbb{R}^+, W_0). \tag{5.57}$$

2. **(Stability)** the closed-loop system is stable when $w(t) \equiv 0$.

A general theory of dissipative systems has been studied by Willems [88], where dissipativity is defined in terms of an inequality involving the *storage function* and the *supply rate*. (Asymptotic) stability of a dissipative system can be obtained

with a further assumption on detectability of the system [44]. James [48] has shown that a system is dissipative if and only if a partial differential inequality (PDI) admits a lower semicontinuous solution in the viscosity sense. Van der Schaft made use of the dissipativity theory in the $\mathcal{H}_\infty$ control setting and derived the Hamilton-Jacobi-Isaacs (HJI) equation for nonlinear affine systems with state feedback [70].

The connection between $\mathcal{H}_\infty$ control and differential games has been well-known [6, 10, 49]. The value function of a differential game (when it exists) is the viscosity solution of the HJI equation under very general assumptions [31]. The relationship between $\mathcal{H}_\infty$ control and viscosity solutions of the appropriate HJI equations has been pursued by [59, 5, 75, 92, 90, 76], to name a few. Here we mention that in particular, Soravia has shown that the $\mathcal{H}_\infty$ control problem is solvable if and only if the corresponding HJI equation admits a nonnegative lower semicontinuous supersolution, which is null and continuous at the origin [76]. This result is the parallel of that in [48] for dissipative systems.

The differential game corresponding to the problem (5.57) is

$$V_\gamma(x) = \inf_K \sup_{w(\cdot)} \sup_T \int_0^T |z(t)|^2 - \gamma^2 |w(t)|^2 dt, \tag{5.58}$$

where V_γ is called the *lower* value function since the controller has advantage over the disturbance. If we let the disturbance have advantage over the controller, the corresponding $\bar{V}_\gamma$ will be called the *upper* value function. In our problem, since the control pair $\alpha = \{d, u\}$ and the disturbance w are seperate in the dynamics and the cost, the Isaacs condition is satisfied and $V_\gamma = \bar{V}_\gamma$.

One can show V_γ satisfies the following HJI equation in the viscosity sense:

$$H(x, DV_\gamma(x)) = 0, \tag{5.59}$$

where the Hamiltonian

$$H(x,p) \triangleq \inf_{w\in W}\{-g(x)w\cdot p \quad + \quad \gamma^2|w|^2\} + \max\{\max_{u\in U_+}\{-uf_+(x)\cdot p - |h(x,u)|^2\}, \max_{u\in U_-}\{-uf_-(x)\cdot p - |h(x,u)|^2\}\}.$$

From the previous discussion, if we can obtain a supersolution of (5.59) which satisfies certain conditions, then the sub-optimal $\mathcal{H}_\infty$ problem is solvable. We note that in general, (5.59) has many supersolutions and one does not seek the uniqueness of the solution. Some computational techniques for solving a PDI in the viscosity sense can be found in James and Yuliar [50]. Controller synthesis based on a (super)solution of the HJI equation has been investigated under various assumptions in, e.g., [5, 75, 92, 90], but it remains an open problem for general cases.

5.4 Optimal Control Based on the Dynamic Hysteresis Model

In this section we briefly discuss how to extend the viscosity solutions approach to optimal control problems based on the dynamic hysteresis model (3.2).

Consider the system (3.2). Given the initial memory curve $\psi \in \Psi$ with corresponding H, the cost functional associated with a control input $I(\cdot)$ is defined as

$$J(H,\psi,I(\cdot)) = \int_0^\infty l(H(t),M(t),I(t))e^{-\lambda t}dt,$$

where $\{H(\cdot),M(\cdot)\}$ is the solution of (3.2) under $I(\cdot)$ with the initial condition ψ, and $\lambda \geq 0$. The value function is defined as

$$V(H,\psi) = \inf_{I(\cdot)} J(H,\psi,I(\cdot)).$$

Remark 5.4.1 *We know the true state space for (3.2) is Ψ. In the definitions above, we "augment" the state space by including the H component, which will be useful in applying the viscosity solutions approach. Note the H component must be consistent with ψ.*

From our analysis in Chapter 3, $\{H(\cdot), M(\cdot)\}$ is bounded if $I(\cdot)$ is so. Hence it's natural to make the following assumptions about the running cost l: l is continuous,

$$0 \leq l(H, M, I) \leq C_0, \forall H, M, \forall I \in [-I_0, I_0], \text{ and}$$

$$|l(H_1, M_1, I) - l(H_2, M_2, I)| \leq C_l(|H_1 - H_2| + |M_1 - M_2|), \forall H_1, H_2, M_1, M_2,$$

$\forall I \in [-I_0, I_0]$, where $C_0 > 0, C_l > 0$ are constants, and I_0 is the limit on the input current of the actuator.

From Proposition 3.3.9 and the assumptions on l, one can easily show that V is bounded and uniformly continuous.

In [4], the author considered an optimal control problem for a controlled system with the form:

$$\begin{cases} \dot{y}(t) = f(y(t), z(t), u(t)) \\ z(t) = \Gamma[y, \psi](t) \end{cases}, \tag{5.60}$$

where Γ is the Preisach operator. The value function was shown to be the unique bounded, uniformly continuous solution of a discontinuous, infinite dimensional HJB equation in an adapted viscosity sense. In [12], the authors studied optimal control of the following system:

$$\begin{cases} \dot{y}(t) = f(t, y(t), u(t), z(t)) \\ z(t) = \Gamma[u, \psi](t) \end{cases}, \tag{5.61}$$

and proposed a new type of HJB equations, where one of the arguments is the active set ($P_+(t)$ in Figure 2.2).

The approach in [4] can be extended to our problem after we rewrite (3.2) as

$$\dot{H}(t) = \frac{c_1}{1 + \frac{dM}{dH}(\psi_t, sgn(I(t) - \frac{H(t)}{c_0}))}(I(t) - \frac{H(t)}{c_0}), \tag{5.62}$$

where $\frac{dM}{dH}(\cdot, \cdot)$ is as defined in Subsection 3.4.1. Although ψ_t appears in (5.62), it does not cause extra difficulty since ψ is an argument in the HJB equation.

Chapter 6

Conclusions

This dissertation has been centered around modeling and control of hysteresis in smart actuators. Extensive simulation and experimental work based on a commercial magnetostrictive actuator have been conducted to validate the modeling approach and the control schemes.

The contribution of this dissertation in the modeling aspect is the proposal of a novel dynamic hysteresis model, consisting of a Preisach operator coupled to an ODE. We have established the well-posedness of the model from two different perspectives. Apart from being useful for the control purpose, the model presents many interesting system-theoretic problems due to its special structure. We have studied the following properties of the model: stability of the equilibria, input-output stability, reachability and observability. We have also looked at algorithms to numerically integrate the system. In addition, the existence of periodic solutions under periodic forcing has been proved. This helps validate the model and provides a theoretical basis for an identification scheme.

We have pursued the problem of hysteresis control along three different but connected paths: inverse control, robust control and optimal control.

The idea of inverse compensation is to construct an inverse operator to cancel out the hysteretic nonlinearity in smart actuators. This is done for the Preisach operator based models. We have presented parameter identification methods and proposed several efficient inversion schemes, all of which can be implemented in real-time. A special type of inversion problem, the *value inversion* problem, has also been formulated and solved.

Inverse control is open-loop in nature and its performance is susceptible to model uncertainties and to errors introduced in the inversion process. To combat this problem, we have come up with a robust control framework for smart actuators. The inversion error is modeled as an exogenous disturbance whose magnitude is quantifible, and then robust control techniques are employed to attenuate its impact. We have also been able to incorporate the saturation constraint into the controller design.

We have studied optimal control problems mainly based on a low dimensional hysteresis model. We have adopted the dynamic programming approach and studied the Hamilton-Jacobi-Bellman equation satisfied by the value function in the viscosity sense.

There are several possible directions to extend the work reported in this dissertation.

We observe that the hysteretic behavior of the actuators varies slowly, possibly due to fluctuation of the temperature. An interesting research direction is to include this variability in hysteresis modeling, for example, proposal of a generalized Preisach operator having extra parameters to account for the variability. We note that a time-dependent Preisach model has been proposed in [27], where the thresholds (β, α) of hysterons are allowed to be time-varying.

An alternative approach to tackle the above problem would be adaptive parameter identification and adaptive inverse control. Although this idea has been pursued for several other (relatively simple) hysteretic operators [80, 57], adaptive inverse control remains an open problem for the Preisach operator.

With fast development of the micro-electro-mechanical systems (MEMS) technology, many applications will involve thousands of smart sensors, actuators, and processors, where information processing and decision making should be done in a distributed but coordinated way. In such a setting, control with communication and compuation constraints is currently an active research area, and how to take into account the hysteresis in sensors and actuators becomes an important and challenging problem.

Appendix A

Elements of Functional Analysis

In this appendix, we review some basic notions and results of functional analysis which have been used in the development of this dissertation. In particular, we introduce metric spaces, Banach spaces and fixed point theorems. The material in this appendix can be found in, e.g., [69, 93].

A.1 Metric Spaces

Definition A.1.1 (Metric spaces) *A metric space $< X, \rho >$ is a nonempty set X of elements together with a real-valued function ρ defined on $X \times X$ such that for all x, y and z in X:*

$$
\begin{aligned}
&1.\ \rho(x,y) \geq 0,\\
&2.\ \rho(x,y) = 0 \text{ if and only if } x = y,\\
&3.\ \rho(x,y) = \rho(y,x), \text{ and}\\
&4.\ \rho(x,y) \leq \rho(x,z) + \rho(z,y).
\end{aligned}
$$

The function ρ is called a metric.

For a metric space $< X, \rho >$, $O \subset X$ is called *open* if, $\forall x \in O$, $\exists \delta > 0$ such that $\{y \in X : \rho(x, y) < \delta\} \subset O$. A point $x \in X$ is called a *point* of closure of the set $E \subset X$ if, $\forall \delta > 0$, $\exists y \in E$, such that $\rho(x, y) < \delta$. The set of points of closure of E is denoted as $\bar{E}$. A set E is called *closed* if $\bar{E} = E$. If $\bar{E} = X$, E is said to be *dense* in X. A metric space $< X, \rho >$ is called *seperable* if it has a subset D which has a countable number of points and is dense in X.

A function f on a metric space $< X, \rho_X >$ into a metric space $< Y, \rho_Y >$ is said to be *continuous* at x if, $\forall \epsilon > 0$, $\exists \delta > 0$ such that if $\rho_X(x, z) < \delta$, then $\rho_Y(f(x), f(z)) < \epsilon$. It is called continuous if it is continuous at every $x \in X$. f is called *injective* if it is one-to-one, and is called *surjective* if it is onto, i.e., $f(X) \stackrel{\triangle}{=} \{z \in Y : z = f(x) \text{ for some } x \in X\} = Y$.

A sequence $\{x_n\}$ from a metric space $< X, \rho >$ *converges* to $x \in X$ if given $\epsilon > 0$, there is an N such that $\rho(x, x_n) < \epsilon$ for all $n \geq N$. The point x is called the *limit* of $\{x_n\}$, and we write $x_n \to x$. We call x a *cluster* point of $\{x_n\}$ if a subsequence of $\{x_n\}$ converges to x.

A sequence $\{x_n\}$ from a metric space $< X, \rho >$ is called a *Cauchy sequence*, if given $\epsilon > 0$, there is an N, such that $\rho(x_n, x_m) < \epsilon$ for all $n, m > N$. A convergent sequence is a Cauchy sequence, but the converse is not generally true. If the metric space has the property that every Cauchy sequence converges, we say that space is *complete*.

A collection $\mathcal{U}$ of open sets in a metric space is an *open covering* of a set E if E is contained in the union of the sets in $\mathcal{U}$. A set E is said to be *compact* if every open covering $\mathcal{U}$ of E has a finite subcovering, i.e., if there is a finite collection $\{O_1, O_2, \cdots, O_N\} \subset \mathcal{U}$ such that $E \subset \cup_{i=1}^{N} O_i$.

We say that a set E in a metric space $< X, \rho >$ is *relatively sequentially compact* if any sequence $\{x_n\}$ in E has a convergent subsequence $x_{n_k} \to x \in X$. E is *sequentially compact* if any sequence $\{x_n\}$ in E has a convergent subsequence $x_{n_k} \to x \in E$.

For a metric space, the notions of compactness and sequential compactness are equivalent.

A family $\mathcal{F}$ of functions from a metric space $< X, \rho_X >$ to a metric space $< Y, \rho_Y >$ is called *equicontinuous* at $x \in X$ if, $\forall \epsilon > 0$, $\exists$ an open set O containing x such that $\rho_Y(f(x), f(z)) < \epsilon$ for all $z \in O$ and $f \in \mathcal{F}$. The family is said to be equicontinuous on X if it is equicontinuous at each point $x \in X$.

Theorem A.1.2 (The Ascoli-Arzelá theorem) *Let $\mathcal{F}$ be an equicontinuous family of functions from a seperable space $< X, \rho_X >$ to a metric space $< Y, \rho_Y >$. Let $\{f_n\}$ be a sequence in $\mathcal{F}$ such that for each $x \in X$, the closure of the set $\{f_n(x) : n \geq 0\}$ is compact. Then there is a subsequence $\{f_{n_k}\}$ that converges pointwise to a continuous function f, and the convergence is uniform on each compact subset of X.*

Corollary A.1.3 *Let $\mathcal{F}$ be an equicontinuous family of real-valued functions on a seperable space X. Then each sequence $\{f_n\}$ in $\mathcal{F}$ which is bounded at each point has a subsequence $\{f_{n_k}\}$ that converges pointwise to a continuous function, and the convergence is uniform on each compact subset of X.*

A.2 Banach Spaces

In the following $\mathbb{K} = \mathbb{R}$ or $\mathbb{K} = \mathbb{C}$, where $\mathbb{R}$ denotes the set of real numbers and $\mathbb{C}$ denotes the set of complex numbers.

Definition A.2.1 (Vector spaces) *A set X of elements is called a vector space (or linear space) over $\mathbb{K}$ if we have a function $+$ on $X \times X$ to X and a function $\cdot$ on $\mathbb{K} \times X$ to X that satisfy the following conditions: for any $x, y \in X$, $\alpha, \beta \in \mathbb{K}$,*

$$
\begin{aligned}
&1.\ x + y = y + x,\\
&2.\ (x + y) + z = x + (y + z),\\
&3.\ \exists\, \theta \in X,\ \textit{such that } x + \theta = x, \forall x \in X,\\
&4.\ \alpha \cdot (x + y) = \alpha \cdot x + \alpha \cdot y,\\
&5.\ (\alpha + \beta) \cdot x = \alpha \cdot x + \beta \cdot x,\\
&6.\ \alpha \cdot (\beta \cdot x) = (\alpha\beta) \cdot x,\\
&7.\ 0 \cdot x = \theta, 1 \cdot x = x.
\end{aligned}
$$

For a vector space X over $\mathbb{K}$, the elements $u_1, u_2, \cdots, u_N$ of X are called *linearly independent* if and only if

$$\alpha_1 u_1 + \alpha_2 u_2 + \cdots + \alpha_N u_N = 0,\ \ \alpha_i \in \mathbb{K},\ 1 \leq i \leq N,$$

implies $\alpha_i = 0$, $1 \leq i \leq N$. The maximal number N of linearly independent elements in X is called the dimension of X. We say X is *finite dimensional* if $N < \infty$, and X is *infinite dimensional* otherwise.

Definition A.2.2 (Norms) *A nonnegative real-valued function $\| \cdot \|$ defined on a vector space is called a norm if for $x, y \in X$, $\alpha \in \mathbb{K}$,*

$$
\begin{aligned}
&1.\ \| x \| = 0 \textit{ if and only if } x = \theta,\\
&2.\ \| x + y \| \leq \| x \| + \| y \|,\\
&3.\ \| \alpha x \| = |\alpha| \, \| x \| .
\end{aligned}
$$

A normed vector space becomes a metric space if we define a metric ρ by $\rho(x, y) = \| x - y \|$. If a normed vector space is complete in this metric, it is called a *Banach space*.

A point x is called a fixed point of a mapping f if $f(x) = x$.

Theorem A.2.3 (The Banach fixed point theorem) *Let E be a closed nonempty subset of a Banach space X. Let the mapping $f : E \to E$ be k-contractive, i.e., for all $x, y \in E$,*

$$\| f(x) - f(y) \| \leq k \| x - y \|,$$

where $0 \leq k < 1$. Then there exists a unique $x^* \in E$ satisfying $f(x^*) = x^*$, and starting from any $x_0 \in E$, we have $x_n \to x^*$, where

$$x_n = f(x_{n-1}), \forall\, n \geq 1.$$

The Banach fixed point theorem is also known as the contraction mapping theorem.

A subset E of a vector space X is called *convex* if $\alpha x + (1 - \alpha)y \in E$ for all $x, y \in E$, $0 \leq \alpha \leq 1$.

Theorem A.2.4 (The Brouwer fixed point theorem) *Let E be a compact, convex, nonempty subset of a finite dimensional normed vector space X. Let the mapping $f : E \to E$ be continuous. Then f has a fixed point in E.*

Let X and Y be normed spaces over $\mathbb{K}$. The mapping $f : E \subset X \to Y$ is called *compact* if f is continuous and it maps bounded sets into relatively compact sets.

The Brouwer fixed point theorem has been generalized to the setting of a Banach space:

Theorem A.2.5 (The Schauder fixed point theorem) *Let E be a bounded, closed, convex, nonempty subset of a Banach space X. Let the mapping $f : E \to E$ be compact. Then f has a fixed point in E.*

Appendix B

Measure and Integration

The material in this appendix can be found in, e.g., [69].

B.1 Measure

A *σ-algebra* $\mathscr{A}$ is a family of subsets of a given set X which contains $\emptyset$ and is closed with respect to complements and with respect to countable unions. *A set function* ν is a function which assigns an extended real number to certain sets.

Definition B.1.1 (Measurable space) *A measurable space is a couple $(X, \mathscr{A})$ consisting of a set X and a σ-algebra $\mathscr{A}$ of subsets of X. A subset A of X is called measurable (with respect to $\mathscr{A}$) if $A \in \mathscr{A}$.*

Definition B.1.2 (Measure) *A measure ν on a measurable space $(X, \mathscr{A})$ is a nonnegative set function defined for all members of $\mathscr{A}$ and satisfying $\nu(\emptyset) = 0$ and*

$$\nu(\bigcup_{i=1}^{\infty} E_i) = \sum_{i=1}^{\infty} \nu(E_i),$$

for any sequence $\{E_i\}$ of disjoint measurable sets. By a measure space $(X, \mathscr{A}, \nu)$, we mean a measurable space $(X, \mathscr{A})$ together with a measure ν defined on $\mathscr{A}$.

A measure ν is called *finite* if $\nu(X) < \infty$. It is called σ-*finite* if there is a sequence $\{X_n\}$ of sets in $\mathscr{A}$ such that

$$X = \bigcup_{n=1}^{\infty} X_n,$$

and $\nu(X_n) < \infty$.

A measure space $(X, \mathscr{A}, \nu)$ is *complete* if $\mathscr{A}$ contains all subsets of sets of measure zero.

Proposition B.1.3 *If $(X, \mathscr{A}, \nu)$ is a measure space, then we can find a complete measure space $(X, \mathscr{A}_0, \nu_0)$ such that*

1. $\mathcal{A} \subset \mathscr{A}_0$,
2. $E \in \mathcal{A} \Rightarrow \nu(E) = \nu_0(E)$, *and*
3. $E \in \mathcal{A}_0 \Leftrightarrow E = A \cup B$ *where* $B \in \mathscr{A}$ *and* $A \subset C, C \in \mathscr{A}, \nu(C) = 0$.

The measure space $(X, \mathscr{A}_0, \nu_0)$ given in Proposition B.1.3 is called the *completion* of $(X, \mathscr{A}, \nu)$.

For a metric space $< X, \rho >$, the *Borel algebra* $\mathscr{B}$ is the smallest σ-algebra containing all the closed subsets of X, and any member of $\mathscr{B}$ is called a *Borel set*. A *Borel measure* ν is a measure defined on the Borel algebra $\mathscr{B}$ or the completion of such a measure. We assume that a Borel measure has finite values on compact sets.

For the space $\mathbb{R}^N$, the unique Borel measure that assigns the standard volume $\prod_{i=1}^{N}(b_i - a_i)$ to every rectangular cube

$$[a_1, b_1] \times \cdots \times [a_N, b_N],$$

is called the *Lebesgue measure* .

Let $(X, \mathscr{A})$ be a fixed measurable space. Two measures ν_1 and ν_2 are called *mutually singular* if there are disjoint sets A and B in $\mathscr{A}$ such that $X = A \cup B$ and $\nu_1(A) = \nu_2(B) = 0$. A measure ν_1 is said to be *absolutely continuous* with respect to the measure ν_2 if $\nu_1(A) = 0$ for each set A satisfying $\nu_2(A) = 0$.

Definition B.1.4 (Signed measure) *A signed measure on the measurable space $(X, \mathscr{A})$ is an extended real-valued set function ν defined for the members of $\mathscr{A}$ and satisfying the following conditions:*

1. *ν assumes at most one of the values $\infty, -\infty$,*
2. *$\nu(\emptyset) = 0$, and*
3. *for any sequence $\{E_i\}$ of disjoint measurable sets*

$$\nu(\bigcup_{i=1}^{\infty} E_i) = \sum_{i=1}^{\infty} \nu(E_i),$$

where the equality is taken to mean that the series on the right converges absolutely if $\nu(\bigcup E_i)$ is finite and that it properly diverges otherwise.

Proposition B.1.5 (Jordan decomposition) *A signed measure ν on the measurable space $(X, \mathscr{A})$ can be uniquely decomposed as $\nu = \nu^+ - \nu^-$, where ν^+ and ν^- are mutually singular measures on $(X, \mathscr{A})$.*

The measure $|\nu|$ defined by $|\nu| = \nu^+ + \nu^-$ is called the *absolute value* of ν.

B.2 Integration

For a measurable space $(X, \mathscr{A})$, a function $f : X \to [-\infty, \infty]$ is called *measurable* if

$$f^{-1}(U) \stackrel{\triangle}{=} \{x \in X : f(x) \in U\} \in \mathscr{A},$$

for any open subset U of $[-\infty, \infty]$, and f is called *Borel measurable* if the $\mathscr{A}$ is the Borel algebra $\mathscr{B}$. A function ϕ is called *simple* if it is a finite linear combination

$$\phi(x) = \sum_{i=1}^{n} c_i \chi_{E_i}(x), \tag{B.1}$$

of characteristic functions of measurable sets E_i.

For a measure space $(X, \mathscr{A}, \nu)$, if E is a measurable set and ϕ is a nonnegative simple function of the form (B.1), we define

$$\int_E \phi d\nu \triangleq \sum_{i=1}^{N} c_i \nu(E_i \cap E).$$

For a nonnegative measurable function f and a measurable set E, we define

$$\int_E f d\nu \triangleq \sup_{\phi \text{ simple }, 0 \le \phi \le f} \int_E \phi d\nu.$$

A measurable function $f : X \to [-\infty, \infty]$ is *integrable* on X with respect to ν, if $\int_X |f| d\nu$ is finite. For an integrable function f, for a measurable set E, we define

$$\int_E f d\nu \triangleq f_+ d\nu - \int_E f_- d\nu,$$

where $f_+ \triangleq \max\{f, 0\}$ and $f_- \triangleq \max\{-f, 0\}$.

Theorem B.2.1 (The Radon-Nikodym theorem) *Let $(X, \mathscr{A}, \nu_1)$ be a σ-finite measure space, and let ν_2 be a measure defined on $\mathscr{A}$ which is absolutely continuous with respect to ν_1. Then there is a nonnegative measurable function μ such that*

$$\nu_2(E) = \int_E \mu d\nu_1, \ \forall E \in \mathscr{A}.$$

Appendix C

Basics of Robust Control

In this appendix we collect some fundamental results of robust control from [29]. Following [29], we carry out the discussions in the discrete-time setting. For other references on linear robust control, in particular, $\mathcal{H}_\infty$ control, please see [33, 39, 94]. A dynamic game approach for $\mathcal{H}_\infty$ control can be found in [10]. For a treatment on nonlinear $\mathcal{H}_\infty$ control, please refer to [43].

C.1 Signals and Systems

Denote $\mathbb{Z}_+$ the set of nonnegative integers. Denote $l^n(\mathbb{Z}_+)$ the space of all vector-valued real sequences on $\mathbb{Z}_+$, of dimension n, i.e., $\forall x = \{x[k]\}_{k=0}^{\infty} \in l^n(\mathbb{Z}_+)$, $x[k] \in \mathbb{R}^n$, $k = 0, 1, \cdots$. For an integer $1 \leq p < \infty$, we define the space

$$l_p^n \stackrel{\triangle}{=} \{x \in l^n(\mathbb{Z}_+) : \| x \|_p < \infty\},$$

where

$$\| x \|_p \stackrel{\triangle}{=} (\sum_{k=0}^{\infty} \sum_{i=1}^{n} |x_i[k]|^p)^{\frac{1}{p}}$$

and $x_i[k]$ denotes the i-th component of $x[k]$. For instance, l_2^n is the space of finite energy signals. For $p = \infty$, we define l_∞^n to be the space of bounded magnitude signals:

$$l_\infty^n \stackrel{\triangle}{=} \{x \in l^n(\mathbb{Z}_+) : \sup_k \max_i |x_i[k]| < \infty\}.$$

A system $\mathcal{T}$ is an operator between two signal spaces X and Y. Denote by $\mathcal{P}_k$, $k \in \mathbb{Z}_+$, the truncation operator on $l^n(\mathbb{Z}_n)$, i.e.,

$$\mathcal{P}_k(x[0], x[1], \cdots) = (x[0], x[1], \cdots, x[k], 0, 0, \cdots).$$

Denote by S the unit shift operator, i.e.,

$$S(x[0], x[1], \cdots) = (0, x[1], x[2], \cdots).$$

Definition C.1.1 (Linearity, causality, and time-invariance) *An operator $\mathcal{T} : X \to Y$ is linear if*

$$\mathcal{T}(\alpha x + \beta y) = \alpha \mathcal{T}(x) + \beta \mathcal{T}(y),\ \forall \alpha,\ \beta \in \mathbb{R},\ \forall x, y \in X.$$

An operator $\mathcal{T}$ is causal if for all k, $\mathcal{P}_k \mathcal{T} = \mathcal{P}_k \mathcal{T} \mathcal{P}_k$, and is strictly causal if $\mathcal{P}_k \mathcal{T} = \mathcal{P}_k \mathcal{T} \mathcal{P}_{k-1}$ for all k. $\mathcal{T}$ is time-invariant if $S\mathcal{T} = \mathcal{T}S$.

Definition C.1.2 (Stability) *Let X, Y be two normed linear spaces. An operator $\mathcal{T} : X \to Y$ is stable if*

$$\| \mathcal{T} \| \stackrel{\triangle}{=} \sup_{x \neq 0} \frac{\| \mathcal{T} x \|_Y}{\| x \|_X} < \infty,$$

where $\| \cdot \|_X$ and $\| \cdot \|_Y$ denote the norms on X and Y, respectively. We call $\| \mathcal{T} \|$ the induced norm of $\mathcal{T}$.

We now characterize classes of linear time-invariant (LTI) systems on l_∞^n and l_2^n. Causality is implicitly assumed for a LTI system.

Let $\mathcal{R}$ be a LTI system from $l^n(\mathbb{Z}_+)$ to $l^m(\mathbb{Z}_+)$. Then for any $x \in l^n(\mathbb{Z}_+)$, $y = \mathcal{R}x \in l^m(\mathbb{Z}_+)$ can be expressed as

$$y[k] = \sum_{i=0}^{k} R[k-i]x[i],\ k = 0, 1, \cdots,$$

where $R = \{R[k]\}_{k=0}^{\infty} \in l^{m\times n}(\mathbb{Z}_+)$ is called the impulse response of $\mathcal{R}$. Write the (i,j)-th component of $R[k]$ as $R_{ij}[k]$, then $R_{ij} \in l^1(\mathbb{Z}_+)$, $1 \le i \le m, 1 \le j \le n$. From now on we will denote $\mathcal{R}$ by its impulse response R.

Theorem C.1.3 *A LTI system R is stable from l_∞^n to l_∞^m if and only if*

$$\| R \|_1 \stackrel{\triangle}{=} \max_{1\le i\le m} \sum_{j=1}^{n} \| R_{ij} \|_1 < \infty, \tag{C.1}$$

and $\| R \|_1$ is the induced norm of the system.

Remark C.1.4 *Recall that a matrix $A = (A_{ij}) \in \mathbb{R}^{m\times n}$ is a mapping from $\mathbb{R}^n$ to $\mathbb{R}^m$. When we equip the vector spaces $\mathbb{R}^n$ and $\mathbb{R}^m$ with the $|\cdot|_\infty$ norms, the induced norm of A is the so called l_1 norm $|A|_1 \stackrel{\triangle}{=} \max_{1\le i\le m} \sum_{j=1}^{n} |A_{ij}|$. Now write $\bar{R} = (\bar{R}_{ij})$ with $\bar{R}_{ij} = \| R_{ij} \|_1$. Then $\| R \|_1$ defined in (C.1) is just composition of the l_1 norm of $\bar{R}$ with the l_1 norms of R_{ij}'s. This is the reason we use notation $\|\cdot\|_1$ for R.*

We will denote by l_1 the space of LTI systems with finite l_∞-induced norm.

For $R \in l^{m\times n}(\mathbb{Z}_+)$, we define the λ-transform of R:

$$\widehat{R}(\lambda) = \sum_{k=0}^{\infty} R[k]\lambda^k.$$

Note the λ-transform is connected to the z-transform by $z = \frac{1}{\lambda}$. A remark on notation: for a LTI system, say G, we will also use G to denote its impulse response and will use $\widehat{G}$ to denote its λ-transform.

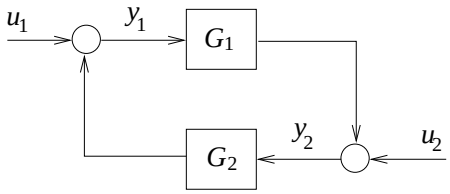

Figure C.1: Feedback connection.

Denote by $\mathcal{H}_\infty^{m\times n}$ the space of complex functions that are analytic on the open unit disc and bounded on the unit circle, and denote by $\mathcal{RH}_\infty^{m\times n}$ the space of real rational functions inside $\mathcal{H}_\infty^{m\times n}$. For any $\widehat{R} \in \mathcal{H}_\infty^{m\times n}$, the $\mathcal{H}_\infty$ norm is defined as

$$\| \widehat{R} \|_{\mathcal{H}_\infty} \triangleq \sup_\theta \sigma_{max}[\widehat{R}(e^{j\theta})],$$

where σ_{max} denotes the largest singular value of the matrix.

Theorem C.1.5 *A LTI system R is stable from l_2^n to l_2^m if and only if*

$$\| \widehat{R} \|_{\mathcal{H}_\infty} < \infty.$$

We write $\| R \|_\infty = \| \widehat{R} \|_{\mathcal{H}_\infty}$.

The following result is at the heart of the robust control theory and it applies to general nonlinear time-varying systems. Consider the feedback connection of two systems G_1 and G_2 as shown in Figure C.1. The closed-loop system is said to be well posed if for any u_1, u_2, there exists a unique solution y_1, y_2.

Theorem C.1.6 (Small gain theorem) *Let $G_1 : l_p^n \to l_p^m$ and $G_2 : l_p^m \to l_p^n$ be two l_p-stable systems and assume that the closed-loop system is well posed. Then the closed-loop system is l_p-stable (taking u_1, u_2 as the input, y_1, y_2 as the output) if $\| G_1 \| \cdot \| G_2 \| < 1$.*

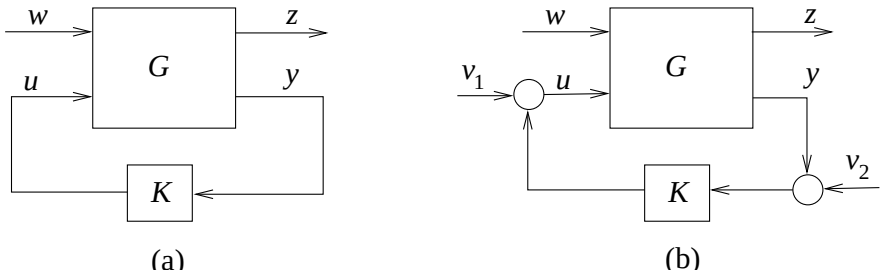

Figure C.2: General setup.

C.2 Parametrization of Stabilizing Controllers and Achievable Closed-Loop Maps

Figure C.2(a) shows a general setup for formulating performance objectives (trajectory tracking, disturbance attenuation, etc.), where u is the controlled input, y is the measured output, w is the exogenous input and z is the regulated output. The operator G is a 2×2 block matrix mapping w and u to z and y:

$$\begin{pmatrix} z \\ y \end{pmatrix} = \begin{bmatrix} G_{11} & G_{12} \\ G_{21} & G_{22} \end{bmatrix} \begin{pmatrix} w \\ u \end{pmatrix}.$$

K is the feedback controller. As we will see shortly, to solve the robust control problem (either robust stability problem, or robust performance problem, or both), one always ends up with the problem of finding a stabilizing K to minimize the induced norm of the closed-loop map from w to z.

Consider Figure C.2(b). Let $H(G, K)$ denote the following map:

$$\begin{pmatrix} z \\ u \\ y \end{pmatrix} = H(G, K) \begin{pmatrix} w \\ v_1 \\ v_2 \end{pmatrix}.$$

We assume the map $H(G, K)$ is well posed.

Definition C.2.1 *The closed-loop system is l_p-stable if the l_p-induced norm of $H(G,K)$ is finite. In such a case, K is said to be stabilizing in the l_p sense.*

We will be interested in the map Φ between w and z:

$$\Phi = G_{11} + G_{12}K(I - G_{22}K)^{-1}G_{21}. \tag{C.2}$$

In literature, Φ is called the *lower Linear Fractional Transformation (LFT)* of G and K and it can be written as $\Phi = F_l(G,K)$.

We now restrict ourselves to the case that G is a LTI system. We make the assumption that all the unstable poles of G are reachable from u and observable from y. With this assumption, K stabilizes G if and only if it stabilizes G_{22} and it suffices to parametrize all stabilizing controllers for G_{22}.

Definition C.2.2 (Doubly-coprime factorization) *A doubly-coprime factorization of G_{22} is a set of maps $N, M, \widetilde{N}, \widetilde{M}$, with $G_{22} = NM^{-1} = \widetilde{M}^{-1}\widetilde{N}$ satisfying*

$$\begin{pmatrix} \widetilde{X} & -\widetilde{Y} \\ -\widetilde{N} & \widetilde{M} \end{pmatrix} \begin{pmatrix} M & Y \\ N & X \end{pmatrix} = I, \tag{C.3}$$

for some stable $X, Y, \widetilde{X}$ and $\widetilde{Y}$, where I is the identity map. M and N are called the right coprime factors of G_{22} while $\widetilde{M}$ and $\widetilde{N}$ are called the left coprime factors of G_{22}.

Theorem C.2.3 *Let a doubly-coprime factorization of G_{22} be given as in (C.3). All stabilizing controllers are given by*

$$K = (Y - MQ)(X - NQ)^{-1} = (\widetilde{X} - Q\widetilde{N})^{-1}(\widetilde{Y} - Q\widetilde{M}),\ Q \text{ is stable.} \tag{C.4}$$

Remark C.2.4 *Theorem C.2.3 gives a complete parametrization of stabilizing controllers in the following two senses:*

1. *If Q is l_∞-stable, K is stabilizing in the l_∞ sense; if Q is l_2-stable, K is stabilizing in the l_2 sense.*

2. *The parametrization covers cases of LTI controllers, linear time-varying (LTV) controllers and nonlinear controllers. For instance, all LTI stabilizing controllers in the l_∞ sense are parametrized by $Q \in l_1$, all finite-dimensional LTI (FDLTI) stabilizing controllers in the l_∞ sense are parametrized by $Q \in \mathcal{RH}_\infty$, all LTV stabilizing controllers in the l_∞ sense are parametrized by Q in the set of all LTV l_∞-stable operators, and all nonlinear time-varying stabilizing controllers in the l_∞ sense are parametrized by Q in the set of all nonlinear time-varying l_∞-stable operators.*

Corollary C.2.5 *If G_{22} is stable, then the parametrization of stabilizing controllers is given by*

$$K = -Q(I - G_{22}Q)^{-1}. \tag{C.5}$$

Proof When G_{22} is stable, we obtain a doubly-coprime factorization by letting $M = \widetilde{X} = I$, $\widetilde{M} = X = I$, $N = \widetilde{N} = G_{22}$ and $Y = \widetilde{Y} = \mathbf{0}$, where the dimensions of the identity matrices I and the zero matrix $\mathbf{0}$ should be compatible with the operators. ∎

Substituting (C.4) into (C.2), we get a parametrization of achievable closed-loop maps from w to z:

$$\Phi = E - UQV, \ Q \text{ is stable}, \tag{C.6}$$

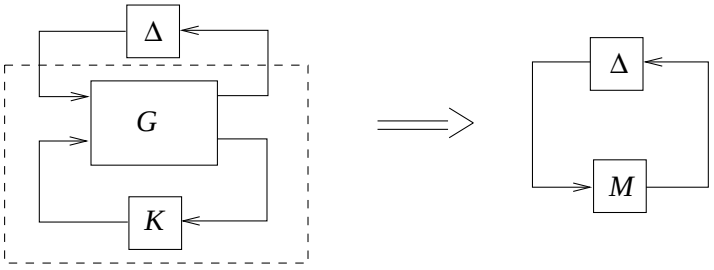

Figure C.3: Robust stability analysis.

where $E = G_{11} + G_{12}Y\widetilde{M}G_{21}$, $U = G_{12}M$, and $V = \widetilde{M}G_{21}$. We note that the closed-loop map Φ is affine in the free parameter Q, and as we will see, this plays a fundamental role in developing synthesis techniques for robust control.

C.3 Stability and Performance Robustness

In this section, we give the sufficient and necessary condition for a closed-loop system to be stable in the presence of uncertainties. We also indicate how to address the performance robustness problem by converting it to a stability robustness problem. Here by "performance" we mean the induced norm of the mapping from the exogenous input w to the regulated output z.

Consider Figure C.3, where Δ represents the uncertainty block. Let $\mathbf{\Delta}$ denote the class of uncertainties. $\mathbf{\Delta}$ can have certain structure, e.g., a block diagonal structure, as a result of our knowledge about uncertainty locations. The structural information of $\mathbf{\Delta}$ is exploited to reduce the conservativeness in robust controller synthesis.

Let $M = F_l(G, K)$.

Definition C.3.1 (Structured norm) *Given the class* $\mathbf{\Delta}$ *of uncertainties and*

p, the structured norm (SN) of M is defined as

$$SN_{\mathbf{\Delta},p}(M) \stackrel{\triangle}{=} \frac{1}{\inf_{\Delta\in\mathbf{\Delta}}\{\| \Delta \|_{l_p-ind}\text{: } (I-M\Delta)^{-1} \textit{ is not } l_p\textit{-stable}\}},$$

where $\| \cdot \|_{l_p-ind}$ denotes the l_p-induced norm. If for any $\Delta \in \mathbf{\Delta}$, $(I-M\Delta)^{-1}$ is l_p-stable, then $SN_{\mathbf{\Delta},p}(M)$ is defined to be 0.

Define $\mathbf{B}_{\mathbf{\Delta},p} = \{\Delta \in \mathbf{\Delta} :\| \Delta \|_{l_p-ind}< 1\}$. From Definition C.3.1, we have the following theorem:

Theorem C.3.2 (Structured small gain theorem) *The feedback connection of M and Δ (Figure C.3) is stable, for all $\Delta \in \mathbf{B}_{\mathbf{\Delta},p}$ if and only if $SN_{\mathbf{\Delta},p}(M) \leq 1$.*

Remark C.3.3 *From the small gain theorem, $SN_{\mathbf{\Delta},p}(M) \leq\| M \|_{l_p-ind}$.*

To make use of Theorem C.3.2, one need know how to compute $SN_{\mathbf{\Delta},p}(M)$ or its upper bound. Define the set $\mathbf{D} = \{D : D, D^{-1}$ are l_p-stable, $D^{-1}\Delta D \in \mathbf{\Delta}$, and $\| D^{-1}\Delta D \|_{l_p-ind}=\| \Delta \|_{l_p-ind}$ for all $\Delta \in \mathbf{\Delta}\}$. From Definition C.3.1, $SN_{\mathbf{\Delta},p}(M) = SN_{\mathbf{\Delta},p}(D^{-1}MD)$. Then by the small gain theorem, we have

$$SN_{\mathbf{\Delta},p}(M) \leq \inf_{D\in\mathbf{D}} \| D^{-1}MD \|_{l_p-ind} . \tag{C.7}$$

It turns out that equality holds in (C.7) for many important cases.

Theorem C.3.4 *Let $\mathbf{\Delta} = \{diag(\Delta_1, \Delta_2, \cdots, \Delta_n)$: each Δ_i is a nonlinear or linear time-varying uncertainty block of dimension $l_i \times l_i$, $1 \leq i \leq n\}$. Define*

$$\mathbf{D} = \{diag(d_1 I_{l_1}, d_2 I_{l_2}, \cdots, d_n I_{l_n}) : d_i \in \mathbb{R}, d_i > 0,\ 1 \leq i \leq n\},$$

where I_{l_i} denotes the identity matrix of dimension l_i. Then

$$SN_{\mathbf{\Delta},\infty}(M) = \inf_{D\in\mathbf{D}} \| D^{-1}MD \|_1, SN_{\mathbf{\Delta},2}(M) = \inf_{D\in\mathbf{D}} \| D^{-1}MD \|_\infty . \tag{C.8}$$

Corollary C.3.5 $\| M \|_1 \leq 1$ *if and only if the closed-loop system in Figure C.3 is* l_∞*-stable for arbitrary nonlinear or LTV* Δ *with* $\| \Delta \|_{l_\infty - ind} < 1$. *Similarly,* $\| M \|_\infty \leq 1$ *if and only if the closed-loop system is* l_2*-stable for arbitrary nonlinear or LTV* Δ *with* $\| \Delta \|_{l_2 - ind} < 1$.

For the case of FDLTI uncertainties, the concept of *structured singular value* is useful. Let $\mathbf{\Delta}_{LTI} = \{diag(\Delta_1, \Delta_2, \cdots, \Delta_n) : \Delta_i \in \mathcal{RH}_\infty^{l_i \times l_i},\ 1 \leq i \leq n\}$.

Definition C.3.6 (Structured singular value μ**)** *Consider the feedback connection in Figure C.3. For each* $\theta \in [0, 2\pi]$*, the structured singular value*

$$\mu_{\mathbf{\Delta}}[\widehat{M}(e^{j\theta})] \stackrel{\triangle}{=} \frac{1}{\inf_{\Delta \in \mathbf{\Delta}_{LTI}} \{\sigma_{max}[\widehat{\Delta}(e^{j\theta})] :\ det(I - \widehat{M}\widehat{\Delta})(e^{j\theta}) = 0\}},$$

and if $det(I - \widehat{M}\widehat{\Delta})(e^{j\theta}) \neq 0$ *for all* $\Delta \in \mathbf{\Delta}_{LTI}$*, then* $\mu_{\mathbf{\Delta}}[\widehat{M}(e^{j\theta})]$ *is defined to be 0.*

Theorem C.3.7 *Let* $\bar{l} = \max_i l_i$. *Then*

$$SN_{\mathbf{\Delta}_{LTI},2}(M) = \sup_{\theta \in [0,2\pi]} \mu_{\mathbf{\Delta}}[\widehat{M}(e^{j\theta})], \tag{C.9}$$

$$\frac{1}{\sqrt{\bar{l}}} \sup_{\theta \in [0,2\pi]} \mu_{\mathbf{\Delta}}[\widehat{M}(e^{j\theta})] \leq SN_{\mathbf{\Delta}_{LTI},\infty}(M) \leq \sqrt{\bar{l}} \sup_{\theta \in [0,2\pi]} \mu_{\mathbf{\Delta}}[\widehat{M}(e^{j\theta})]. \tag{C.10}$$

For single-input single-output (SISO) blocks, equality holds in (C.10).

Consider Figure C.4. From Corollary C.3.5, the robust performance problem (System I) can be converted to a robust stability problem by adding a fictitious uncertainty block mapping z to w (System II).

Theorem C.3.8 *Let* $\Delta \in \mathbf{\Delta}$. *Let* $\mathbf{\Delta}_P$ *be the class of arbitrary nonlinear or LTV uncertainties. Define the new set of uncertainties*

$$\widetilde{\mathbf{\Delta}} \stackrel{\triangle}{=} \{\widetilde{\Delta} = diag(\Delta, \Delta_P) : \Delta \in \mathbf{\Delta}, \Delta_P \in \mathbf{\Delta}_P\}.$$

Denote the mapping from w *to* z *as* $\mathcal{T}_{zw}$. *Then for* $p = \infty$ *or* $p = 2$, *System I is stable and* $\| \mathcal{T}_{zw} \|_{l_p - ind} \leq 1$ *for all* $\Delta \in \mathbf{B}_{\mathbf{\Delta},p}$ *if and only if* $SN_{\widetilde{\mathbf{\Delta}},p}(M) \leq 1$.

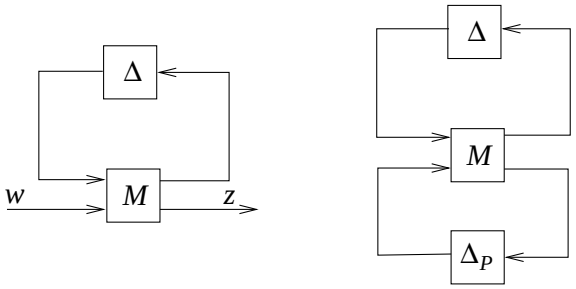

Figure C.4: Performance robustness vs. stability robustness.

C.4 The l_1 Model Matching Problem

We have seen from the previous section that solving a robust control problem involves computation of $\inf_{D\in\mathbf{D}} \parallel D^{-1}MD \parallel_{l_p-ind}$. Recall $M = F_l(G, K)$, therefore the controller synthesis problem is often posed as:

$$\inf_{\text{stabilizing } K} \inf_{D\in\mathbf{D}} \parallel D^{-1}MD \parallel_{l_p-ind} . \tag{C.11}$$

Optimizing (C.11) simultaneously with respect to K and D is hard. One method to approximately solve (C.11) is the so called *D-K iteration method*. The iteration goes as follows:

- **Step 1.** For a fixed $D \in \mathbf{D}$, solve

$$\inf_{\text{stabilizing } K} \parallel D^{-1}MD \parallel_{l_p-ind}, \tag{C.12}$$

  and denote the optimal controller as K^*.

- **Step 2.** Fix K^*, and search for the optimal D^* to minimize $\parallel D^{-1}MD \parallel_{l_p-ind}$.

- **Step 3.** Go back to Step 1 with $D = D^*$.

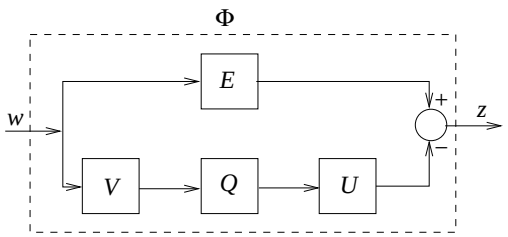

Figure C.5: The model matching problem.

By redefining G, the minimization problem in Step 1 above is equivalent to a model matching problem (recall Eq. (C.6) and Remark C.2.4)

$$\inf_{Q \text{ stable}} \| E - UQV \|_{l_p - ind}, \tag{C.13}$$

as illustrated in Figure C.5.

For $p = 2$, the problem (C.13) becomes the $\mathcal{H}_\infty$ model matching problem when we consider $Q \in \mathcal{RH}_\infty$ and it can be elegantly solved through the theory of Hankel operators. Since we are mainly interested in the case $p = \infty$ in robust control of smart actuators, here we focus on how to solve the l_1 model matching problem:

$$\inf_{Q \in l_1} \| E - UQV \|_1 . \tag{C.14}$$

C.4.1 Interpolation conditions

The approach to solve (C.14) is to first characterize the subspace

$$\mathcal{S} \stackrel{\triangle}{=} \{R \in l_1 : R = UQV \text{ for some } Q \in l_1\}$$

and then solve the minimum distance problem

$$\inf_{R \in \mathcal{S}} \| E - R \|_1 . \tag{C.15}$$

An element $R \in \mathcal{S}$ should preserve the *zero structures* of U and V: intuitively speaking, non-minimum phase zeros (zeros inside the open unit disk $\mathcal{D}$) of U and

V can not be cancelled by poles of Q since Q is stable. In addition, some rank conditions may need to be satisfied. We first review the concepts of zeros and poles for a rational matrix $\widehat{G}(\lambda)$.

Definition C.4.1 *A square polynomial matrix $\widehat{P}(\lambda)$ is called unimodular if its determinant is a nonzero constant.*

By definition, unimodular matrices have polynomial inverses.

Theorem C.4.2 *Let $\widehat{G}(\lambda)$ be an $m \times n$ rational matrix of normal rank r (i.e., of rank r for almost all λ). Then $\widehat{G}(\lambda)$ can always be factored as:*

$$\widehat{G}(\lambda) = \widehat{L}_G(\lambda)\widehat{M}_G(\lambda)\widehat{R}_G(\lambda), \tag{C.16}$$

where $\widehat{L}_G(\lambda)$ and $\widehat{R}_G(\lambda)$ are unimodular matrices of the appropriate dimensions, and

$$\widehat{M}_G(\lambda) = \begin{pmatrix} \frac{\widehat{\epsilon}_1(\lambda)}{\widehat{\psi}_1(\lambda)} & & & 0 & \cdots & 0 \\ & \ddots & & \vdots & \ddots & \vdots \\ & & \frac{\widehat{\epsilon}_r(\lambda)}{\widehat{\psi}_r(\lambda)} & 0 & \cdots & 0 \\ 0 & \cdots & 0 & 0 & \cdots & 0 \\ \vdots & \ddots & \vdots & \vdots & \ddots & \vdots \\ 0 & \cdots & 0 & 0 & \cdots & 0 \end{pmatrix}$$

is $m \times n$, where the monic polynomials $\{\widehat{\epsilon}_i(\lambda), \widehat{\psi}_i(\lambda)\}$ are coprime for all $i = 1, 2, \cdots, r$ and have the following divisibility property: $\widehat{\epsilon}_i(\lambda)$ divides $\widehat{\epsilon}_{i+1}(\lambda)$ and $\widehat{\psi}_{i+1}(\lambda)$ divides $\widehat{\psi}_i(\lambda)$ for $i = 1, 2, \cdots, r-1$.

Definition C.4.3 *$\widehat{M}_G(\lambda)$ is called the Smith-McMillan form of $\widehat{G}(\lambda)$. The roots of $\prod_{i=1}^{r} \widehat{\epsilon}_i(\lambda)$ are called the zeros of $\widehat{G}(\lambda)$ and the roots of $\prod_{i=1}^{r} \widehat{\psi}_i(\lambda)$ are called the poles of $\widehat{G}(\lambda)$.*

Definition C.4.4 *Let λ_0 be a zero of $\widehat{G}(\lambda)$. Let $\sigma_{G_i}(\lambda_0)$ denote the multiplicity of λ_0 as a root of $\widehat{\epsilon}_i(\lambda)$. $\sigma_{G_i}(\lambda_0)$ is known as the algebraic multiplicity of λ_0. The total number of indices i for which $\sigma_{G_i}(\lambda_0)$ is strictly positive is known as the geometric multiplicity of λ_0.*

Recall Figure C.2. We denote the dimensions of w, z, u, y as n_w, n_z, n_u and n_y, respectively. Without loss of generality, we assume that $\widehat{U}(\lambda)$ has full column normal rank n_u and $\widehat{V}(\lambda)$ has full row normal rank n_y.

Characterization of the subspace $\mathcal{S}$ is given by a set of interpolation conditions:

Theorem C.4.5 *Let the Smith-McMillan decompositions of $\widehat{U}$ and $\widehat{V}$ be $\widehat{U} = \widehat{L}_U\widehat{M}_U\widehat{R}_U$ and $\widehat{V} = \widehat{L}_V\widehat{M}_V\widehat{R}_V$, respectively. Let Λ_{UV} denote the set of zeros of $\widehat{U}$ or $\widehat{V}$ in the closed unit disk $\bar{\mathcal{D}}$. Define the polynomial row and column vectors:*

$$\widehat{\alpha}_i(\lambda) = (\widehat{L}_U^{-1})_i(\lambda),\ i = 1, 2, \cdots, n_z$$
$$\widehat{\beta}_j(\lambda) = (\widehat{R}_V^{-1})^j(\lambda),\ j = 1, 2, \cdots, n_w,$$

where $(M)_i$ denotes the i-th row of matrix M and $(M)^j$ denotes the j-th column of M. Assume that $\Lambda_{UV} \subset \mathcal{D}$. Given $R \in l_1^{n_z \times n_w}$, there exists a $Q \in l_1^{n_u \times n_y}$ such that $R = UQV$ if and only if for all $\lambda_0 \in \Lambda_{UV}$, the following conditions are satisfied:

1. *Zero interpolation conditions:*

$$(\widehat{\alpha}_i\widehat{R}\widehat{\beta}_j)^{(k)}(\lambda_0) = 0 \ \ for \begin{cases} i = 1, \cdots, n_u \\ j = 1, \cdots, n_y \\ k = 0, \cdots, \sigma_{U_i}(\lambda_0) + \sigma_{V_j}(\lambda_0) - 1 \end{cases}.$$

2. *Rank interpolation conditions:*

$$\begin{cases} (\widehat{\alpha}_i\widehat{R})(\lambda) \equiv 0 \ \ for\ i = n_u + 1, \cdots, n_z \\ (\widehat{R}\widehat{\beta}_j)(\lambda) \equiv 0 \ \ for\ j = n_y + 1, \cdots, n_w \end{cases}.$$

Corollary C.4.6 *The result in Theorem C.4.5 holds for $\Lambda_{UV} \subset \bar{\mathcal{D}}$ if $\widehat{R} \in \mathcal{RH}_\infty$.*

From Theorem C.4.5, if $n_w = n_y$ and $n_u = n_z$, the rank interpolation conditions disappear and we call such problems *one-block problems*. A problem is called *multi-block* if it is not one-block.

C.4.2 The one-block problem

The zero interpolation conditions in Theorem C.4.5 can be reformulated in terms of *null chains* of U and V, which avoids explicit computation of the Smith-McMillan decomposition. We assume that locations of zeros are known.

Definition C.4.7 (Null chains) *Given a $m \times n$ real rational matrix $\widehat{E}(\lambda)$ analytic at λ_0 and a positive integer σ, define the Toeplitz matrix:*

$$T_{\lambda_0,\sigma}(\widehat{E}) = \begin{pmatrix} E_0 & 0 & 0 & \cdots & 0 \\ E_1 & E_0 & 0 & \cdots & 0 \\ \vdots & & & \ddots & \vdots \\ E_{\sigma-1} & E_{\sigma-2} & E_{\sigma-3} & \cdots & E_0 \end{pmatrix},$$

where $E_i = \frac{1}{i!}\widehat{E}^{(i)}(\lambda_0)$, $i \geq 0$. A right null chain of order σ of $\widehat{E}(\lambda)$ at λ_0 is an ordered set of column vectors in $\mathbb{R}^n$, $\{x_1, x_2, \cdots, x_\sigma\}$, such that $x_1 \neq 0$ and

$$T_{\lambda_0,\sigma}(\widehat{E}) \begin{pmatrix} x_1 \\ x_2 \\ \vdots \\ x_\sigma \end{pmatrix} = \mathbf{0}.$$

A left null chain of order σ of $\widehat{E}(\lambda)$ at λ_0 is, by definition, a right null chain of order σ of $\widehat{E}^T(\lambda)$ at λ_0.

Definition C.4.8 *A canonical set of right null chains of $\widehat{E}(\lambda)$ at λ_0 is an ordered set of right null chains, i.e., $x^i = (x_1^i, \cdots, x_{\sigma_i}^i)$ for $i = 1, \cdots, l$, such that*

1. *$\{x_1^1, \cdots, x_1^l\}$ are linearly independent,*
2. *$span\{x_1^1, \cdots, x_1^l\}$ = the null space of $\widehat{E}(\lambda_0)$, and*
3. *$\sigma_1 \geq \sigma_2 \geq \cdots \geq \sigma_l$.*

A canonical set of left null chains is defined similarly.

Definition C.4.9 *An extended set of right null chains of a full rank $n \times n$ rational matrix $\widehat{E}(\lambda)$ at λ_0, is a canonical set of right null chains augmented with $n - l$ vectors in $\mathbb{R}^n$, $\{x_1^{l+1}, \cdots, x_1^n\}$ such that $span\{x_1^1, x_1^2, \cdots, x_1^n\} = \mathbb{R}^n$. Each $\{x_1^k\}$ is treated as a chain with order 0, $l + 1 \leq k \leq n$. An extended set of left null chains is defined similarly.*

An algorithm to compute the extended set of null chains is provided in [29], page 134.

Given an element of an extended set of right null chains at λ_0, x^j of order σ_j, define

$$\widehat{x}_{\lambda_0}^j(\lambda) \stackrel{\triangle}{=} x_1^j + (\lambda - \lambda_0)x_2^j + \cdots + (\lambda - \lambda_0)^{\sigma_j - 1}x_{\sigma_j}^j$$

if $\sigma_j > 0$ and $\widehat{x}_{\lambda_0}^j(\lambda) \stackrel{\triangle}{=} x_1^j$ if $\sigma_j = 0$. Similarly, define $\widehat{y}_{\lambda_0}^i(\lambda)$ for an element of an extended set of left null chains, y^i, of order σ_i. With this notation, we have

Theorem C.4.10 *Given a one-block problem, the zero interpolation conditions in Theorem C.4.5 are equivalent to the following: for all $\lambda_0 \in \Lambda_{UV}$,*

$$((\widehat{y}_{\lambda_0}^i)^T \widehat{R} \widehat{x}_{\lambda_0}^j)^{(k)}(\lambda_0) = 0 \ \ for \begin{cases} i = 1, \cdots, n_u \\ j = 1, \cdots, n_y \\ k = 0, \cdots, \sigma_{U_i}(\lambda_0) + \sigma_{V_j}(\lambda_0) - 1 \end{cases}, \qquad \text{(C.17)}$$

where y^i and x^j are elements of the extended sets of left and right null chains of $\widehat{U}$ and $\widehat{V}$, respectively, and σ_{U_i}, σ_{V_j} are the corresponding orders.

The problem (C.15) can now be solved by a linear programming approach. Recall a closed-loop map $\Phi = E - R$. Therefore (C.17) leads to a set of linear equality constraints on Φ:

$$\mathcal{A}_{zero}\Phi = b,$$

where $\mathcal{A}_{zero}$ is some linear operator on $l_1^{n_z \times n_w}$, $b \in \mathbb{R}^{n_c}$ and n_c is the total number of constraints imposed by (C.17).

For $\Phi \in l_1^{n_z \times n_w}$, we define $\Phi^+, \Phi^- \in l_1^{n_z \times n_w}$ as follows:

$$\Phi_{ij}^+[k] = \max\{0, \Phi_{ij}[k]\}, \text{ and } \Phi_{ij}^-[k] = \max\{0, -\Phi_{ij}[k]\},$$

for all $k \geq 0, 1 \leq i \leq n_z, 1 \leq j \leq n_w$. Thus $\Phi = \Phi^+ - \Phi^-$. $\| \Phi \|_1$ can be expressed as $\mathcal{A}_{l_1}(\Phi^+ + \Phi^-)$ where $\mathcal{A}_{l_1}$ is a linear functional.

The one-block l_1 model match problem is transformed into the following linear program:

$$\begin{aligned} \nu^0 = \inf_{\nu, \Psi^+, \Psi^-} \nu, \qquad & \text{such that} \\ \mathcal{A}_{zero}(\Phi^+ - \Phi^-) &= b, \\ \mathcal{A}_{l_1}(\Phi^+ + \Phi^-) &\leq \nu, \\ \Phi^+, \Phi^- &\geq 0. \end{aligned} \tag{C.18}$$

When $\Lambda_{UV} \subset \mathcal{D}$, one can show that the optimal Φ has a finite impulse response (FIR) through analysis on the dual linear program of (C.18).

From the optimal Φ, one obtains the optimal controller by plugging the corresponding Q into (C.4).

C.4.3 The multi-block problem

The rank interpolation conditions in Theorem C.4.5 also imposes linear constraints on Φ, but the number of constraints is infinite. Therefore in general the resulting linear programming problem has infinite number of variables and infinite number of constraints. Three approximation methods are available to solve the infinite dimensional linear programming problem:

1. Finitely Many Variables (FMV) approximation: approximate Φ by a finite impulse response of length N which results in finite number of variables.

2. Finitely Many Equations (FME) approximation: approximate the dual variables by a finite vector of dimension N which is equivalent to retaining finite number of constraints in the primal problem.

3. Delay Augmentation (DA) approximation: Embedding the problem into a one-block problem by augmenting U and V with N pure delays.

The DA approximation carries richer information about the structure of the optimal solution than FMV and FME. It is also the method we use in our computation. We now give a brief introduction to the DA method.

We first partition the original system (C.6) as:

$$\begin{pmatrix} \Phi_{11} & \Phi_{12} \\ \Phi_{21} & \Phi_{22} \end{pmatrix} = \begin{pmatrix} E_{11} & E_{12} \\ E_{21} & E_{22} \end{pmatrix} - \begin{pmatrix} U_1 \\ U_2 \end{pmatrix} Q(V_1\ V_2),$$

where $U_1 \in l_1^{n_u \times n_u}$ and $V_1 \in l_1^{n_y \times n_y}$. Denote by S_N the N-th order delay operator, i.e., $\widehat{S}_N = \lambda^N$. Augment U, V and Q accordingly:

$$\underbrace{\begin{pmatrix} \Phi_{11,N} & \Phi_{12,N} \\ \Phi_{21,N} & \Phi_{22,N} \end{pmatrix}}_{\Phi_N} \triangleq \begin{pmatrix} E_{11} & E_{12} \\ E_{21} & E_{22} \end{pmatrix} - \underbrace{\begin{pmatrix} U_1 & 0 \\ U_2 & S_N I_{n_z - n_u} \end{pmatrix}}_{U_N} \underbrace{\begin{pmatrix} Q_{11} & Q_{12} \\ Q_{21} & Q_{22} \end{pmatrix}}_{Q_N} \underbrace{\begin{pmatrix} V_1 & V_2 \\ 0 & S_N I_{n_w - n_y} \end{pmatrix}}_{V_N}.$$

Theorem C.4.11 *For $N > 0$, let*

$$\nu^0 = \inf_{Q_{11} \in l_1^{n_u \times n_y}} \| E - UQV \|_1, \text{ and}$$

$$\underline{\eta}_N = \Phi_N^0 \triangleq \inf_{Q_N \in l_1^{n_z \times n_w}} \| \Phi_N \|_1 .$$

If Φ_N^0 is achievable, let Q_N^0 be the corresponding minimizer. Let $\bar{\eta}_N = \| E - UQ_{11}^0 V \|$. Then

$$\underline{\eta}_N \leq \nu^0 \leq \bar{\eta}_N. \tag{C.19}$$

Proof We have

$$\nu^0 = \inf_{Q_{11} \in l_1^{nu \times ny}} \inf_{Q_{12} = Q_{21} = Q_{22} = 0} \| \Phi_N \|_1 \geq \underline{\eta}_N.$$

Sine $Q_{11}^0 \in l_1^{n_u \times n_y}$, it's clear that $\nu^0 \leq \bar{\eta}_N$. ∎

Theorem C.4.11 tells us that we can obtain a sub-optimal controller by plugging Q_{11}^0 into (C.4).

Convergence results for the DA method can be found in [29].

BIBLIOGRAPHY

[1] A. A. Adly, I. D. Mayergoyz, and A. Bergqvist. Preisach modeling of magnetostrictive hysteresis. *Journal of Applied Physics*, 69(8):5777–5779, 1991.

[2] F. Bagagiolo. Dynamic programming for some optimal control problems with hysteresis. Technical Report 38, Max-Planck Institute for the Mathematics in the Sciences, Leipzig, Germany, 2000.

[3] F. Bagagiolo. An infinite horizon optimal control problem for some switching systems. *Discrete and Continuous Dynamical Systems, Series B*, 1(4):443–462, 2001.

[4] F. Bagagiolo. Viscosity solutions for an optimal control problem with Preisach hysteresis nonlinearities. Technical Report 594, Department of Mathematics, University of Trento, June 2001.

[5] J. A. Ball and J. W. Helton. Viscosity solutions of Hamilton-Jacobi equations arising in nonlinear $\mathcal{H}_\infty$ control. *Journal of Mathematical Systems, Estimation, and Control*, 6(1):1–22, 1996.

[6] J. A. Ball, J. W. Helton, and M. L. Walker. $\mathcal{H}_\infty$ control for nonlinear systems with output feedback. *IEEE Transactions on Automatic Control*, 38(4):546–559, 1993.

[7] H. T. Banks, A. J. Kurdila, and G. Webb. Identification of hysteretic control influence operators representing smart actuators, Part I: Formulation. *Mathematical Problems in Engineering*, 3(4):287–328, 1997.

[8] H. T. Banks, A. J. Kurdila, and G. Webb. Identification of hysteretic control influence operators representing smart actuators, Part II: Convergent approximations. *Journal of Intelligent Material Systems and Structures*, 6(8):536–550, 1997.

[9] M. Bardi and I. Capuzzo-Dolcetta. *Optimal Control and Viscosity Solutions of Hamilton-Jacobi-Bellman Equations*. Birkhäuser, Boston, 1997.

[10] T. Basar and P. Bernhard. $\mathcal{H}_\infty$-*Optimal Control and Related Minimax Design Problems*. Birkhäuser, Boston, 1995.

[11] S. A. Belbas and I. D. Mayergoyz. Optimal control of dynamic systems with hysteresis. *International Journal of Control*, 73(1):22–28, 2000.

[12] S. A. Belbas and I. D. Mayergoyz. Dynamic programming for systems with hysteresis. *Physica B*, 306(1-4):200–205, 2001.

[13] D. P. Bertsekas. *Dynamic Programming and Optimal Control*. Athena Scientific, Belmont, Massachusetts, 1995.

[14] P. A. Bliman, A. M. Krasnosel'skii, M. Sorine, and A. A. Vladimirov. Nonlinear resonance in systems with hysteresis. *Nonlinear Analysis, Theory, Methods and Applications*, 27(5):561–577, 1996.

[15] L. S. Bobrow and M. A. Arbib. *Discrete Mathematics: Applied Algebra for Computer and Information Science*. W. B. Saunders Company, 1974.

[16] M. S. Branicky. *Studies in hybrid systems: modeling, analysis, and control*. PhD thesis, MIT, Cambridge, 1995.

[17] M. S. Branicky, V. S. Borkar, and S. K. Mitter. A unified framework for hybrid control: model and optimal control theory. *IEEE Transactions on Automatic Control*, 43(1):31–45, 1998.

[18] M. Brokate. Optimal control of ODE systems with hysteresis nonlinearities. In K. H. Hoffman, J. B. Hiriart-Urruty, C. Lemarechal, and J. Zowe, editors, *Trends in Mathematical Optimization*, pages 25–41. Birkhäuser Verlag, 1988.

[19] M. Brokate and A. V. Pokrovskii. Asymptotically stable oscillations in systems with hysteresis nonlinearities. *Journal of Differential Equations*, 150:98–123, 1998.

[20] M. Brokate and J. Sprekels. *Hysteresis and Phase Transitions*. Springer Verlag, New York, 1996.

[21] M. Brokate and A. Visintin. Properties of the Preisach model for hysteresis. *Journal ür die reine und angewandte Mathematik*, 402:1–40, 1989.

[22] W. F. Brown. *Magnetoelastic Interactions*. Springer-Verlag, 1966.

[23] S. Chikazumi. *Physics of Magnetism*. John Wiley & Sons, Inc., 1966.

[24] W. A. Coppel. *Stability and Asymptotic Behavior of Differential Equations*. Heath, Boston, 1965.

[25] M. G. Crandall, L. C. Evans, and P. L. Lions. Some properties of viscosity solutions of Hamilton-Jacobi equations. *Transactions of the American Mathematical Society*, 282(2):487–502, 1984.

[26] M. G. Crandall and P. L. Lions. Viscosity solutions of Hamilton-Jacobi equations. *Transactions of the American Mathematical Society*, 277(1):1–42, 1983.

[27] R. Cross, A. M. Krasnosel'skii, and A. V. Pokrovskii. A time-dependent Preisach model. *Physica B*, 306(1-4):206–210, 2001.

[28] J. M. Cruz-Hernández and V. Hayward. Phase control approach to hysteresis reduction. *IEEE Transactions on Control Systems Technology*, 9(1):17–26, 2001.

[29] M. A. Dahleh and I. J. Diaz-Bobillo. *Control of Uncertain Systems: A Linear Programming Approach*. Prentice-Hall, Englewood Cliffs, NJ, 1995.

[30] M. J. Dapino. *Nonlinear and Hysteretic Magnetomechanical Model for Magnetostrictive Transducers*. PhD thesis, Iowa State University, Ames, Iowa, 1999.

[31] L. C. Evans and P. E. Souganidis. Differential games and representation formulas for solutions of Hamilton-Jacobi-Issacs equations. *Indiana University Mathematics Journal*, 33(5):773–793, 1984.

[32] W. H. Fleming and H. M. Soner. *Controlled Markov Processes and Viscosity Solutions*. Springer-Verlag, New York, 1993.

[33] B. A. Francis. *A Course of $\mathcal{H}_\infty$ Control Theory*. Springer-Verlag, Berlin, New York, 1987.

[34] W. S. Galinaitis and R. C. Rogers. Compensation for hysteresis using bivariate Preisach models. In V. V. Varadan and J. Chandra, editors, *Mathematics and Control in Smart Structures*, volume 3039 of *SPIE*, pages 538–547, 1997.

[35] W. S. Galinaitis and R. C. Rogers. Control of a hysteretic actuator using inverse hysteresis compensation. In V.V. Varadan, editor, *Mathematics and Control in Smart Structures*, volume 3323 of *SPIE*, pages 267–277, 1998.

[36] P. Ge and M. Jouaneh. Tracking control of a piezoceramic actuator. *IEEE Transactions on Control Systems Technology*, 4(3):209–216, 1996.

[37] R. B. Gorbet, K. A. Morris, and D. W. L. Wang. Control of hysteretic systems: a state-space approach. In Y. Yamamoto and S. Hara, editors, *Learning, Control and Hybrid Systems*, volume 241 of *Lecture Notes in Control and Information Sciences*, pages 432–451, New York, 1998. Springer.

[38] R. B. Gorbet, D. W. L. Wang, and K. A. Morris. Preisach model identification of a two-wire SMA actuator. In *Proceedings of IEEE International Conference on Robotics and Automation*, pages 2161–2167, 1998.

[39] M. Green and D. J. N. Limebeer. *Linear Robust Control*. Prentice Hall, Englewood Cliffs, NJ, 1995.

[40] E. Hairer, S. P. N∅rsett, and G. Wanner. *Solving Ordinary Differential Equations I: Nonstiff Problems*. Springer-Verlag, 1993.

[41] E. Hairer and G. Wanner. *Solving Ordinary Differential Equations II: Stiff and Differential-Algebraic Problems*. Springer-Verlag, 1996.

[42] S. Hedlund and A. Rantzer. Optimal control of hybrid systems. In *Proceedings of the 38th IEEE Conference on Decision and Control*, pages 3972–3977, Phoenix, Arizona, December 1999.

[43] J. W. Helton and M. R. James. *Extending $\mathcal{H}_\infty$ Control to Nonlinear Systems: Control of Nonlinear Systems to Achieve Performance Objectives*. Society for Industrial and Applied Mathematics, 1999.

[44] D. Hill and P. Moylan. The stability of nonlinear dissipative systems. *IEEE Transactions on Automatic Control*, AC-21:708–711, 1976.

[45] D. Hughes and J. T. Wen. Preisach modeling and compensation for smart material hysteresis. In G. L. Anderson and D. C. Lagoudas, editors, *Active Materials and Smart Structures*, volume 2427 of *SPIE*, pages 50–64, 1994.

[46] D. Hughes and J. T. Wen. Preisach modeling of piezoceramic hysteresis; independent stress effect. In V. V. Varadan, editor, *Mathematics and Control in Smart Structures*, volume 2442 of *SPIE*, pages 328–336, 1995.

[47] H. Ishii. Uniqueness of unbounded viscosity solution of Hamilton-Jacobi equations. *Indiana University Mathematics Journal*, 33(5):721–748, 1984.

[48] M. R. James. A partial differential inequality for dissipative nonlinear systems. *Systems and Control Letters*, 21:315–320, 1993.

[49] M. R. James and J. S. Baras. Partially observed differential games, infinite-dimensional Hamilton-Jacobi-Isaacs equations, and nonlinear $\mathcal{H}_\infty$ control. *SIAM Journal on Control and Optimization*, 34(4):1342–1364, 1996.

[50] M.R. James and S. Yuliar. Numerical approximation of the $\mathcal{H}_\infty$ norm for nonlinear systems. *Automatica*, 31(8):1075–1086, 1995.

[51] D. C. Jiles and D. L. Atherton. Theory of ferromagnetic hysteresis. *Journal of Magnetism and Magnetic Materials*, 61:48–60, 1986.

[52] K.-H. Hoffmann and G. H. Meyer. A least squares method for finding the Preisach hysteresis operator from measurements. *Numerische Mathematik*, 55:695–710, 1989.

[53] K.-H. Hoffmann, J. Sprekels, and A. Visintin. Identification of hysteretic loops. *Journal of Computational Physics*, 78:215–230, 1988.

[54] H. K. Khalil. *Nonlinear Systems*. Prentice Hall, Upper Saddle River, NJ, 1996.

[55] M. A. Krasnosel'skii and A. V. Pokrovskii. *Systems with Hysteresis*. Springer-Verlag, 1989.

[56] M. A. Krasnosel'skii and A. V. Pokrovskii. Operators in the problem of forced oscillations in systems with hysteresis. *Soviet Mathematics Doklady*, 44(1):228–232, 1992.

[57] K. Kuhnen and H. Janocha. Adaptive inverse control of piezoelectric actuators with hysteresis operators. In *Proceedings of European Control Conference (ECC)*, Karsruhe, Germany, 1999. Paper F 0291.

[58] I. D. Mayergoyz. *Mathematical Models of Hysteresis*. Springer Verlag, 1991.

[59] W. M. McEneaney. Robust control and differential games on a finite time horizon. *Mathematics of Control, Signals and Systems*, 8:138–166, 1995.

[60] W. M. McEneaney. Uniqueness for viscosity solutions of nonstationary Hamilton-Jacobi-Bellman equations under some a priori conditions (with applications). *SIAM Journal on Control and Optimization*, 33(5):1560–1576, 1995.

[61] R. K. Miller and A. N. Michel. *Ordinary Differential Equations*. Academic Press, 1982.

[62] C. Natale, F. Velardi, and C. Visone. Modelling and compensation of hysteresis for magnetostrictive actuators. In *Proceedings of IEEE/ASME International Conference on Advanced Intelligent Mechatronics*, pages 744–749, 2001.

[63] B. Piccoli. Hybrid systems and optimal control. In *Proceedings of the 37th IEEE Conference on Decision and Control*, pages 13–18, Tampa, Florida, December 1998.

[64] A. V. Pokrovskii, K. Abodayeh, and J. McInerney. Recurrent oscillations in systems with hysteresis nonlinearities. Technical Report 99-008, Institute for Nonlinear Science at University College, Cork, Ireland, 1999. Available at http://www.ucc.ie/ucc/depts/physics/ins/preprints.html.

[65] A. V. Pokrovskii, K. Abodayeh, and J. McInerney. Recurrent oscillations in systems with hysteresis nonlinearities. *Physica B*, 306(1-4):191–194, 2001.

[66] D. Rachinskii. Asymptotic stability of large-amplitude oscillations in systems with hysteresis. *Nonlinear Differential Equations and Applications*, 6:267–288, 1999.

[67] A. Rantzer and M. Johansson. Piecewise linear quadratic optimal control. *IEEE Transactions on Automatic Control*, 45(4):629–637, 2000.

[68] P. Riedinger, F. Kratz, C. Iung, and C. Zanne. Linear quadratic optimization for hybrid systems. In *Proceedings of the 38th IEEE Conference on Decision and Control*, pages 3059–3064, Phoenix, Arizona, December 1999.

[69] H. L. Royden. *Real Analysis*. Prentice Hall, Englewood Cliffs, NJ, 1988.

[70] A. J. van der Schaft. L_2-gain analysis of nonlinear systems and nonlinear state feedback $\mathcal{H}_\infty$ control. *IEEE Transactions on Automatic Control*, 37(6):770–784, 1992.

[71] R. C. Smith. Inverse compensation for hysteresis in magnetostrictive transducers. Technical Report CRSC-TR98-36, CRSC, North Carolina State University, 1998.

[72] R. C. Smith and C. L. Hom. A domain wall theory for ferroelectric hysteresis. Technical Report CRSC-TR99-01, CRSC, North Carolina State University, 1999.

[73] H. M. Soner. Optimal control with state-space constraint. *SIAM Journal on Control and Optimization*, 24(3):552–561, 1986.

[74] E. D. Sontag. *Mathematical Control Theory: Deterministic Finite Dimensional Systems*. Springer, New York, 1998.

[75] P. Soravia. $\mathcal{H}_\infty$ control of nonlinear systems: differential games and viscosity solutions. *SIAM Journal on Control and Optimization*, 34(3):1071–1097, 1996.

[76] P. Soravia. Equivalence between nonlinear $\mathcal{H}_\infty$ control problems and existence of viscosity solutions of Hamiltion-Jacobi-Isaacs equations. *Applied Mathematics and Optimization*, 39:17–32, 1999.

[77] X. Tan and J. S. Baras. Control of smart actuators: A viscosity solutions approach. Technical Report TR2001-39, Institute for Systems Research, University of Maryland at College Park, 2001.

[78] X. Tan and J. S. Baras. Optimal control of hysteresis in smart actuators: a viscosity solutions approach. In C. J. Tomlin and M. R. Greenstreet, editors, *Proceedings of the 5th International Workshop on Hybrid Systems: Computation and Control*, volume 2289 of *Lecture Notes in Computer Science*, pages 451–464. Springer, 2002.

[79] X. Tan, R. Venkataraman, and P. S. Krishnaprasad. Control of hysteresis: Theory and experimental results. In V. S. Rao, editor, *Modeling, Signal Processing, and Control in Smart Structures*, volume 4326 of *SPIE*, pages 101–112, 2001.

[80] G. Tao and P. V. Kokotović. Adaptive control of plants with unknown hysteresis. *IEEE Transactions on Automatic Control*, 40(2):200–212, 1995.

[81] E. Della Torre. *Magnetic Hysteresis*. IEEE Press, Piscataway, NJ, 1999.

[82] R. Venkataraman. *Modeling and Adaptive Control of Magnetostrictive Actuators*. PhD thesis, University of Maryland, College Park, 1999.

[83] R. Venkataraman and P. S. Krishnaprasad. A model for a thin magnetostrictive actuator. In *Proceedings of the 32nd Conference on Information Sciences and Systems, Princeton, NJ*, Princeton, March 1998.

[84] R. Venkataraman and P. S. Krishnaprasad. Qualitative analysis of a bulk ferromagnetic hysteresis model. In *Proceedings of the 37th IEEE Conference on Decision and Control, Tampa, FL*, pages 2443–2448, December 1998.

[85] R. Venkataraman and P. S. Krishnaprasad. Approximate inversion of hysteresis: theory and numerical results. In *Proceedings of the 39th IEEE Conference on Decision and Control*, pages 4448–4454, Sydney, Australia, December 2000.

[86] A. Visintin. *Differential Models of Hysteresis*. Springer, 1994.

[87] W. Walter. *Ordinary Differential Equations*. Springer, 1998.

[88] J. C. Willems. Dissipative dynamical systems, Part I: General theory. *Arch. Rational Mech. Anal.*, 45:321–351, 1972.

[89] H. S. Witsenhausen. A class of hybrid-state continuous-time dynamic systems. *IEEE Transactions on Automatic Control*, 11(2):161–167, 1966.

[90] M. Xiao and T. Basar. Nonlinear $\mathcal{H}_\infty$ controller design via viscosity supersolutions of the Isaacs equation. In W. M. McEneaney, G. Yin, and Q. Zhang, editors, *Stochastic Analysis, Control, Optimization and Applications*, pages 151–170. Birkhäuser, Boston, 1999.

[91] J. Yong. Systems governed by ordinary differential equations with continuous, switching and impulse controls. *Applied Mathematics and Optimization*, 20:223–235, 1989.

[92] S. Yuliar, M. R. James, and J. W. Helton. Dissipative control systems synthesis with full state feedback. *Mathematics of Control, Signals, and Systems*, 11:335–356, 1998.

[93] E. Zeidler. *Applied Functional Analysis: Applications to Mathematical Physics*. Springer-Verlag, 1995.

[94] K. Zhou and J. C. Doyle. *Essentials of Robust Control*. Prentice Hall, Upper Saddle River, NJ, 1998.